

SYMPOSIUM ON THE STABILITY AND OXIDATION CHEMISTRY OF MIDDLE DISTILLATE
FUELS, DIVISION OF FUEL AND PETROLEUM CHEMISTRY, AMERICAN CHEMICAL
SOCIETY, WASHINGTON D.C. MEETING, AUGUST 1990

THE ROLE OF A METAL DEACTIVATOR ADDITIVE IN IMPROVING
THE THERMAL STABILITY OF AVIATION KEROSESINES:
ADDITIVE ADSORPTION STUDIES

By

R.H. Clark, K.M. Delargy and R.J. Heins
Shell Research Ltd., Thornton Research Centre, P.O. Box 1, Chester CH1 3SH

INTRODUCTION

SCOPE OF PREVIOUS WORK

In an earlier paper¹, we reported studies that elucidated the mechanisms whereby MDA can affect the stability of jet fuel. The work not only investigated MDA in its claimed role as a metal chelating agent, but, more significantly, assessed the role of this additive within engine fuel system environments and within the thermal stability specification test (JFTOT). Thus the experimental work was on three parallel fronts:

- Realistic-large scale simulations of engine components
- Specification testing - the JFTOT
- Fundamental mechanistic studies

Glassware fuel oxidation studies clearly demonstrated the ability of MDA to act as a metal chelator, resulting in a near-unity chelation ratio. However, in the dynamic stability tests (i.e. fuel system simulators and the JFTOT), where fuel flows over a heated metal surface, the action of MDA was less clearcut. In particular, in spite of eliminating the metal chelation mechanism by using a metal-free fuel, benefits to fuel stability were still evident in our oil-cooler simulation² (Single-Tube Heat-Transfer Rig, STHTR) and the JFTOT. This improvement in fuel stability was attributed to MDA acting as a metal passivator and retarding the formation of lacquers on metal surfaces.

The passivating role of MDA was most evident on clean metal surfaces; once sufficient fuel lacquer had coated the metal surface, passivation ceased to be a factor controlling lacquer deposition. This differing response of a clean versus lacquered surface was of great concern for the specification test (JFTOT); given its short duration and low lacquer loadings, the JFTOT responds particularly strongly to the passivating action when compared with a more realistic rig (e.g. the STHTR) employing a longer test duration (25 - 100 hours). Thus, any improvement in fuel performance in the JFTOT obtained from the use of MDA may not necessarily be manifest in service. Figure 1, taken from reference 1, illustrates the different benefits of MDA on a low-metal-content fuel in a variety of systems.

CURRENT OBJECTIVE

Our use of a wide range of experimental systems has provided strong empirical evidence for the passivation mechanism of MDA, and, in particular, the overresponse of the JFTOT to MDA. Nevertheless, it was thought desirable to confirm such a mechanism by independent means. It was reasoned that a surface analysis technique would offer the opportunity of directly observing the adsorption of MDA molecules onto a metal surface. The chosen technique should be (i) sensitive enough to resolve a monolayer of MDA, and (ii) sufficiently discriminating to observe MDA in the presence of fuel or fuel lacquers. SIMS (Secondary Ion Mass Spectrometry) appeared a viable option, thus the overall aims became:

- To apply SIMS to observe directly the adsorption of MDA molecules onto aluminium surfaces, in particular JFTOT test specimens.
- To continue SIMS work to elucidate how MDA influences the lacquer patterns on a JFTOT test specimen

EXPERIMENTAL

SIMS

Secondary Ion Mass Spectrometry (SIMS) is a highly surface sensitive analytical technique (sampling depth = 0.5 - 1 nm) which involves the bombardment of a sample surface with a primary beam of energetic particles (normally ions or atoms). This results in the emission of a range of secondary particles, including positively and negatively charged ions. These secondary ions, both atomic and molecular species, are subsequently mass analysed to generate surface mass spectra similar to those obtained in conventional organic mass spectrometry. The technique, therefore, provides elemental analysis in addition to detailed and highly specific chemical structure information.

This study was carried out using a VG IX23S instrument equipped with a Poschenrieder time-of-flight analyser and a pulsed liquid metal ion source (Ga^+ , 30 KeV)³. For each sample, secondary ion spectra were recorded from an area of 0.5 mm x 0.5 mm. All spectra were generated under static SIMS conditions, where sufficiently low primary ion doses are used such that the samples are effectively undamaged throughout the course of the analysis. Both positive and negative ion spectra were recorded in the mass range 0 - 1500.

JFTOT

In essence, the JFTOT rig⁴ provides a system for passing a small sample of fuel (600 cm³) over a heated metal test section. The JFTOT assesses the stability of a fuel by its propensity to lacquer the test section and from the associated blockage of a downstream filter by decomposition products. For specification purposes, the hottest temperature on the test section (aluminium tube) is controlled to 260°C for 2.5 hours.

To pass the test, the tube lacquer must not be darker than the specified limit, and the filter pressure drop should not exceed 25 mm Hg. This results in a go/no go specification test. For research purposes, various refinements may be made to the procedure to allow fuel ranking.

TEST FUEL AND ADDITIVE

The test fuel was chosen so as to represent current refinery production. However, to minimise potential interference from other polar species within the SIMS analysis, the fuel was taken from commercial hydrotreated stock with a low intrinsic sulphur content. The fuel was pre-filtered to 0.45 μm before use. Two sources of the MDA concentrate were used:

- (i) 75% w/w MDA in xylene, proprietary name DuPont DMD No. 1.
- (ii) 50% w/w MDA in xylene, proprietary name DuPont DMD No. 2.

SAMPLE PREPARATION

Table 1 summarises the various sample preparation procedures. Samples comprised three basic types:

- (i) Sections of aluminium foil (approx 0.5 x 0.5 cm) for static/soaking experiments. These were pre-treated by ultrasonic cleaning with a trisolvent solution (an equivolume blend of toluene, isopropyl alcohol and acetone).
- (ii) Sections from JFTOT tubes (1.8 cm long) used in static/soaking experiments. The position of the sample along the tube was not critical.
- (iii) Sections from JFTOT tubes (1.8 cm long) used in a dynamic experiment, i.e. the uncut tubes had been run in the conventional JFTOT rig. These samples were taken to bracket the position on the test section corresponding to the hot spot (38.7 mm from the fuel inlet).

Except where indicated, all JFTOT tubes were used straight from the pack without any pre-treatment in compliance with the specification test conditions. Similarly, after exposure to the fuel or MDA solutions, the samples were rinsed with Analar grade heptane and allowed to dry (in accordance with the ASTM D3241 method⁷). The 1.8 cm samples were sectioned from the JFTOT tubes using a Beuhler saw. A stream of compressed air was used to remove any metallic debris from the sample surface.

RESULTS AND DISCUSSION

SIMS SPECTRUM - FRAGMENTATION PATTERN

Positive and negative ion spectra were taken in the mass range 0 - 1500; examples of spectra are given in Figures 2 and 3. The molecular weight (M) of MDA is 282, and ions corresponding to (M+H)⁺, at 283 daltons, and (M-H)⁻, at 281 daltons, were detected. A number of other ionic species were also observed but only in the presence of MDA; these are listed in

Table 2 together with the most probable assignments for molecular fragments arising from MDA. In addition to these characteristic ion fragments, a number of low-mass species were also detected in the positive and negative ion spectra, e.g. $C_2H_3^+$, Ph^+ , $PhCH_2^+$, C_n^- , C_nH^- , CN^- and PhO^- . Of all the fragments, the species at 118^- is considered to be, analytically, the most useful. The signal is of good intensity and is a highly characteristic indicator of MDA. Quasimolecular ions at 283^+ and 281^- are of limited use only: the intensity of the 283^+ signal is likely to be strongly dependent on the surface structure of MDA. Whilst the 281^- species is analytically more useful for assessing intact MDA molecules on a surface, it overlaps with a signal from an oleate-containing species. Consequently, any conclusions based on the 281^- signal alone are subject to some uncertainty. Thus for the purpose of comparison between samples the 118^- peak was used. As this peak lies adjacent to a characteristic reference peak for the substrate, $Al_2O_3H^-$ at 119^- , peak area ratios could be used with confidence to monitor the concentration of adsorbate. The relative surface concentration (C) of MDA was monitored using computed peak areas (A_{118} and A_{119}) in the following manner:

$$XC = \frac{A_{118}}{A_{118} + A_{119}} \times 100 \quad \dots(1)$$

The surface concentrations for each sample are shown diagrammatically in Figures 4 - 7. Interpretation of all results with equation 1 requires care, in that SIMS is considered only semi-quantitative. It is more important to consider trends within a series of specimens rather than absolute values.

PRELIMINARY FINDINGS

Initial experiments made use of simple samples in the form of aluminium foil sections. With these, there was a close similarity between the SIMS spectrum of the foil wetted by an MDA solution (derived from a DMD No 2 concentrate) and that of foil exposed to the same solution and then rinsed in heptane. Those features common to these two spectra were not evident in the third spectrum, which corresponded to a foil sample that had not been in contact with MDA. In addition, differences between the samples could be seen in the surface concentrations of MDA as determined from equation 1.

However, there were various features of the SIMS MDA spectrum which corresponded to mass numbers higher than the molecular weight of the additive, suggesting that this sample of MDA had degraded or polymerised. This potential problem of storage stability accordingly led us to seek a fresh sample of MDA for the main body of experimentation.

JFTOT TUBE SAMPLES - STATIC PREPARATION

These preliminary findings having shown that SIMS had sufficient sensitivity to detect MDA adsorbed onto aluminium surfaces, subsequent samples were prepared to reflect more closely the reality of the

specification test:

- solutions of MDA were made up with commercial jet fuel
- aluminium samples were taken from JFTOT test sections

Whilst it was clearly desirable for all JFTOT tubes to be used without any surface pre-treatment (i.e. as ASTM D3241), there were concerns that residual cutting oils on the aluminium could interfere with the SIMS detection or alternatively reduce the number of surface sites available for additive adsorption. As a precaution, two similar sets of samples were prepared: one untreated and the other pre-cleaned. However, it was recognised that these various preparations suffered from the shortcoming of being static immersion tests at ambient temperature. SIMS spectra were recorded for the following untreated JFTOT tubes:

- (i) Fuel wetted and heptane rinsed
- (ii) Fuel + 5.7 mg/l MDA wetted and heptane rinsed
- (iii) Fuel + 64.8 g/l MDA wetted and heptane rinsed
- (iv) Neat MDA cast onto a JFTOT tube as a reference spectrum
- (v) Sample (ii) was then repeated using a pre-cleaned JFTOT tube.

The results in terms of MDA surface concentrations are illustrated in Figure 4. SIMS could detect MDA in all samples that had been exposed to the additive. Moreover, the concentration of additive within the original bulk solution had a strong effect on the resultant surface concentration; the 5.7 mg/l MDA solution gave a spectrum in which the additive was only just discernible, whereas the 64.8 g/l solution resulted in an MDA signal comparable to that of the neat additive. This effect of concentration suggests an equilibrium between the MDA in the fuel solution and the molecules adsorbed onto the metal, presumably following a simple adsorption-type mechanism (e.g. Langmuir isotherm). From this, it can be concluded that, at the specification MDA concentration, not all the surface sites will be occupied by the MDA molecule. Comparison of the pre-cleaned tubes and the as-received examples indicated better adsorption of the additive onto a cleaned tube, presumably because more surface sites have become available. However, the cleaned system is less relevant to the specification conditions.

JFTOT TUBE SAMPLES - DYNAMIC PREPARATION

Data from the first two sets of experiments gave the necessary confidence to dispense with the idealised model systems and to use samples actually generated within the JFTOT rig and covering a range of temperature and additive concentration. In particular, it was seen as crucial that at least one condition should reflect the current specification test conditions (260°C maximum tube temperature, 2.5 hours duration, MDA concentration 5.7 mg/l maximum).

(a) Concentration dependence

Figure 5 illustrates the amount of MDA present on the surface as a function of the original additive concentration for tests at ambient temperature. The results agree with those seen in the static experiments where the MDA adsorbed onto the surface increased with bulk additive

concentration. However, more detail can be derived by applying a simple Langmuir-type adsorption model. The surface concentration approaches a limiting value for the two highest bulk additive concentrations (570 mg/l and 57 g/l), indicating that the surface sites are approaching saturation. This further confirms that at the specification concentration (5.7 mg/l) only a small fraction of available sites are occupied by adsorbed MDA molecules.

(b) Effect of temperature

An increase in the surface concentration of MDA is observed with increasing temperature (Figures 6 and 7). A small increment accompanies the change from 25°C to 140°C, but a dramatic one results on further increasing the test temperature to 260°C. This temperature dependence of MDA adsorption is unexpected; one might predict an exothermic heat of adsorption, and thus a decreasing amount of MDA adsorbed with increasing temperature. This anomalous increase in surface MDA concentration coupled with the strong non-Arrhenius temperature response suggests that a simple adsorption mechanism is not occurring. A plausible explanation could be that, in addition to reaching the surface by an adsorption mechanism, the MDA molecules can also add to the surface by polymerising to form an MDA matrix on the surface. Alternatively, fuel lacquer could entrain MDA molecules on the surface.

A MODEL FOR MDA PASSIVATION

In our previous paper¹, we discussed how MDA could modify and passivate a metal surface. This latest work allows us to hypothesise as to the nature of the mechanism by which MDA passivates. It is doubtful that the passivation results solely from MDA molecules adsorbed onto the metal surface. A two-stage mechanism is proposed: firstly, the MDA molecules adsorb onto some of the available surface sites and then subsequently, under the influence of heat, the adsorbed MDA molecules crosslink with each other and those in solution to form an MDA matrix; alternatively, the MDA molecules could be entrapped within a fuel lacquer film. It is proposed that such a polymerised MDA layer presents a less favourable substrate for lacquer formation than a bare Al/Al₂O₃ surface. Since our previous work has shown that this passivation is short-lived, it is assumed that either the fuel lacquer grows thick enough on the surface to hide the passivating layer, or, alternatively, the passivating layer is metastable and is eventually displaced by fuel lacquer. Unfortunately, in its current form the SIMS approach is unable to confirm such a mechanism. If the MDA is undergoing reaction, one would expect a decrease in the parent ion signals at higher temperatures. In the event these signals are rather weak and obscured by other species. However, it has been noted that at higher temperatures there is an increase in the CN⁻ signal relative to the 118⁻ signal, which suggests breakdown of the MDA molecule.

CONCLUSIONS

SIMS offers the sensitivity and discrimination required to detect the MDA molecule on an aluminium surface. The surface concentration of adsorbed MDA is a function of the original bulk MDA concentration and

appears to reach a saturation for bulk concentrations of ~ 57 g/l, indicating a simple Langmuir-type adsorption model. A fuel doped with MDA at the specification limit (5.7 mg/l) when run in the JFTOT will result in MDA being adsorbed onto the aluminium test specimen. However, relatively few surface sites will be occupied at this lower concentration.

The strong influence of temperature and the non-Arrhenius behaviour of the MDA surface concentration indicate that more than an adsorption mechanism is in operation at elevated temperatures. This evidence indicates that MDA passivation of the JFTOT test section does not result solely from surface adsorption; the MDA molecule may well be present as a polymer or in a fuel decomposition matrix.

ACKNOWLEDGEMENTS

The authors are indebted to Dr. Alan J. Paul of the Centre for Surface and Materials Analysis, UMIST, Manchester for his experimental expertise, interpretation and helpful discussions. The support of the British Ministry of Defence is gratefully acknowledged.

REFERENCES

1. R.H. Clark, The Role of a Metal Deactivator Additive in improving the Thermal Stability of Aviation Kerosines, presented at the 3rd International Conference on the Stability and Handling of Liquid Fuels, London, September 1988, Paper #47, p. 283, Institute of Petroleum (1989).
2. J.S. Mills and D.R. Kendall, The Quantification and Improvement of the Thermal Stability of Aviation Fuels, presented at the 30th International Gas Turbine Conference, Houston, Tex., March 1985, ASME Paper 85-GT-33.
3. A.J. Eccles and J.C. Vickerman, The Characterisation of an Imaging Time-of-flight Secondary Ion Mass Spectrometry Instrument, J. Vac. Sci. Technol. A7(2), 234, (Mar/Apr 1989).
4. Manual of ASTM Standards, ASTM D3241, Vol 05.02 (1989).

Table 1
A summary of the sample preparation stages

Sample Group	Pre-treatment of specimen	MDA conc. (mg/l)	Heptane rinse after MDA exposure	Use of JFTOT	JFTOT test Temperature (°C)
(i) Aluminium foil (MDA No. 2)	Ultrasonic clean with trisol	0	✓	x	
		160,000	✓	x	
		160,000	x	x	
(ii) JFTOT test sections (MDA No. 1)	Ultrasonic clean with HPLC grade methanol. In addition duplicate set of uncleaned specimens.	0	✓	x	
		5.7	✓	x	
		64,800	✓	x	
		concentrate	x	x	
(iii) JFTOT test sections (MDA No. 1)	None	5.7	✓	✓	25
		57	✓	✓	25
		570	✓	✓	25
		57,000	✓	✓	25
		5.7	✓	✓	140
		5.7	✓	✓	260
		57	✓	✓	260

Table 2
Fragmentation of MDA in TOF SIMS:

ION MASS	FRAGMENT ION
107 ⁺	C ₆ H ₄ (OH)CH ₂ ⁺
120 ⁺	C ₆ H ₄ (OH)CNH ⁺
134 ⁺	C ₆ H ₄ (OH)CHNCH ₂ ⁺
148 ⁺	C ₆ H ₄ (OH)CHNCH(CH ₃) ⁺
162 ⁺	C ₆ H ₄ (OH)CHNCH(CH ₃) ⁺ CH ₂ ⁺
283 ⁺	(M + H) ⁺
118 ⁻	C ₆ H ₄ (CN)O ⁻
120 ⁻	C ₆ H ₄ (OH)CNH ⁻ OR C ₆ H ₄ (CHNH)O ⁻
281 ⁻	(M - H) ⁻

NOTES: (1) M = molecular species (mol. wt. = 282)
= C₆H₄(OH)CHNCH(CH₃)CH₂NCHC₆H₄(OH)

(2) ALSO DETECTED WERE: C_xH_y⁺, Ph⁺, PhCH₂⁺, C_n⁻, C_nH⁻, CN⁻, PhO⁻ ETC.

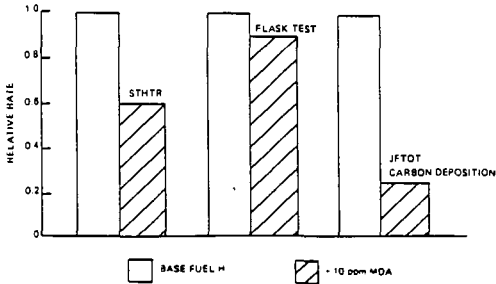


FIG. 1 - The influence of MDA on the behaviour of a sweetened fuel H. STHTR operated at 225°C condition, Flask at 160°C, JFTOT at 350°C to determine carbon deposit weight (Reference 1).

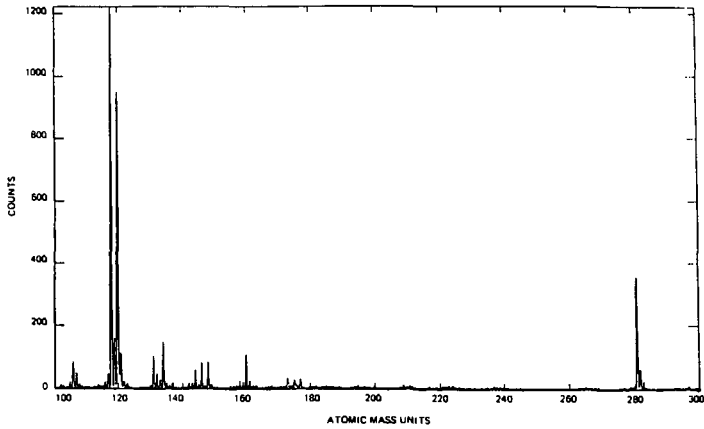
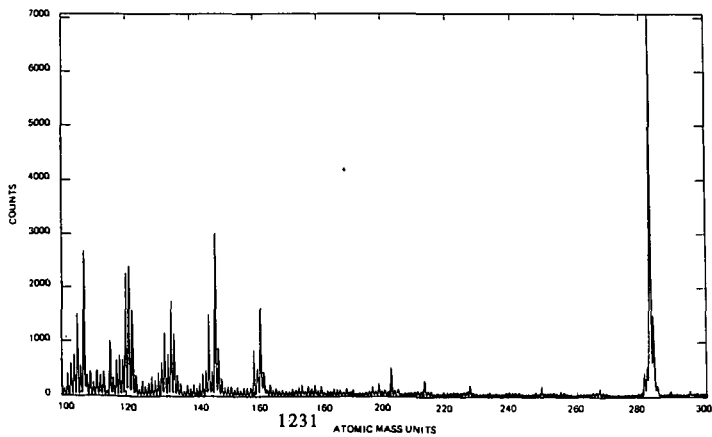


FIG. 2 - Negative ion TOF SIMS spectrum of MDA concentrate cast onto aluminium JFTOT tube.



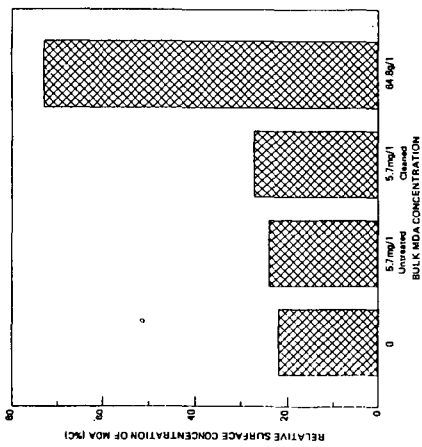


FIG. 4 - The influence of MDA bulk concentration on the resulting MDA surface concentration of JFTOT test specimens. Samples generated within a static experiment.

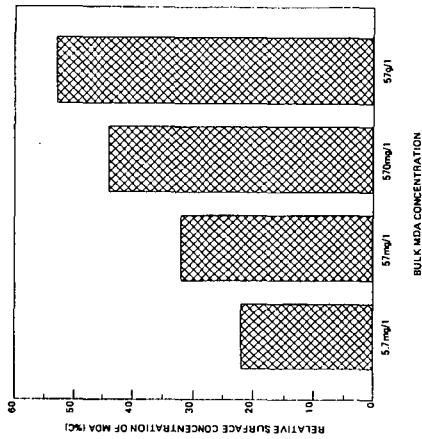


FIG. 5 - The influence of MDA bulk concentration on the resulting MDA surface concentration of JFTOT test specimens. Samples generated within a JFTOT rig at ambient temperature.

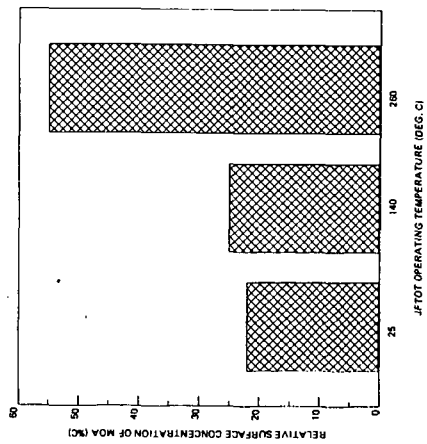


FIG. 6 - The influence of JFTOT operating temperature on the resulting MDA surface concentration of JFTOT test specimens (MDA bulk concentration 5.7 mg/l).

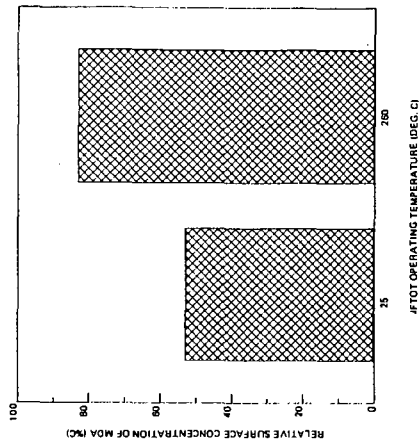


FIG. 7 - The influence of JFTOT operating temperature on the resulting MDA surface concentration of JFTOT test specimens (MDA bulk concentration 570 mg/l).

**CHARACTERISATION AND QUANTIFICATION OF DEPOSITS
FROM THERMALLY STRESSED AVIATION FUELS**

Clive Baker, Peter David, Robert Finney
Diane Hall, Ray Swatridge

BP Research Centre, Chertsey Road, Sunbury-on-Thames, Middx, TW16 7LN, UK

1. INTRODUCTION

Deposits generated during thermal stressing of jet fuels in the JFTOT (Jet Fuel Thermal Oxidation Tester) hold a great deal of potential information about the mechanism and chemistry of fuel degradation, providing a suitable technique can be found for "unlocking" the data. Previous work at the BP Research Centre at Sunbury-on-Thames (RCS) using Auger Electron Spectroscopy has shown that magnesium (present in the tube alloy) will segregate at the tube surface and inhibit carbon deposition (1). The aims of recent work are to investigate further the causes and mechanisms of deposition, both in terms of chemical species and physical parameters.

JFTOT tube deposits have been examined by Scanning Electron Microscopy/Energy Dispersive Analysis of X-rays (SEM/EDX). This non-destructive technique enables a "profile" of the relative abundance of different elements present in the deposit along the tube length to be drawn. Further chemical characterisation of deposits has been made using Laser Ionisation Mass Analysis (LIMA); again, analysis has been performed along the length and through the depth of the deposit, providing information on deposit profiles in relation to tube temperature. It is now possible to obtain reproducible and reliable information about deposition levels enabling the influence of different factors such as temperature, time and fuel composition to be studied.

Much effort has been devoted during the past decade to characterisation of JFTOT tube deposits with less attention being given to the formation of particulate material during thermal stressing of fuels. It is believed that these could have as equally deleterious effects in aircraft fuel systems as surface layer deposits. Specific fuels are known to produce sufficient particulate material during normal JFTOT tests to give a measurable pressure differential across the standard JFTOT 17 μm Dutch weave test filter. To study the formation of filterable deposits, an Alcor HLPS (Hot Liquid Process Simulator) has been modified at RCS to incorporate a 0.45 μm Millipore membrane downstream of the heater tube test section, as a direct replacement for the standard filter. Filterable particulate deposits are collected during tests and characterised in terms of total mass and chemical composition.

Use of LIMA and SEM/EDX to characterise deposits generated in the JFTOT and the modified HLPS apparatus is described in this paper, with particular reference to the influence of fuel composition and test operating conditions on tube deposition and filterable deposit formation.

2. APPLICATION OF SEM/EDX TO JFTOT TUBE DEPOSIT ANALYSIS

In SEM/EDX, bombardment of the deposit with a low energy probe (3.0kv) enables X-rays to be generated from the individual elements present at the point of analysis. This energy is sufficient to ensure that an aluminium signal from the tube itself is seen whilst maximising the surface sensitivity. Thus a ratio of the particular element under investigation to the aluminium can be given. As the thickness of the deposit varies, the response due to both carbon and aluminium will alter respectively. It is therefore not possible to give an absolute value to the carbon content, but by quoting it as a ratio to the aluminium, a comparative value is obtained. Repetitive analysis at points along the deposit length enables a profile of C/Al values with tube position to be plotted. Calibration of the peak areas, using

carbon films of known thickness would allow at least semi-quantitative measurement of deposit thickness. Owing to the varying response of the technique to different elements, it is not possible to establish relationships between different elements in one deposit, only to compare the abundance of any one element from deposit to deposit.

Typical profiles are given (Fig 1) with the profile obtained from an unused tube included for comparison. Uniformity of the deposit was checked by determining the profile on two sides of the tube. A small difference was observed, but this was not thought to be significant.

From the profile obtained from a typical JFTOT deposit, the carbon concentration is seen to be symmetrical about a point which occurs downstream of the maximum tube temperature (39mm). There is a substantial increase in the amount of deposition after the maximum tube temperature. Where TDR traces show "splitting" of peaks, SEM/EDX has shown the deposit to consist of a single gaussian distribution envelope mainly of carbon. This throws some doubt on the validity of the TDR for tubes with thicker deposits.

2.1 Relationship between deposition and tube assessment

The relationship between visual ratings, TDR values and SEM/EDX traces is shown (Figs 2,3). There is good agreement, although SEM/EDX can identify trace levels of degradation carbon on a tube that has been given a visual rating of 1 and a TDR rating of zero. It is clear that the sensitivity of any assessment technique must be taken into account when defining the breakpoint of fuel as the temperature at which "onset of deposition" occurs.

2.2 Prediction of fuel breakpoint

The deposit C/Al ratio at any point in the profile can be plotted against the corresponding tube temperature; two values for each temperature are obtained, one upstream and one downstream of the maximum tube temperature (Fig 4). For a given fuel run at different temperatures in JFTOT tests, the C/Al ratios at equivalent tube temperatures on the upstream side of the maximum tube temperature show good agreement (Fig 5). This suggests that the thickness of deposits generated during JFTOT tests may be constant at a specific tube temperature for a given fuel. Thus with knowledge of carbon thickness associated with a visual rating of 3, it may be possible to estimate the breakpoint temperature of a fuel from the SEM/EDX profile generated from a single JFTOT test at a temperature higher than the breakpoint. This procedure may find applications for research purposes.

2.3 Kinetics of deposition

Maximum C/Al ratios obtained for one fuel at a constant temperature are plotted against test duration in Fig 6. The extent to which the non-linear response of the SEM/EDX to deposits of varying thickness affects these results is not known. However, the extended "induction period" observed implies a genuine change in mechanism, with deposition perhaps being governed by either a catalytic reaction with the tube surface or by an adherence effect. Others have also noticed this so-called "induction period" before the onset of deposition (2). The significance of this "induction period" with respect to aircraft fuel system operation needs to be established.

2.4 Role of metals and MDA (Metal Deactivator Additive)

The presence of metals in fuel causes a reduction in thermal stability, although it is not known whether the metal plays an integral part in deposition or acts only in a catalytic capacity. Addition of MDA generally produces an apparent increase in thermal stability as perceived by the JFTOT. The mechanism for this "improvement" is not understood clearly and may be ascribed either to a bulk fuel reaction or to a "passivation" of the tube surface. In order to address some of these aspects, experiments were carried out using one fuel with differing levels of metals, MDA and metal/MDA; results are shown in Table 1.

It is shown (Table 1, Fig 7) that copper had a deleterious effect on the thermal stability of the fuel, with an increase in carbon deposition with increasing levels of copper. Interestingly, copper was observed in the deposit and was also seen to increase as fuel copper levels were increased (Fig 8). When MDA was added, the thermal stability was seen to improve over and above that of the base fuel. This time, however, there was no evidence for copper in the deposit, indicating that the metal chelate plays no part in deposition. This would imply that the free copper reacts with species in the fuel to cause deposition, but will preferentially bind to the MDA. It is apparent that the MDA performs its accepted role well in metal chelation, and also appears to have some other additional effect on JFTOT results as yet not fully understood. Tubes run with dodecane doped with copper showed that in the absence of a deposit no copper was detected on the tube surface.

Addition of iron to the fuel was seen to promote deposition to a much greater extent, but, in contrast to the copper, iron was not found to be present in the deposit. Although MDA was found to negate the effect of the iron, the additive was not as efficient as with the copper at improving JFTOT breakpoint.

Iron appears to play a catalytic role in deposit formation. Although chelation with MDA reduces its activity, it may be that some limited catalysis can still occur even in the chelated form or that the chelate is not thermodynamically stable at higher temperatures.

3. APPLICATION OF LIMA TO JFTOT TUBE DEPOSIT ANALYSIS

LIMA analysis of the deposits has shown variations in the chemical composition with respect to temperature and tube location. The proportion of aromatic to aliphatic hydrocarbons is seen to increase towards the maximum tube temperature and also nearer the tube surface in a deposit, where presumably a temperature gradient exists across the deposit. As such, it may be that chemical changes occur in the deposit after it has been laid down and that therefore characterisation of the deposit in this way may not be a fruitful exercise.

3.1 MDA studies

The presence of MDA on tube surfaces has been shown by LIMA. The negative ion spectrum generated from analysis of MDA on stainless steel or aluminium substrates shows characteristic peaks at 119 and 146 amu (atomic mass units) (Fig 9). These peaks have been observed in spectra from tubes which have been contacted with dodecane or fuel containing MDA, at ambient or at elevated temperatures (Fig 10). They have not been observed during analyses of new JFTOT tubes or deposits generated from fuels which had not been treated with MDA, when peaks characteristic of fuel degradation products only are observed.

Immersion of a new JFTOT tube in fuel containing MDA at ambient temperature results in a layer of MDA on the tube surface, identifiable by LIMA. Variation in contact time does not appear to alter the level of coating, although absolute levels of MDA were not quantifiable. These tests are confirmation of the affinity of MDA for virgin metal of the JFTOT tube surface. The "strength" of the MDA coating can be demonstrated by performing tests on tubes pre-coated with MDA by immersion in treated fuel; the MDA is not removed in subsequent JFTOT tests using untreated fuel. There is however, some evidence for carryover of MDA from previous JFTOT tests although the extent of carryover is insufficient to have a measurable influence on visual rating or TDR assessments.

The passivation role attributed to MDA in the JFTOT test is undoubtedly related to the affinity of the additive for the metal surface. LIMA provides the opportunity to study the phenomenon in detail.

4. FORMATION OF PARTICULATE MATERIAL DURING THERMAL STRESSING

Tests on the modified HLPS have shown that in addition to tube deposition, substantial filterable deposits are formed which are not normally detected in standard JFTOT tests, and at temperatures below the recognised breakpoint of the fuel. These increase exponentially with temperature (Fig 11).

The influence of fuel metal content was demonstrated by addition of copper and iron (as naphthenate) to the fuel, when there was a significant increase in the mass of deposit at a given temperature (Figs 12, 13). With copper, the level of tube and filterable deposits increased with fuel copper content and copper was observed to be inherent in the deposits in increasing amounts. In contrast, while iron had a detrimental effect, there appeared to be a limiting level of iron above which formation of filterable deposits was not increased. Also, iron was not present in the tube deposits, but was observed in the filter deposits. These data coupled with results from other JFTOT studies (Section 2.4) suggest that the deleterious effects of iron and copper are caused by different mechanisms. In particular, iron appears to behave as a catalyst and is not inherently involved in deposit formation on the tube, whereas copper appears to combine with fuel species to promote deposition, in addition to any catalytic role it may have.

Addition of excess MDA to the metal doped fuels restored the quality to that of the base fuel (Figs 12, 13) indicating that the MDA was effective in negating the effect of the metals. To what extent this was caused by passivation of the tube surface and hence reduced reactivity, or by a genuine bulk fuel improvement is at this stage unclear.

The rate of formation of filterable deposits is shown in Fig 14. Initially, there was a linear increase, but thereafter, the rate of formation was reduced. (The fuel flow rate is kept constant throughout the test by adjusting the variable speed pump to compensate for the increase in pressure differential across the test filter.) It is proposed that the rate of formation of filterable deposits is affected by two factors. As deposition occurs on the tube surface, (i) the surface reactivity of the tube is inhibited, leading to reduced overall fuel degradation, and (ii), the tube exhibits enhanced adhesion properties, such that bulk fuel degradation products are retained, leading to an increase in tube deposition and a decrease in filterable deposits. This is shown schematically (Fig 14) where the tube deposits have been calculated as the difference between linearly increasing filterable deposits and actual measured levels. The variation in tube deposits with time is in good agreement with SEM/EDX data generated from JFTOT deposits (Section 2.3). Also, the mass of tube deposits predicted is of the same order of magnitude as measured by others in carbon burn-off assessment of JFTOT tube deposits (3).

Particle size measurements performed using laser diffraction techniques (Fig 15) demonstrate large increases in the number of particulates after thermal stressing, with the majority in the sub-micron size range. The implications for aircraft fuel system operation need to be established.

5. CONCLUSIONS

SEM/EDX and LIMA have been used for reliable characterisation of JFTOT and HLPS tube deposits providing information about deposit formation in relation to operating parameters and fuel composition. Tentative mechanisms for the role of metals and MDA on thermal stability have been proposed.

Tests on a modified HLPS have shown that substantial filterable deposits are formed during thermal stressing of fuels which are not detected in standard JFTOT tests. These have been shown to occur at temperatures below the JFTOT breakpoint of the fuel and to vary with temperature and fuel composition. Models have been proposed to demonstrate the relationship between tube and filterable deposits. These initial investigations will form the basis for more detailed studies on jet fuel thermal stability.

6. REFERENCES

1. An AES Depth Profiling Study of the Deposits formed on Aluminium during Jet Fuel Thermal Oxidation Test.
Baker C, David P and Hazell L.
Surface and Interface Analysis Vol 9 507-513 (1986)
2. The Thermal Degradation of Aviation Fuels in Jet Engine Injector Feed-Arms Part 1 - Results from a Full-Scale Rig.
Kendall D R et al.
Tokyo International Gas Turbine Congress (1987)
3. The Influence of Polar Compounds on the Stability of Jet Fuel
Kendall D R et al.
Presented at 2nd International Conference on Long-Term Storage Stabilities of Liquid Fuels. San Antonio, Texas (1986)

7. ACKNOWLEDGEMENTS

The authors would like to thank Air BP and UK MOD(PE) for their sponsorship of this work.

TABLE 1

JFTOT DATA OBTAINED ON MEROX TREATED KEROSENE SHOWING THE EFFECTS OF METALS AND MDA ON TUBE RATING

FUEL			Temp °C	TDR			PRESSURE Δ p-mmHg	VISUAL RATING	MAXIMUM C/A1 RATIO
Cu (ppb)	Fe (ppb)	MDA (ppm)		Spun	Spot	Posn			
-	-	-	260	2.5	3.5	45	0.1	<2	0.08
83	-	-	260	14	15	44	0.2	4	0.74
166	-	-	260	16	17.5	31/49	0.3	4	1.36
83	-	5.70	305	5.5	8.5	44	>25	A	0.38
83	-	0.57	260	0	0	-	0.2	1	0.03
-	-	0.57	305	50	50	38	2.5	>4	2.50(9kv)
-	-	1.14	305	9	11	43	0.7	2A	ND
-	-	2.28	305	0	0	-	0.3	1	ND
-	78	-	260	44	45	38	0.4	1	ND
-	78	5.7	260	0	0	-	>25	4	10.1(5kv)
-	78	5.7	305	22	25	42	3.3	1	ND
-	-	-	305	22	25	42	>25	4P	0.64(5kv)

ND - Not Determined

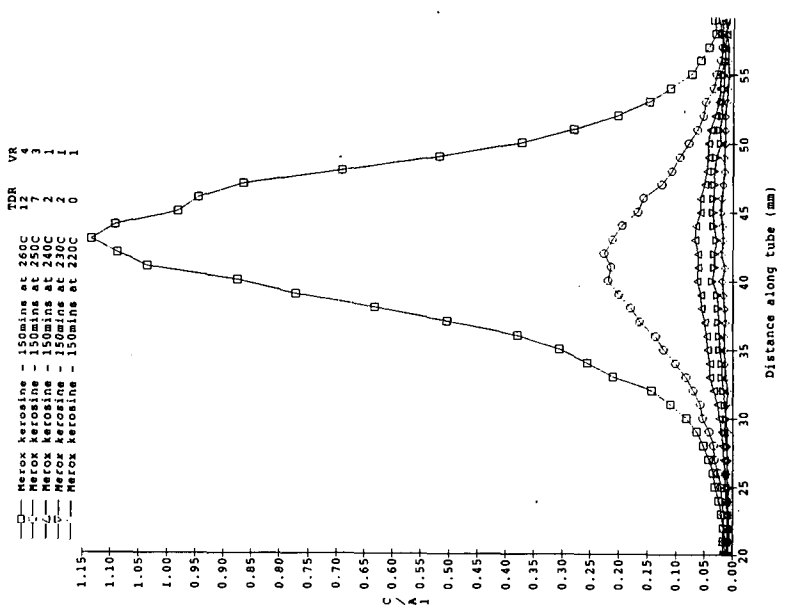


Figure 2. Carbon deposition on JFTOT tubes: Correlation with TDR and VR.

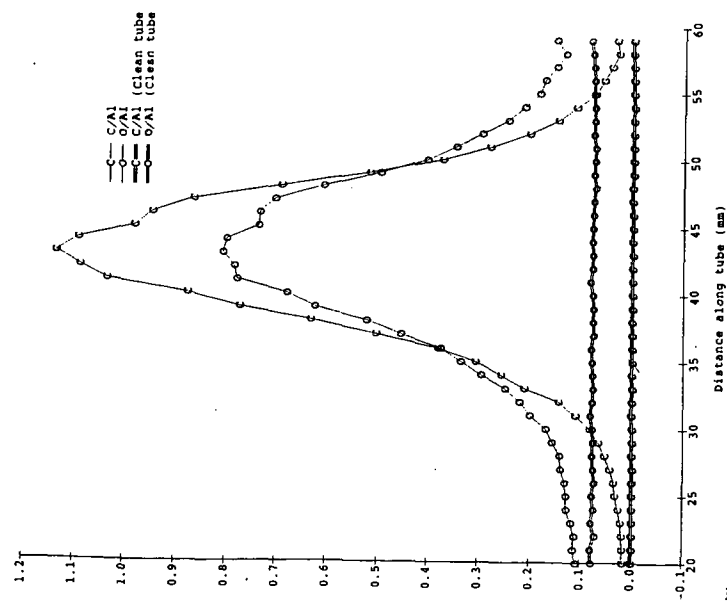


Figure 1. Typical SEM / EDX profile for JFTOT deposit with result from clean tube for comparison.

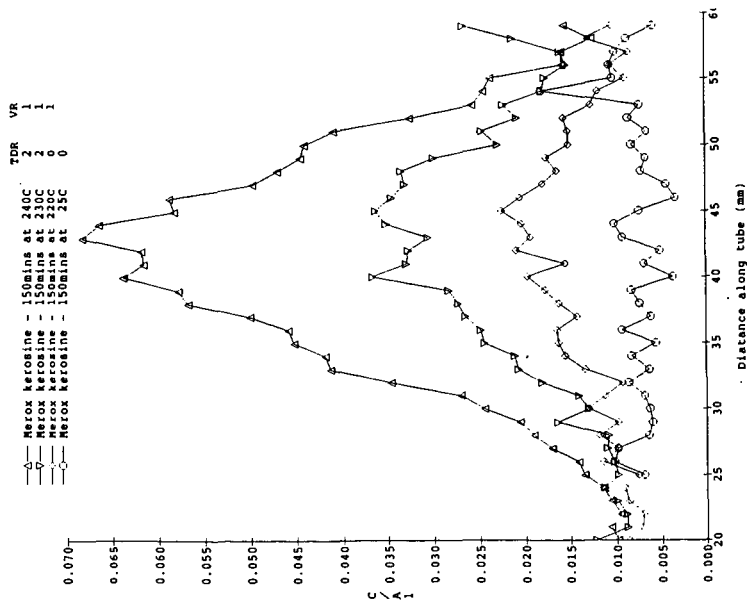


Figure 3. Carbon deposition on JFTOT tubes: Correlation with TDR and VR.

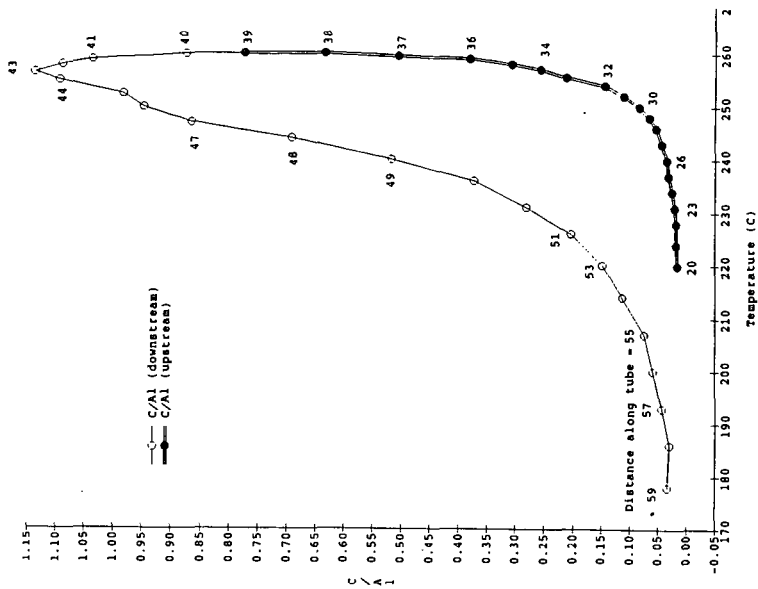


Figure 4. Temperature profile of carbon deposit Merox kerosene at 260°C.

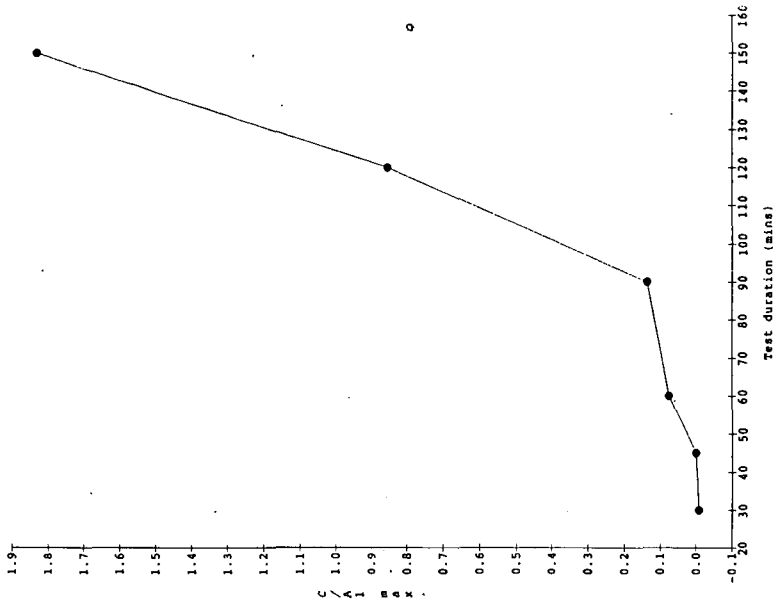


Figure 5. Relationship of upstream C / Al ratios to temperature of deposition (Merox kerosine).

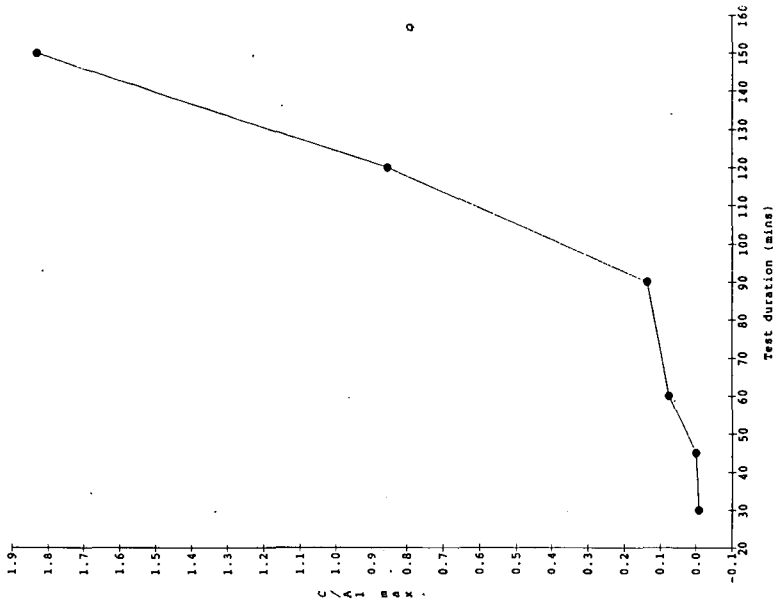


Figure 6. Maximum C / Al ratios against test duration -Merox kerosine at 275°C.

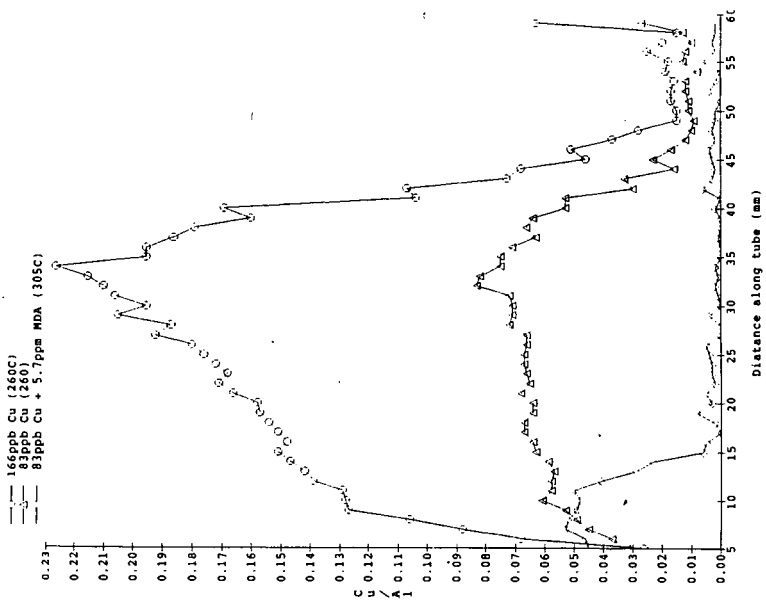


Figure 8. Comparison of Cu / Al ratios for Merox kerosene blends.

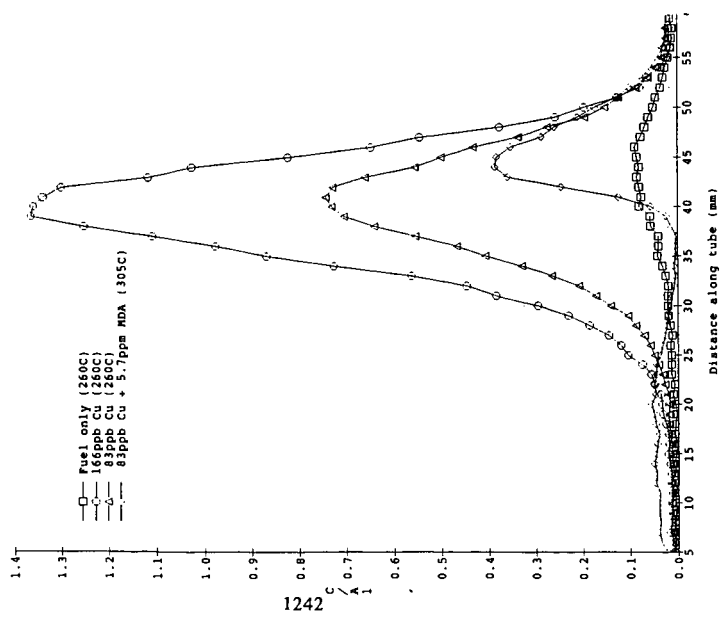
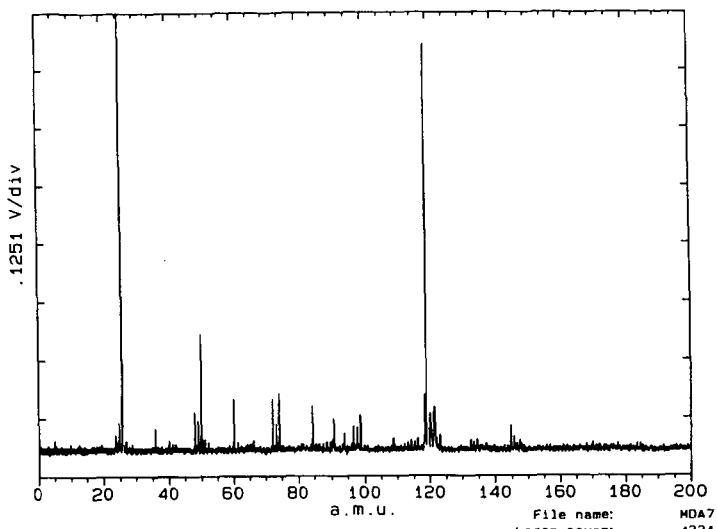


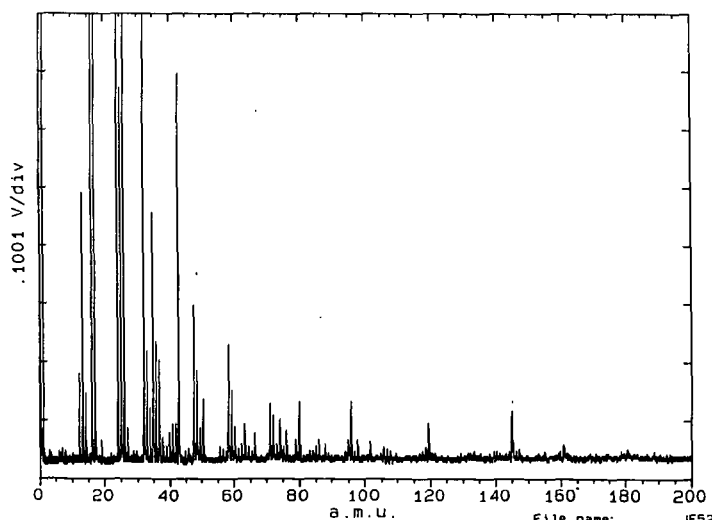
Figure 7. Comparison of C / Al ratios for Merox kerosene blends.



REFERENCE MDA SMEAR LIMA NEG. IONS

File name: MDA7
 Laser power: 4331
 8 Mar 1990

Figure 9. Metal deactivator additive.



MEROX JET A-1 + 2.3 mg.\ ml. MDA

File name: JF52
 Laser power: 3157
 13 Feb 1990

Figure 10. Merox Jet A-1/2.3 mg/litre MDA 150 minutes at 305°C.

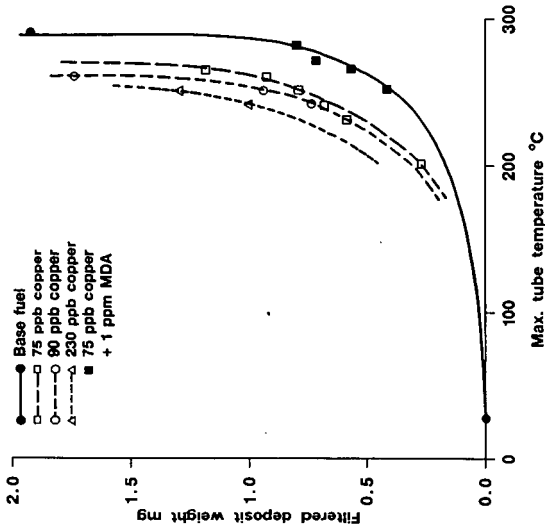


Figure 12. Modified HPLPS tests. Influence of soluble copper and MDA on filtered deposit levels.

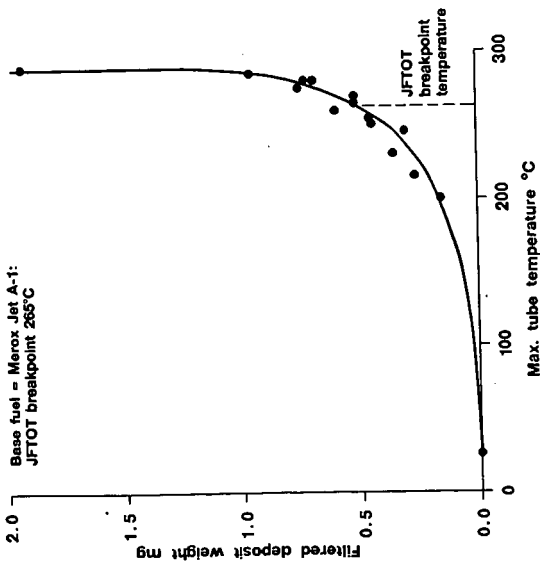


Figure 11. Modified HPLPS tests. Influence of temperature on filtered deposit levels.

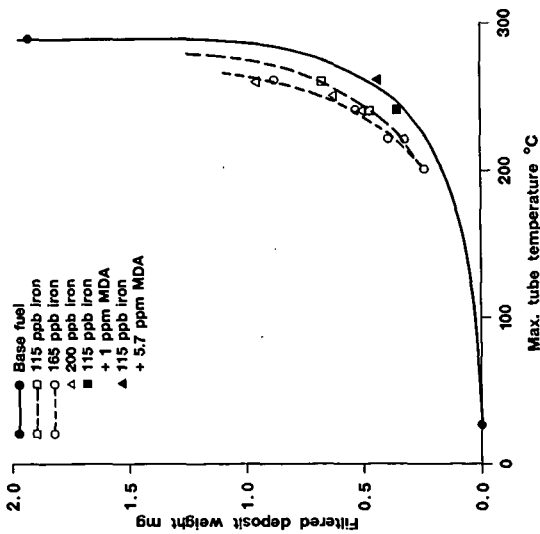


Figure 13. Modified HPLPS tests. Influence of soluble iron and MDA on filtered deposit levels.

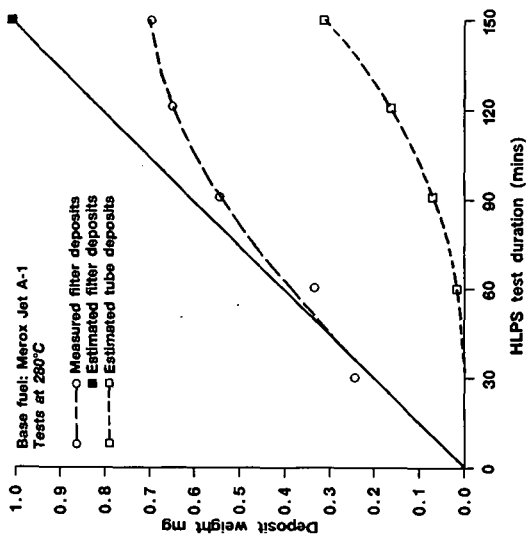


Figure 14. Modified HPLPS tests. Relationship between tube and filter deposits.

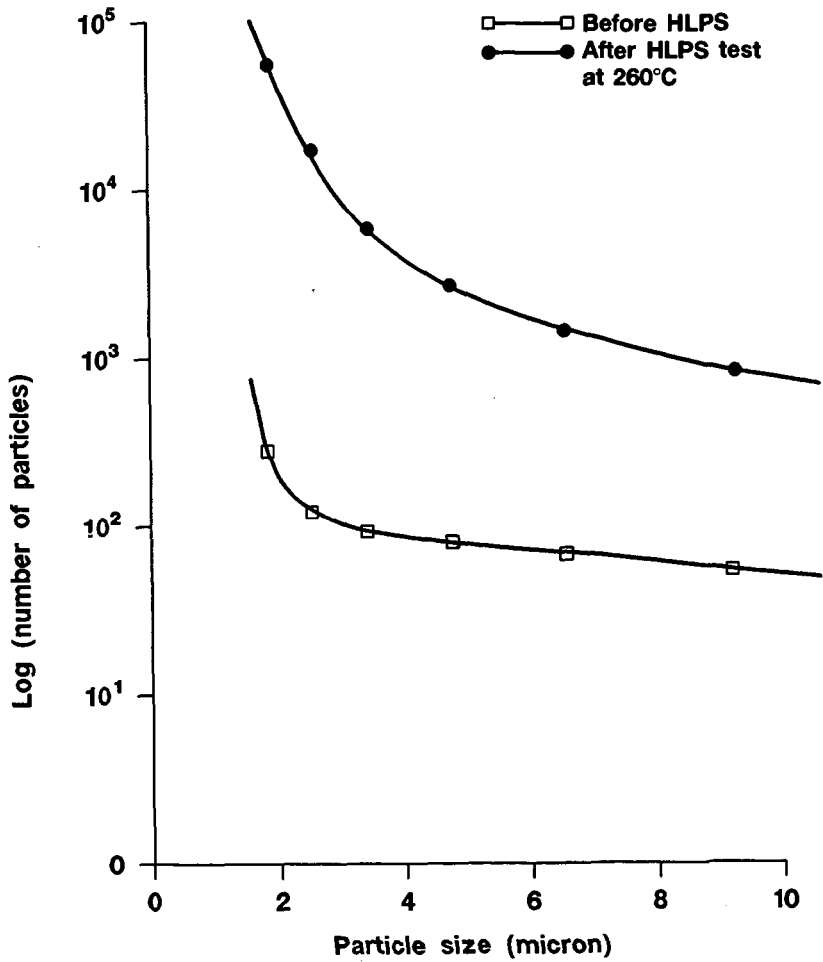


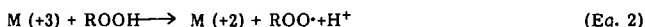
Figure 15. Influence of thermal stressing on particle size (number) distribution. Fuel: Merox Jet A-1 + 75 ppb copper.

The Catalytic Activity of Transition Metal Complexes in Oxidation Reactions Utilizing Hydroperoxides

J. J. Weers and C. E. Thomasson
Petrolite Corporation
Research & Development
369 Marshall Avenue
St. Louis, MO. 63119

INTRODUCTION

Hydroperoxides and oxy-based radicals have often been identified as residue and color formation precursors in hydrocarbon fuels during storage¹. Typically the peroxides are generated during the propagation step of an air autoxidation mechanism and their formation is continuous as long as initiators and oxygen are present for the reaction to occur. A study performed in jet fuel determined that the square root of peroxide concentration is proportional to fuel storage duration². The peroxide species, once formed in the fuel, have a wide range of possible reactions in which they can participate. For example, the reaction with olefins³, nitrogen compounds⁴ and sulfur compounds⁵ present in the hydrocarbon yields epoxides, amine oxides or nitro compounds, and disulfides, sulfoxides, sulfones, etc., respectively. The reactivity of the peroxide species toward the above derivatives can be modified in a number of ways. One of the more common methods is the introduction of a metal catalyst. The metal, when present even in catalytic amounts, may cause rapid degradation of the peroxides into oxy or peroxy radicals⁶.



The formation of esters, olefins or even alkyl halides is possible depending on the catalyst present, its oxidation state and the counter ion associated with it⁷. Vanadium complexes for example have been shown to be excellent catalysts for the oxidation of tertiary amines to amine oxides⁸. Iron and cobalt were found to be poor catalysts for the same reaction. Phenols have also been shown to be oxidatively unstable in fuels⁹ yielding an additional reagent for the peroxides to interact with in these systems.

A factor which has not been as widely studied is the influence of ligands on the catalytic activity of the metal¹⁰. When the metal is in a mid-distillate, there are a variety of nitrogen and sulfur, etc., species present to act as ligands to complex the metal. The complex may have a much different redox potential than the metal itself as well as having ligands blocking potential coordination sites for the peroxide and thereby preventing its decomposition from occurring.

A study was thus conducted to investigate the influence various ligands have on the oxidation of olefins and phenols by hydroperoxides in the presence of various metal catalysts. The reactions were investigated without added solvent as well as in a No. 2

diesel fuel to determine if the reactivity was similar or if other fuel components present in the hydrocarbon would alter the results. Reactions were conducted under conditions commonly used for mid-distillate fuel stability testing.

EXPERIMENTAL

In the cyclohexene oxidation studies, samples were prepared using 0.1 mole cyclohexene, 0.1 mole 90% tert-butyl hydroperoxide, 1×10^{-3} mole metal catalyst and 5×10^{-3} mole of the ligand where applicable. The samples were heated at the specified temperature for the desired time period and then analyzed by ^1H and ^{13}C NMR (Varian Gemini 300) and by GC mass spectroscopy (DuPont DP-1 mass spectrometer). Product yields were determined by capillary GC (HP-5710A). Fuel studies utilized the above amounts of dopants added to a 300 mL sample. All samples were stirred until homogeneous and then stored in an oven at 43°C until analyzed for residue content as specified in ASTM D-4625.

Experiments for phenol oxidation were performed using 0.1 mole p-cresol, 0.1 mole 90% tert-butyl hydroperoxide, 1×10^{-3} mole catalyst and 5×10^{-3} mole ligand. Product yield was determined by gas chromatography after conversion of the phenol mixture to their methyl ethers by treatment with Me_4NOH and MeI to increase their volatility. Fuel studies were run using 1000 ppm p-cresol and hydroperoxide, 1 ppm metal catalyst and 5 ppm ligand. The p-cresol, cyclohexene, tert-butyl hydroperoxide and the metal catalysts, cobalt acetate monohydrate ($\text{Co}(\text{OAc})_2$), copper acetate tetrahydrate ($\text{Cu}(\text{OAc})_2$), nickel acetate tetrahydrate ($\text{Ni}(\text{OAc})_2$), vanadium pentoxide, anhydrous ferric chloride and the ligands pyridine and tetrahydrothiophene (THT) were purchased from Aldrich Chemical Co. and used as received. The ligands chelant 1 and chelant 2 are proprietary commercial metal chelants used as mid-distillate fuel stability additives. Fuel utilized in the studies was a No. 2 diesel fuel produced at a Gulf Coast refinery containing a 80/20 mixture of straight run distillate and LCO.

RESULTS

Analysis of the cyclohexene oxidation products present after heating, indicated each contained a complex mixture of tert-butanol, acetone, cyclohexene, 2-cyclohexene-1-ol, 2-cyclohexene-1-one, tert-butoxy-2-cyclohexene and 2-cyclohexenyl-tert-butyl peroxide. The wide variety of products is indicative of the complexity of the reaction and of the many different reaction mechanisms available for the peroxides and radicals. The ether and peroxide products formed by oxidation of cyclohexene most likely resulted from attack of $\text{RO}\cdot$ and $\text{ROO}\cdot$ radicals on the olefin, followed by hydrogen elimination and double bond formation. Both oxy and peroxy radicals are present in the reaction mixtures from the metal catalyzed decomposition reactions illustrated in equations 1 and 2. The 2-cyclohexene-1-one is probably present as a thermal decomposition product of the 2-cyclohexenyl-tert-butyl peroxide. This peroxide is quite thermally stable and thus the decomposition is likely occurring in the injector of the gas chromatograph during analysis rather than in the experiment itself. The 2-cyclohexene-1-ol could be formed by several mechanisms. Attack of a hydroxyl radical, generated by thermal or radical induced decomposition of the hydroperoxide, is a possible mechanism. Hydrogen abstraction by a cyclohexenyl oxy radical generated by decomposition of the peroxide is also possible. It is not possible from these data to determine which mechanism is occurring under our reaction conditions.

The high yield of 2-cyclohexenyl-tert-butyl peroxide compared to the yield of the ether was surprising as both $\text{RO}\cdot$ and $\text{ROO}\cdot$ radicals should be present if the cycle shown in equations 1 and 2 was operative. The higher yield of the peroxide suggest a second

process is occurring in which the $RO\cdot$ radicals are converted to $ROO\cdot$ followed by reaction with cyclohexene. A likely mechanism for this reaction is the hydroperoxide oxidation of the oxy radical¹¹,



This reaction apparently is faster than the reaction of the $RO\cdot$ radical with cyclohexene.

In the absence of added ligand, a relative ranking of the activity of the catalyst in the order $V(V) \gg Co(II) > Fe(III) > Cu(II) > Ni(II)$ was obtained (Table 1). All of the ligands reduced the activity of the vanadium catalyst and increased the activity of nickel. Apparently the ligands present in the vanadium experiment compete for coordination sites on the metal, either as free ligand or as an oxidized species (amine oxide, sulfoxide, etc.), and thereby decrease the ability of the catalyst to complex the hydroperoxide and initiate oxidation¹². In the case of the nickel catalyst, the opposite effect is observed. The ligands can modify the catalyst's solubility, redox potential, etc., with a resulting increase in activity. The results with the other metals were mixed with some ligands promoting oxidation while others inhibited it. For copper, the oxidation of cyclohexene by $t\text{-BuOOH}$ has been studied in the absence of added ligand¹³. A copper naphthenate catalyst was used and the peroxide and ketone were the only cyclohexene based oxidation products detected. The alcohol and ether were not detected in their study, and indeed, were minor products in our study until pyridine or tetrahydrothiophene ligands were present. The ligands increased the total yield of the alcohol and ether as well as the overall yield of all cyclohexene oxidation products with copper as a catalyst. Both of the metal chelants (chelant 1 and chelant 2) decreased the amount of oxidation product obtained. These materials are used commercially as "metal deactivators" in fuels and thus the lower oxidation product yield would be expected. The total amount of material identified in the mixture containing chelant 1 was low (78%) indicating a lot of unidentified material was present. Pyridine and chelant 1 increased the activity of the iron and cobalt catalyst while tetrahydrothiophene and chelant 2 had the opposite effect. The nature of the ligand is thus important in determining if a metal catalyst is an inhibitor or a pro-oxidant.

The activity of the iron, copper and cobalt catalysts, with and without pyridine or tetrahydrothiophene ligands, in a real diesel fuel was also investigated. In this case sulfur, nitrogen etc., components of the fuel may also influence the oxidation reactions. On monitoring the samples, it was observed that very significant degradation of the samples had occurred after only 1.5 weeks storage at 43°C. The insoluble (filterable + adherent) residue values were thus obtained (Table 2) and compared to the results in Table 1. A high level of sedimentation was assumed to be indicative of a high level of oxidation occurring in the fuel. The results were surprising however, in that the sample doped with only the hydroperoxide was much more unstable than the untreated fuel, while the sample containing both hydroperoxide and cyclohexene was only slightly more unstable. This would suggest the peroxide reacts with the cyclohexene in the fuel to give soluble products, while in its absence, the hydroperoxide reacts with other fuel components to give insoluble products. Addition of the metals to these systems greatly increased the amount of residue obtained. Copper with the pyridine ligand gave particularly high values of residue. The tetrahydrothiophene ligand gave variable results, increasing sediment with iron but decreasing the level of residue with copper and cobalt.

Analysis of the phenolic components present in mid-distillate fuels has indicated a complex mixture of low molecular weight alkyl phenols are present and that these materials can have an influence on the fuels storage stability¹⁴. Coupling reactions to give biphenyldiols are postulated to be active mechanisms involved in the instability work. Metals are known catalyst for the reaction and thus their influence on the oxidative coupling a model compound, p-cresol under fuel stability test conditions was investigated. The results (Table 3) indicated all metals when mixed with p-cresol even in the absence of added hydroperoxide or ligand gave some coupled product. A relative ranking of the catalyst in the order $V(V) = Cu(II) > Fe(III) > Co(II)$ was obtained. In this case atmospheric oxygen in the sample is the only oxidant present. With the ligands present yields were also relatively low. When the experiment was repeated with added hydroperoxide as oxidant, the yield of coupled products increased dramatically. Copper clearly was the best catalyst for the autoxidation. Not only was the yield of the bis-phenol increased, but large amounts of trimer and even tetramer were measured (Table 4). Copper has been identified previously as an excellent catalyst for this reaction in agreement with our results¹⁵. The ligands were again influential on product yield but the results were variable. All ligands decreased the yield of oxidation products when used in combination with the copper catalyst. The sample containing pyridine was unusual in that the ligand decreased the yield obtained to that obtained in the absence of catalyst. Pyridine has been found to be a poor ligand in previous studies utilizing copper-amine catalyst to oxidize phenols and the studies indicate a strong dependence of the structure of the metal complex in these systems¹⁶. Pyridine was a pro-oxidant for the iron catalyst. Higher yields of trimer in particular being obtained when the ligand was present. The commercial metal chelants were good oxidation inhibitors for this metal, however only 78.9% of the material analyzed by the GC could be identified in the sample containing chelant 1. Compounds other than bisphenyldiols etc., were formed. This is not surprising as products resulting from C-O coupling are possible as well as from addition of the ROO· radicals to the phenol ring. The influence of the ligands on the activity of the cobalt catalyst was smaller, with pyridine again acting as an antioxidant and tetrahydrothiophene acting as a pro-oxidant. The percentage of the products identified with the sample containing chelant 1 was again low indicating additional unidentified products were present. Vanadium pentoxide alone was second only to copper in its ability to catalyze the oxidation. The tetrahydrothiophene and chelant 2 did not seem to influence its activity much while chelant 1 and pyridine again lowered the amount of oxidation occurring.

Many of the above observations were not found to correlate with samples of diesel fuel treated with the reagents and stressed at 149°C for 30 min (Table 5). Using residue pad ratings as an indicator of fuel degradation, it was clear pyridine ligand was not a catalyst deactivator as observed in the above reactions. With each of the metal catalyst evaluated, the amount of residue formed on stressing the fuel was higher in the presence of pyridine. With the exception of cobalt, the two chelant ligands were the only ones which did show some improvement in the amount of residue obtained. Apparently components present in the fuel also participate in the reactions occurring to generate the residue. The p-cresol and hydroperoxide by themselves did not influence the pad ratings.

CONCLUSIONS

The presence of ligands in a metal catalyzed oxidation of an olefin or phenol can have a large influence on product yield and distribution. The influence is, however, dependent on the metal and the species being oxidized. For example pyridine increased the yield of cyclohexene oxidation products with the copper catalyst while it decreased the yield observed with vanadium. In the phenol coupling experiment, the addition of

pyridine gave lower yields of products than did copper itself. Many of the results could also not be correlated with residue values obtained in the real fuel. Residue values did not agree well with the product yields obtained. Apparently other components of the fuel also react with the dopants altering the results.

REFERENCES

1. Taylor, W. F., Frankenfeld, J. W., Conference Proceedings, 2nd Int. Conference on Long Term Storage Stability of Liquid Fuels, 1986, 496-511.
2. Fodor, G. E., Naegeli, K. W., Kohl, D. B., Energy and Fuels, 1988, 2, 729-734.
3. Edwards, J. O., "Peroxide Reaction Mechanisms", Interscience Publishers, 1962, 77.
- 4a. De La Mare, H. E., J. Org. Chem., 1960, 25, 2114-2126.
- b. Capp, C. W., Hawkins, E. G. E., J. Chem. Soc. 1953, 4106-4109.
- c. Murry, R. W., Rajadhyaksha, S. N., Mohan, L., J. Org. Chem. 1989, 54, 5783-5788.
5. Mushrush, G. W., Hazlett, R. N., Hardy, D. R., Watkins, J. M., Conference Proceedings, 2nd Int. Conference on Long Term Storage of Liquid Fuels, 1986, 512-522.
6. Robertson, A., Waters, W. A., Trans. Faraday Soc., 1946, 42, 201.
7. Cardinate, G., Grimmelhuysen, J. C., Laan, J. A., Van Lier, F. P., Van der Steen, D., Ward, J. P., Tetrahedron, 1989, 45, 5971-5978.
8. Sheng, M. N., Zajacek, J. G., J. Org. Chem., 1968, 33, 588-590.
9. Hazlett, R. N., Power, A. J., Conference Proceedings, 2nd Int. Conference on Long Term Storage Stability of Liquid Fuels, 1986, 556-559.
10. Li, N. C., Tzou, J. R., Chang, H., Wang, S. M., Chin, J., J. Chem. Soc. 1987, 34, 91-98.
11. Bell, E. R., Raley, J. H., Rust, F. F., Seubold, F. H., Vaughan, W. E., Discussions Faraday Soc., 1951, 10, 242.
12. Carlin, R. L., J. Am. Chem. Soc., 1961, 83, 3773-3775.
13. Kharasch, M. S., Paulson, P., Nudenberg, W., J. Org. Chem. 1953, 18, 322-327.
14. White, C. M., Jones, L., Li, N. C., Fuel. 1983, 62, 1397-1403.
15. Kushioka, K., J. Org. Chem., 1984, 49, 4456-4459.
16. Hewitt, D. G., J. Chem. Soc., 1971, 2967-2973.

TABLE 1
Product Distribution in Cyclohexene Oxidations

Catalyst	% Cyclohexene Oxidation Product Yield after 24 hrs at 43°C ***					
	Alcohol	Ketone	Ether	Peroxide	Total	Total Identified
None	0.4	0.4	0	0.1	0.9	79.9
Cu(OAc) ₂	0.9	1.4	0	1.0	3.3	90.5
+ Chelant 1	0	1.6	0	0.9	2.5	78.0
+ Chelant 2	0	0.2	0	0.5	0.7	95.5
+ Pyridine	2.9	9.0	0.2	1.8	13.9	76.6
+ THT	1.3	2.0	0	1.1	4.4	89.3
FeCl ₃	1.7	1.6	0	0.8	4.1	91.5
+ Chelant 1	0.9	6.0	0	0.4	7.3	81.6
+ Chelant 2	0.7	2.4	0	0	3.1	84.8
+ Pyridine	1.8	5.0	0.3	0.5	7.6	87.7
+ THT	1.1	1.8	0	0	2.9	81.7
Co(OAc) ₂	2.5	2.5	0	0.3	5.3	95.8
+ Chelant 1	1.8	6.3	0	0.3	8.4	83.5
+ Chelant 2	0.8	2.6	0	0	3.4	87.3
+ Pyridine	1.6	5.7	0.1	0	7.4	85.0
+ THT	2.4	2.6	0	0	5.0	92.1
V ₂ O ₅	0	21.4	0	1.5	22.9	96.9
+ Chelant 1	2.0	5.1	0	0.8	7.9	78.9
+ Chelant 2	1.8	3.1	0	2.4	7.3	79.1
Pyridine	0.6	1.4	0	0	1.0	99.6
+ THT	1.1	8.4	0.3	0.8	10.6	95.2
Ni(OAc) ₂	0.4	0.4	0	0	0.8	99.3
+ Chelant 1	2.1	4.2	0	0.4	6.7	83.8
+ Chelant 2	0.7	3.1	0	0	3.8	79.7
+ Pyridine	0.4	0.5	0	0	0.9	98.7
+ THT	0.7	1.0	0	0	1.7	97.7

* Alcohol = 2-cyclohexene-1-ol; Ketone = 2-cyclohexene-1-one; Ether = t-butoxy-2-cyclohexene; Peroxide = cyclohexenyl-tert-butyl peroxide.

*** Sum of acetone, t-butanol, cyclohexene and alcohol, ketone, ether and peroxide cyclohexene derivatives yields.

TABLE 2
Fuels Stability Studies Utilizing Cyclohexene, Hydroperoxide,
Metal Catalyst and Various Ligands

Dopant	Insoluble Residue (mg/100 mL) *
None	0.3
Cyclohexene	0.3
t-BuOOH	1.7
Cyclohexene + t-BuOOH	0.5
+ FeCl ₃	6.1
+ FeCl ₃ + Pyridine	3.4
+ FeCl ₃ + THT	19.0
+ Cu(OAc) ₂	13.0
+ Cu(OAc) ₂ + Pyridine	32.0
+ Cu(OAc) ₂ + THT	9.3
+ Co(OAc) ₂	2.0
+ Co(OAc) ₂ + Pyridine	2.9
+ Co(OAc) ₂ + THT	1.9

* After 1.5 weeks at 43°C

TABLE 3
Influence of Hydroperoxide on *p*-Cresol Oxidation

Catalyst	% <i>p</i> -Cresol Oxidation Product Yield	
	Without <i>t</i> -BuOOH	With <i>t</i> -BuOOH
None	0	2.0
Cu(OAc) ₂	2.7	37.2
FeCl ₃	1.4	10.8
Co(OAc) ₂	0.3	8.6
V ₂ O ₅	2.8	12.8

* After 90 min storage at 149°C. Total of dimer, trimer and tetramer products.

TABLE 4
Product Distribution in *p*-Cresol Oxidation
by *tert*-Butyl Hydroperoxide

Catalyst	% Oxidation product Yield [*]				Total Identified ^{**}
	Dimer	Trimer	Tetramer	Total	
None	2.0	0	0	2.0	99.8
Cu(OAc) ₂	22.9	9.6	4.7	37.2	94.8
+ Chelant 1	8.2	2.2	2.5	12.9	91.4
+ Chelant 2	11.8	4.8	3.5	20.0	99.0
+ Pyridine	3.4	0	0	3.4	96.5
+ THT	6.5	1.9	0	8.4	95.1
FeCl ₃ [*]	10.4	0.4	0	10.8	97.5
+ Chelant 1	1.3	1.0	0	2.3	78.9
+ Chelant 2	5.1	0	0	5.1	95.0
+ Pyridine	12.6	3.1	0	15.7	96.6
+ THT	9.3	1.7	0	11.0	91.5
Co(OAc) ₂	4.2	4.4	0	8.6	90.4
+ Chelant 1	6.1	0.5	0.1	6.7	82.5
+ Chelant 2	7.6	0.9	0	8.5	95.1
+ Pyridine	4.0	0.4	0	4.4	93.0
+ THT	6.8	4.8	0	11.6	69.6
V ₂ O ₅	10.7	2.1	0	12.8	88.6
+ Chelant 1	6.5	0.9	0	7.4	80.0
+ Chelant 2	11.1	2.0	0	13.1	91.4
+ Pyridine	6.0	0.6	0	6.6	93.0
+ THT	10.9	1.4	0	12.3	87.1

* After 90 min at 149°C.

** Sum of *t*-butanol, *p*-cresol, dimer, trimer and tetramer yields.

TABLE 5

<u>Dopant</u>	<u>Residue Pad Rating[*]</u> <u>Without t-BuOOH</u>	<u>Residue Pad Rating</u> <u>With t-BuOOH</u>
None	4	4
p-Cresol	4	4
+ Cu(OAc) ₂	5	20
+ Chelant 1	4	3
+ Chelant 2	4	3
+ Pyridine	5	20
+ THT	5	17
+ FeCl ₃	14	11
+ Chelant 1	7	3
+ Chelant 2	4	4
+ Pyridine	15	18
+ THT	17	15
+ Co(OAc) ₂	4	3
+ Chelant 1	5	3
+ Chelant 2	3	7
+ Pyridine	4	8
+ THT	3	4
+ V ₂ O ₅	4	4
+ Chelant 1	3	3
+ Chelant 2	3	4
+ Pyridine	4	7
+ THT	3	4

^{*} After 90 min storage at 149°C. Pad rating scale; 1 = clean pad to 20 = heavy residue.

ANALYSIS OF PHENOLIC ANTIOXIDANTS IN JP-5 AVIATION FUELS

Mei-Hsia Alice Huang and Lynda M. Turner
Fluid Sciences Division
Naval Air Propulsion Center, Trenton, NJ 08628

ABSTRACT

The Navy requires the addition of antioxidants to prevent the degradation of JP-5 aviation fuel in storage. Monitoring phenolic compounds commonly used for this purpose is essential to determine the quality of prepositioned aviation fuel supplies. The large number of chemical constituents in JP-5 fuels provides complex chromatograms which, for most approaches, hinder the detection of antioxidants. In this study, however, liquid chromatography with electrochemical detection and a judicious choice of the mobile phase provided good resolution of many antioxidants. Several phenolic antioxidants are evaluated in fuels originating from different crude sources and processing techniques.

INTRODUCTION

The jet fuel supply and distribution system is very complex and unpredictable. The refineries supplying the U.S. Navy with JP-5 fuel change annually depending upon cost, logistics and the political situation in the oil industry. JP-5 properties within a given geographic area, therefore, are becoming more variable.¹

Trends indicate future crude sources will have higher unsaturated hydrocarbon, heteroatom and metallic contents. All of these properties require increased hydroprocessing to produce an acceptable JP-5 product. Jet fuel is changing from a product made by simple distillation to a variable blend of streams from different processing units.²

The Navy is becoming increasingly concerned with the properties of the JP-5 now available for consumption and is relying less on property/performance relationships which existed ten years ago. The Naval Air Propulsion Center (NAPC) has initiated a Fuels Diagnostics Program to facilitate the measurement of JP-5 properties and interpretation of their relationship with aircraft engine performance. An integral part of this program is to collect, modify and/or develop analytical methods which will allow us to make evaluations.

The stability of our current JP-5 supplies must be periodically monitored. This is especially true for fuels placed in strategic storage locations for extended periods. Due to the shortage of pristine, straight distillate fuels, storing fuels with known less-than-desirable stability characteristics is becoming more of a reality. Presently, the Navy does not have regulations to prohibit the storage of fuels processed by techniques other than straight distillation. The Navy must rely heavily upon the addition of antioxidants to

prevent fuel degradation. The additives currently accepted in Specification MIL-T-5624 are phenolic in structure and serve to inhibit the degradation of fuel components by breaking the reaction chain of the peroxy radical which occurs during the hydrocarbon auto-oxidation process.³

A study conducted⁴ had shown that peroxidation will occur only after the additive has been depleted. Therefore, tracking an additive's depletion pattern would give forewarning of fuel degradation. Having this information prior to degradation could assist the Navy in making decisions regarding when to rotate JP-5 stock. This could reduce the number of potential JP-5 fuels which may have to be downgraded to Diesel Fuel Marine (DFM) due to high peroxide content, thus not meeting military aviation fuel stability requirements.

Gas chromatographic and liquid chromatographic techniques for determining commercial phenolic antioxidants in aviation turbine fuels have been reported.⁵⁻⁸ Unfortunately, only a few antioxidants were investigated in these papers. Pearson⁵ presented an internal standard technique using gas chromatography-mass selective detection for two antioxidants. Cunningham and Hillman⁶ reported a liquid chromatographic method with ultraviolet detection that can be applied to measure several hindered phenolic antioxidants. Also in this paper, an extractive procedure was developed to remove part of the "main fuel peak" from the chromatogram. Hayes and Hillman⁷ used liquid chromatography with electrochemical detection (LCEC) for determining a single antioxidant in turbine fuel. A modified LCEC procedure to determine the retention time of several antioxidants was presented by Vogh.⁸ However, the results were obtained with severely hydroprocessed neat (additive-free) jet fuels. Further modifications to this LCEC method were carried out in our study at NAPC to measure additional commercial phenolic antioxidants in actual refinery-produced JP-5 fuels.

EXPERIMENTAL SECTION

The isocratic liquid chromatographic system consisted of a solvent delivery pump (SSI Model 222B Single-Piston) with the flow rate set at 0.5 ml/min., a pulse damper (SSI Model LP-21 Lo-Pulse Damper), a Rheodyne 7176 injector with 20 microliter sample loop, a Rheodyne 73XX column inlet filter, and a 4.6 mm I.D x 25 cm stainless steel Du Pont Zorbax C₈ reversed phase column of 5 micron particle size.

The detector was a flow-by type electrochemical (EC) detector (EG&G Princeton Applied Research Model 400). The EC detector contained a glassy carbon working electrode and a reference electrode. The reference cell was filled with a solution containing 3 M sodium chloride and saturated silver chloride. The EC detector was operated in the DC mode at 1000 mV, a current of 100 nA, a 1.0 second time constant, and a cathodic output. A Perkin-Elmer LCI-100 integrator was used for peak area measurements.

The mobile phase consisted of a mixture of 30% of 0.02 M potassium acetate buffer, 60% of 2-propanol, and 10% methanol. This solution was vacuum filtered through Millipore HVHP 0.45 micron filter paper and degassed for at least ten minutes (sonicated with vacuum).

The response factor and the retention time for each antioxidant in JP-5 fuel samples varied slightly from day to day. This was probably due to slight variances of conditions of the analytical instrumentation and the composition of the mobile phase. Therefore, it was necessary to run a standard solution every day for calibration prior to the analysis of each fuel sample. If more analyses needed to be run the following day, it was essential to pump the mobile phase continuously overnight at a low flow rate. If this was not done, the system might become clogged and damaged by the deposits that could be formed by the buffer solution in the mobile phase. If the instrument was going to be turned off for long period, distilled water with 10% methanol had to be pumped through the system for few hours, followed by acetone for at least half an hour prior to turning off the pump.

RESULTS AND DISCUSSION

Hindered phenolic type antioxidants are typically added into JP-5 fuel at a concentration of 17 to 24 ppm during the refining process. At this level, analytical methods with commonly used detectors do not provide sufficient sensitivity for identifying and quantifying the antioxidants. An electrochemical (EC) detector was chosen in this study due to its selectivity and sensitivity for phenolic compounds. With EC detection, compounds that contain either electro-oxidizable or electro-reducible organic functional groups will be detected. Thus, many hydrocarbon fuel components can be conveniently eliminated from detection making it easier to isolate antioxidant peaks.

Based on initial testing, it was determined that improvements could be made to the mobile phases that had been used and reported in other papers.^{7,9} A variety of solvents and combinations of solvents were evaluated. The mobile phase that was found to be most effective in this study (see Experimental Section) provided much improved resolution of many antioxidants and minimized the miscibility problem between JP-5 fuel and the mobile phase.

Seven antioxidants that are commonly added to JP-5 aviation fuels were studied in this work. The chemical compositions of these antioxidants are listed in Table 1. Most antioxidants that are added to JP-5 fuels at the refinery are phenolic mixtures. Of the antioxidant structures that are or had been used in the military specification, only three antioxidants (AO-A, AO-B, and AO-E) are single component additives.

In the preliminary phase of this study, antioxidants were added at the 17 to 25 ppm level into a "clean" fuel to prepare standards. A hydrocracked JP-5 type additive-free fuel (Fuel X) was used as the "clean" fuel. It was selected

because the high intensity region in its chromatogram (Figure 1) is much narrower than a typical JP-5 fuel (Figure 2, Fuel #1) due to differences in refinery processing (e.g. hydrocracking vs straight run). The antioxidants in the prepared standards were then characterized by their chromatogram retention time (Figures 3 and 4). This "preliminary" information for each antioxidant was then applied to the analyses of "actual" JP-5 fuel samples.

A number of actual JP-5 fuels originating from different crude sources and processing techniques were evaluated. Examples of their typical chromatograms are shown in Figure 5 (Fuel #2) and Figure 6 (Fuel #3). Unfortunately, for most of these fuels, the "main fuel peak" that elutes during the first fifteen minutes retention time completely masks the peaks of a number of the antioxidants in this study. Antioxidants AO-B, AO-C, AO-D, the minor peak for antioxidant AO-F, and the minor peaks for antioxidant AO-G are completely blocked by this "main fuel peak". It is impossible to positively identify antioxidants AO-B, AO-C and AO-D in JP-5 fuel samples unless the "main fuel peak" can be eliminated partially or completely from the chromatogram.

The major component of antioxidant AO-F has the same chemical composition as antioxidant AO-E. Therefore, they will be detected with the same retention time. Thus, when this peak is detected in "real" JP-5 with the large "main fuel peak", it is not known if the minor peak for antioxidant AO-F is being masked. In this case, it is impossible to determine whether antioxidant AO-E or AO-F is present in the JP-5 fuel sample.

Regardless of the difficulty in identifying some antioxidants as mentioned above, antioxidant AO-E (or the major component of antioxidant AO-F), a component of antioxidant AO-G, and antioxidant AO-A in JP-5 fuel samples still can be detected by HPLC analysis. Peak retention times for antioxidant AO-E and antioxidant AO-G are very close to each other (Figure 7, Fuel #4). However, these two antioxidants will never be added simultaneously into JP-5 fuel by the manufacturer. Therefore, the antioxidant which is actually present in the fuel can be identified by spiking one of these antioxidants into the fuel.

Not all fuels contain the large "main fuel peak" in their chromatogram. The intensity of the "main fuel peak" in Figure 7 is much narrower than the one for most typical JP-5 fuel samples as shown in Figure 2. This difference is most likely due to the fact that JP-5 Fuel #4 was produced by different refinery processing. The antioxidant peaks in this chromatogram did not originate from the fuel sample. Antioxidants AO-A, AO-E, and AO-G were added into the fuel before running the chromatogram.

Quantitative analysis of "actual" JP-fuels involved several steps. A chromatogram was run on the as-received JP-5 fuel for a "preliminary" identification of antioxidant peaks. Next, a standard was prepared from a "blank" fuel. Because "actual" JP-5 fuels vary in chemical composition which affects the peak area measurement in the analysis, it is necessary to prepare

a standard for each fuel sample. A "blank" fuel was obtained by filtering the JP-5 fuel through either a silica gel column or an Alumina N Sep-Pak cartridge. This step removed the antioxidant from the fuel and their peaks from the chromatogram. An antioxidant at a concentration of 10 to 25 ppm was added into a "blank" fuel to prepare a standard. The prepared standard was then analyzed to calculate the response factor for each corresponding antioxidant. With the response factor for each antioxidant and the fuel chromatogram that was obtained in the first step, the amount of antioxidant in the JP-5 fuel sample was determined by the external standard technique.

For most fuel samples, there was only a very small peak shown at the chromatogram retention time that corresponds to antioxidant AO-A (Figure 2). It is very difficult to accurately measure such a low concentration directly. However, in this case, the amount of antioxidant AO-A in JP-5 fuels could be more accurately determined by an addition technique than with an external standard technique. The addition method was conducted as follows: A known amount of antioxidant AO-A was added into a "blank" fuel to calculate its response factor. The "blank" fuel was prepared by the same filtration technique described earlier. After spiking a known amount of antioxidant AO-A into an actual JP-5 fuel sample (Figure 8), the total concentration of antioxidant AO-A in the spiked fuel sample was determined. The difference between this measured total amount of antioxidant AO-A and the known amount that was added into the fuel sample was the original concentration of antioxidant AO-A in the JP-5 fuel sample.

The effects of interferences occurring at the location of an antioxidant peak may also be minimized by using the addition technique described in the preceding paragraph. When Fuel #1 was filtered through an Alumina N Sep-Pak cartridge, a small shoulder remained at the prior location of the antioxidant AO-A peak (Figure 9). This demonstrates that care must be taken to account for interferences in quantitative analyses. This process effectively subtracts out baseline interferences since the response factor is determined on a "blank" fuel containing interferences.

CONCLUSIONS

A number of JP-5 aviation fuel samples were examined by liquid chromatography with electrochemical detection. A mobile phase was found which provided good resolution. All antioxidant peak locations were identified and quantitative analysis demonstrated at use levels (17-24 ppm). A detection limit of about 1 ppm was found for all antioxidants. However, many JP-5 fuels have a "main fuel peak" which masks some of the antioxidant peaks. Thus, a complete qualitative/quantitative analysis of actual JP-5 fuel samples was greatly dependent on the location of the antioxidant peaks with respect to the "main fuel peak". A technique for eliminating the "main fuel peak" (partially or completely) from the chromatogram needs to be developed to analyze the antioxidant peaks which are located in that region and will be the objective of subsequent work.

ACKNOWLEDGEMENT

The authors wish to thank Dr. M. N. Sundberg for helpful discussions on this project. Also, the authors would like to express their thanks to Dr. E. Florio for technological assistance.

REFERENCES

1. The Characteristics of Future Fuels Hadallar, O.J., Momentary, A.M., Boeing Commercial Airplanes, August 1984
2. IBID
3. Auto-oxidation and Antioxidants of Petroleum Nixon, Alan C., Interscience Publishers, Shell Development Company, Emeryville, CA
4. Sutterfield, F.D. et al. The Third International Conference on Stability and Handling of Liquid Fuels Conference Proceeding; vol. 1 pg. 321; 13-16 September 1988.
5. Pearson, C.D., J. Chromatogr, 1988, V.449, pp. 440-447
6. Bartl, P., Schaaf, H. Presentius Z. Anal. Chem., 1982, V.310, pp. 250
7. Cunningham, A.F., Hillman, D.E. J. Chromatogr, 1978, V.148, pp. 528-531
8. Hayes, G.E., Hillman, D.E. J. Chromatogr, 1985, V.322, pp. 376-379
9. Vogh, J.W., Unpublished report, National Institute for Petroleum and Energy Research

TABLE I
Antioxidants Commonly Used in JP-5 Aviation Fuels

<u>Antioxidant</u>	<u>Chemical Composition</u>
AO-A	2,6-di- <u>tert</u> -butyl-4-methylphenol
AO-B	6- <u>tert</u> -butyl-2,4-di-methylphenol
AO-C	72% min 6- <u>tert</u> -butyl-2,4-dimethyl-phenol 28% max <u>tert</u> -butyl-methylphenols and <u>tert</u> -butyl- dimethyl-phenols
AO-D	60% min 2,4-di- <u>tert</u> -butylphenol 40% max mixture of <u>tert</u> -butylphenols
AO-E	2,6-di- <u>tert</u> -butylphenol
AO-F	75% min 2,6-di- <u>tert</u> -butylphenol 25% max <u>tert</u> -butylphenols and tri- <u>tert</u> -butylphenols
AO-G	55% min butylated ethyl phenols 45% max butylated methyl and dimethyl-phenols

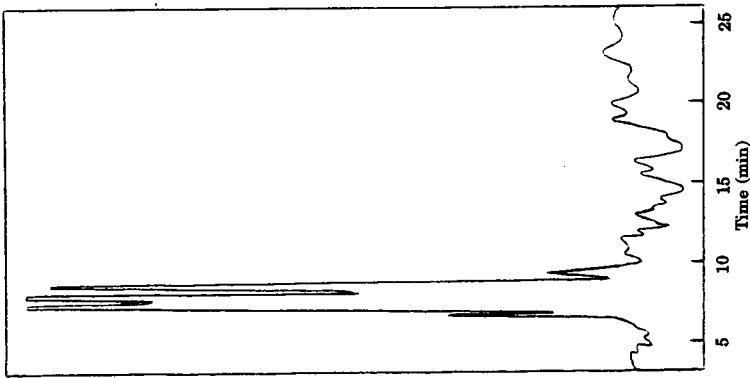


FIGURE 1: Chromatogram of "Clean" Fuel X
(with no antioxidants)

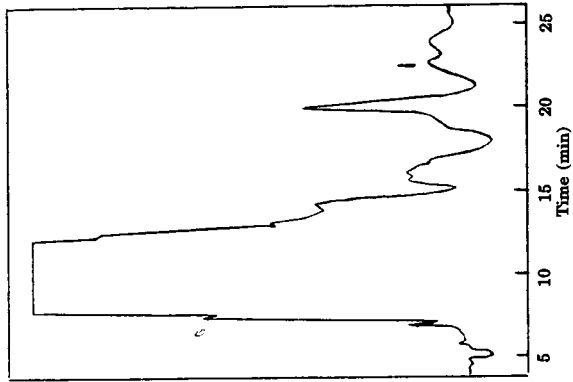


FIGURE 2: Chromatogram of "Typical" JP-5
Fuel #1 containing AO-A (1)

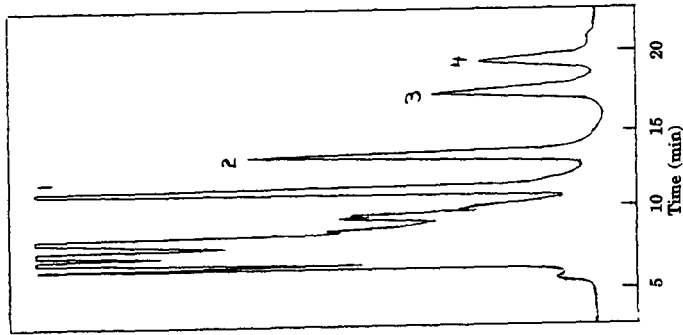


FIGURE 3: Chromatogram of "Clean" Fuel X containing AO-A (4), AO-B (1), AO-C (1), AO-D (2), AO-E (3) and AO-F (3)

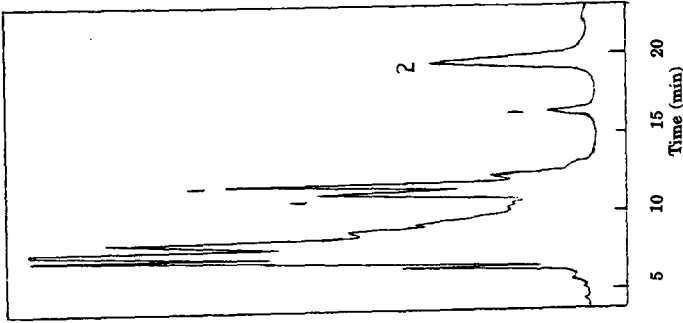


FIGURE 4: Chromatogram of "Clean" Fuel X containing AO-A (2) and AO-G (1)

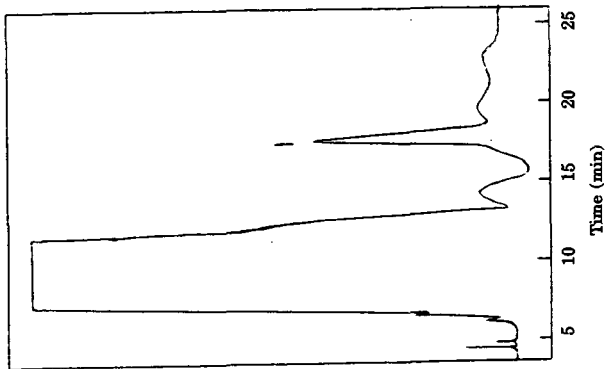


FIGURE 6: Chromatogram of JP-5 Fuel #3 containing AO-E (1) or AO-F (1)

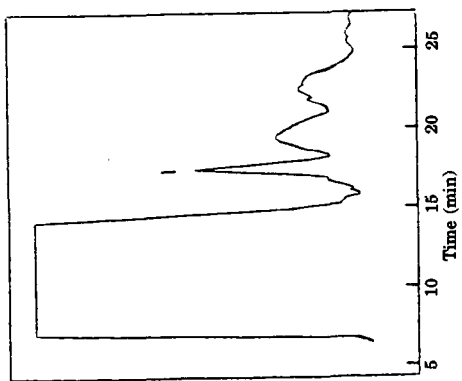


FIGURE 5: Chromatogram of JP-5 Fuel #2 containing AO-E (1) or AO-F (1)

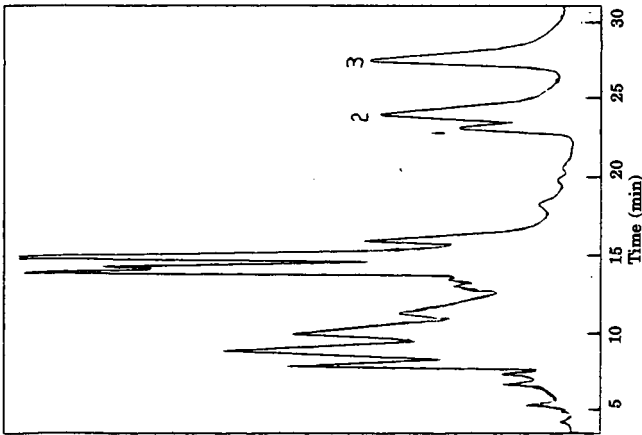


FIGURE 7: Chromatogram of JP-5 Fuel #4 containing AO-A (3), AO-E (2), and AO-G (1)

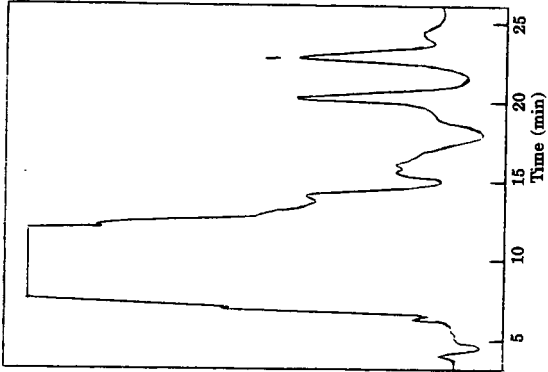


FIGURE 8: Chromatogram of JP-5 Fuel #1 spiked with AO-A (1)

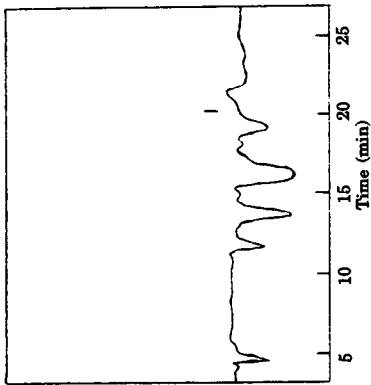


FIGURE 9: Chromatogram of JP-6 Fuel¹ filtered through an Alumina N Sep-Pak cartridge showing interferent (1)

PEROXIDE FORMATION IN JET FUELS

George E. Fodor* and David W. Naegeli
Belvoir Fuels and Lubricants Research Facility, Southwest Research
Institute, 6220 Culebra Road, San Antonio, Texas 78228

ABSTRACT

This paper reports recent results from an ongoing study of the kinetics of peroxide formation and the development of a method to measure potential peroxides in jet fuels. In the earlier work, rates of peroxide formation in six jet fuels were measured over a temperature range of 43 to 120 °C with oxygen partial pressures ranging from 10 to 1140 kPa. Global rate constants for the peroxide formation were based on a kinetic model of the autoxidation process, which showed that the peroxide concentration increased as the square of the stress duration. The rate of peroxide formation was strongly dependent on temperature, but independent of the partial pressure of oxygen. Recently, rates of peroxide formation have been measured in four more jet fuels at temperatures of 80, 100 and 120 °C with an oxygen partial pressure of 240 kPa. Global Arrhenius rate constants for peroxide formation were determined for the induction and post-induction periods in the new fuels. These results were found to be in good agreement with the earlier work, which encouraged the development of a test method to predict rates of peroxide formation at ambient conditions from rate measurements at elevated temperatures.

INTRODUCTION

The need for a method of predicting the potential formation of peroxides in jet fuels arose from fuel pump failures in jet aircraft. Shertzler (1), Hazlett, et al. (2), and Love, et al. (3) found that peroxides cause significant deterioration of neoprene, nitrile rubber, and Buna-N diaphragms and O-rings used in aircraft engine fuel pumps.

To avoid future problems, a program was initiated to study the kinetics of peroxide formation and ultimately to develop a timely method of predicting the potential peroxide content of jet fuels.(4-7) Several test methods have been developed to determine the oxidative stability of fuels, e.g., ASTM D 2274; they are carried out at elevated temperatures to reduce the test duration to an acceptable level. An accelerated high-temperature test is also desired for the timely determination of potential peroxide formation in jet fuels.

It is well-known that peroxides form in fuels by an oxidation process that is slow at room temperature, but relatively fast at temperatures ranging from 80 to 120 °C.(7-9) Since the objective was to provide a basis for a practical test method, not exceeding about 48 hours, the foremost goal was to determine if the mechanism of peroxide formation at elevated temperatures was the same as that at ambient temperature. If the mechanism is unchanged over a limited temperature range (e.g., 0 to 150 °C), it is possible to predict ambient temperature behavior from a global Arrhenius rate expression that can be determined by making two or more rate measurements at higher temperatures.

Recent results have shown that the reaction mechanism responsible for peroxide formation is the same from ambient temperature conditions to at least 120 °C.(7) In that work, rates of peroxide formation in six jet fuels were measured over a temperature range of 43 to 120 °C with oxygen partial pressures ranging from 10 to 1140 kPa. Experiments in the 80 to 120 °C range were performed in a pure oxygen atmosphere in a stirred pressure reactor. Long-term experiments at 65 and 43 °C were accomplished by bottle storage with fuels exposed to air. Global rate constants for peroxide formation, derived from a kinetic model of the autoxidation process, were strongly dependent on temperature and independent of the partial pressure of oxygen. In the present study, global rates of peroxide formation were measured in four more jet fuels in the temperature range of 43 to 120 °C. Additionally, limited oxidation experiments were also performed on dodecane, ethyl benzene, and tetralin. These results support the conclusions of the earlier work (7) and agree favorably with other reported rate measurements.

EXPERIMENTAL SECTION

To establish baseline data on the long-term stability, a modified version of the ASTM D 4625 method of bottle storage at 43 °C was used. (10) The modified procedure ensured that the autoxidation reactions will not become oxygen concentration limited. In the revised procedure, each fuel sample was purged with "synthetic" air until the fuel became saturated with oxygen, as determined by gas chromatography. Then the fuel samples were stored at 43 °C in sealed amber borosilicate bottles. The oxygen contents were determined periodically in both the liquid and vapor phases. If the oxygen concentration in the vapor phase dropped below 10.0 vol%, the remaining bottles of the same fuel were again aerated.

Accelerated oxidative stressing of the test fuels was carried out in replicate in two nominally identical 600-mL, 316 stainless-steel pressure reactors. Temperature was regulated to ± 0.5 °C, and the oxygen pressure was continuously monitored. For details of the experimental procedure, see Ref. 7.

The test fuels selected for this study are described in Table 1. Since the objective of this paper is to compare the new results with those obtained previously, (7), a description of the fuels 1 through 6 examined in the first study will also be included.

The new test fuels 7 through 10 were hydrocracked kerosenes in the Jet A boiling point range.

All the test fuels were claimed by the suppliers to be free of synthetic antioxidant-type additives. Infrared analysis of the polar fraction of the fuels did not show any substituted phenolic or amine-type compounds in excess of the detection limit, < 5 ppm.

MECHANISM

It is well-known that the autoxidation of hydrocarbons is based on a free-radical mechanism (11), which includes the familiar radical initiation, propagation, and termination reaction steps. While several reaction steps are conceivable in the overall autoxidation of hydrocarbon fuels, the formation of alkyl hydroperoxides, ROOH, water and gums may be described by the mechanism shown in Reactions 1 through 6 in Table 2.

In this mechanism, the alkyl peroxide, ROOH, itself initiates the chain mechanism defined by these reactions. For a truly pristine fuel, a chain propagated autoxidation process can not start unless there is a trace of a radical initiator such as ROOH present. In reality, all fuels contain a trace of ROOH even though the concentration is below the detection limits of current analytical methods. In fact, since free radicals are inevitably formed in fuels by exposure to background radiations such as muons, it is highly probable that traces of ROOH will form by Reactions 4 and 5 in Table 2.

The remaining mechanistic arguments and derivation of the kinetic relationships were discussed earlier. (7) Basically, it was concluded from both theory and experiment that the formation of peroxides in jet fuels is independent of the oxygen concentration and appears to depend only on the hydrocarbon concentration, which is assumed to be constant during the autoxidation process. The final relationship based on Reactions 1 through 6, which was used in the analysis of the data, is

$$[\text{ROOH}]^{1/2} = k_2/(k_1/2k_3)^{1/2} [\text{RH}] t \quad (\text{Equ. 1})$$

where the combination of constants $k_2/(k_1/2k_3)^{1/2} [\text{RH}]$ is the global rate constant for peroxide formation. It is important to note (9), however, that if the partial pressure of oxygen is too low (< 7 kPa), Reaction 4 may become the rate controlling step in the mechanism, and Reaction 7 below would then take the place of Reaction 6.



For the oxygen-starved reaction, it may be shown that

$$[\text{ROOH}]^{1/2} = k_g/(k_p/2k_t)^{1/2} [\text{O}_2] t \quad (\text{Equ. 2})$$

where the peroxide concentration now depends on the oxygen concentration, $[\text{O}_2]$, in the fuel.

RESULTS AND DISCUSSION

The basic goal of this study was to develop a method to predict the slow formation of peroxides in jet fuels at ambient conditions from global rate constants obtained at higher temperatures. In the previous work (7) on fuels 1 through 6, the rates of peroxide formation were measured over the temperature range 43 to 120 °C, and the partial pressure of oxygen was varied from 10 to 1140 kPa. In the continuation, global rate constants for the formation of peroxides were measured in fuels 7 through 13.

Existing methods for the evaluation of the storage stability of distillate fuels include "bottle storage" under an atmosphere of air at 43 and 65 °C (10,12) for extended periods ranging from weeks to months. To establish baseline data, bottle storage tests were performed on fuels 1 through 8. Fuels 1 through 4, 7 and 8 were aged at 43 °C, and fuels 5 and 6 were aged at 65 °C. All the test fuels were stressed in the stirred pressure reactors at temperatures ranging from 80 to 120 °C.

Results of the experiments on the new fuels 7 through 10 are shown in Figures 1 through 7. Figure 1 shows the peroxide concentration time curves for fuels 7 and 8 measured in bottle storage experiments at 43 °C. Figures 2 and 3 show the peroxide concentration versus time curves for fuels 7 and 8 measured in the stirred reactor at 80, 100, and 120 °C. Fuels 7 and 8 each had pronounced induction periods that lengthened as the stress temperature was lowered. The induction periods were substantial considering that synthetic antioxidants were not added to these fuels. Previous studies (13) on the autoxidation of hydrocarbons have shown that similar induction periods appear in autoxidations of hydrocarbons when antioxidants are added.

Figure 4 shows the Arrhenius plots of the global rate constants determined for fuels 7 and 8. Figures 5 and 6 show the peroxide concentration time curves for fuels 9 and 10 measured in the stirred reactor at 80, 100, and 120 °C. Fuels 9 and 10 also exhibited pronounced induction periods that increased as the stress temperature was lowered. Figure 7 shows the Arrhenius correlation of the global rate constants measured in the stirred reactors.

The results given in Table 3 show a favorable correlation of global rate constants over the temperature range of 43 to 120 °C. Except for the induction period of fuel 7, the activation energies were also about the same, ≈ 22 kcal/mol. The activation energy for the induction period for fuel 7 (28.4 kcal/mol) is similar to that (29.4 kcal/mol) obtained earlier for fuel 3. Fuels 3 and 7 represent two instances where the activation energy for the induction period is higher than what has been commonly observed for fuels. It is important to note, however, that an activation energy as high as 29.4 kcal/mol is not unusual for the formation of peroxides in hydrocarbons. Rubio, et al. (14) measured rate constants in basically the same way as the present study and found an activation energy of 31 kcal/mol for peroxide formation in C_{10} to C_{16} normal alkanes. Arrhenius parameters given for fuels 9 and 10, which do not include 43° or 65 °C data, are consistent with those of the other fuels.

Two issues arose from the previous study.(7) First, there was a desire for some confirmation of the results obtained from the stirred reactors. To satisfy that need, rates of peroxide formation were determined in dodecane and compared with data in the literature. A second concern was that there were induction periods observed when the test fuels were known to be free of synthetic antioxidants. The induction periods generally lasted until the peroxide concentration reached about 50 to 100 ppm.

To satisfy the above concerns, some experiments were conducted with model compounds. The global rate constant for dodecane was measured at 120 °C and was found to compare favorably with similar rate constants measured

by Rubio, et al. (14) for peroxide formed in decane, dodecane and hexadecane. The rates of peroxide formation in ethyl benzene and tetralin were measured in the stirred reactor at 80 °C. It is interesting to note that there were no induction periods observed in the oxidations of the model compounds. Because these compounds contained traces of peroxides when procured, they were carefully purified by distillation before they were oxidized. The distillation may have removed trace amounts of antioxidant-type impurities that could have caused an induction period. The fact that the test fuels were reportedly free of antioxidants, but nevertheless exhibited induction periods, suggests that fuels contain natural oxidation inhibitors that appear to be quite alien to synthetic antioxidants.

Table 4 shows that the global rate constants for model compounds decrease in the order tetralin > ethyl benzene >> dodecane. The rate constant for dodecane was calculated using a rate expression developed by Rubio, et al. (14)

If the well-known argument is used, i.e., the rate-controlling step in the autoxidation process is the attack on the C-H bond by the $RO_2\cdot$ radical, then the ease of hydrogen abstraction determines the overall rate of oxidation. (9,13,15-17) The results in Table 4 agree with the basic order of free-radical attack on the carbon-hydrogen bond, which is benzylic and allylic H >> aliphatic H.

Since the rate of peroxide formation in alkyl-substituted aromatics is about 100 time faster than in normal alkanes, it would seem that it is the aromatic constituents of the fuel that determine the peroxide potential. This belief seems to concur with the observations in that the rate constants of the test fuels, except for fuel 1, are similar to that of ethyl benzene (3.9×10^6 (mol/L)^{1/2}/s), i.e., they ranged from about 1×10^6 to 4×10^6 (mol/L)^{1/2}/s at 80 °C. The aromatic contents of the fuels ranged from 8.5 to 44.0 percent and the amounts of alkyl groups bonded to the aromatic rings ranged from 4.3 to 17.7 percent. The aromatic alkyl group content was determined as the difference between the total aromatics by FIA and the total aromatic ring carbon measured by UV absorption spectroscopy. It seems reasonable to conclude that the aromatics play a major role in determining the peroxide potential since the concentration of benzylic type C-H bonds appears to be in plentiful supply in all the test fuels.

The above argument seems reasonable except for fuel 1, which formed peroxides at a much slower rate than the other test fuels. In fact, the measured rate of peroxide formation in fuel 1 at 120 °C was somewhat less than that measured in dodecane. There was nothing unusual about the composition of fuel 1. Its total aromatic content was 18.7 percent and the amount of aromatic alkyl groups was 9.3 percent, so there was no obvious reason why the fuel should have oxidized so slowly. Perhaps, because it was a straight run fuel, i.e., not hydrocracked etc., the natural oxidation inhibitors were preserved in the refinement process. A complicating factor is that a later report by the refiner of fuel 1 indicated that this fuel "may have been" Mercox treated. It is interesting that some fuels seem to contain relatively potent natural oxidation inhibitors that are not detectable by the analytical methods used to measure synthetic antioxidants.

CONCLUSION

The new results on fuels 7 through 10 agree with the original observations (7) on fuels 1 through 6. It is evident from the Arrhenius correlations that the mechanism designated by reactions 1 through 6 predominates over the temperature range of 43 to 120 °C.

Potential peroxide formation in jet fuels depends on both the reactivity of the bulk hydrocarbons and the presence of small, possibly undetectable, amounts of (natural) antioxidants.

It is concluded that the peroxide potential of jet fuels at ambient conditions can be predicted from relatively timely measurements at elevated temperatures. However, since the activation energies for peroxide formation in jet fuels range from 19 to 29 kcal/mol, it is concluded that a timely prediction of peroxide potential at ambient conditions would require measurements of global rate constants at two or more elevated temperatures.

ACKNOWLEDGMENT

This work was conducted at the Belvoir Fuels and Lubricants Research Facility, located at Southwest Research Institute (SwRI), for the Naval Research Laboratory (NRL) under Contract No. N00014-85-C-2520. For completeness, this paper includes the results of earlier work funded by the Naval Air Propulsion Center (NAPC). NAPC funding was provided by a Military Interdepartmental Purchase Requisition through the U.S. Army Belvoir Research, Development and Engineering Center under Contract DAAK70-85-C-0007. The project monitors for the Navy were Dr. D.R. Hardy of NRL and C.J. Nowack, G.E. Speck, and L.M. Turner of NAPC. We gratefully acknowledge the invaluable participation by J.P. Cuellar, Jr.; K.B. Kohl; and M. Voigt. Editorial assistance provided by J.W. Pryor, Sherry Douvry, and LuAnn Pierce is also acknowledged with appreciation.

REFERENCES

1. Shertzer, R.H., Final Report No. NAPC-433, Naval Air Propulsion Center: Trenton, NJ, 1978.
2. Hazlett, R.N.; Hall, J.M.; Nowack, C.J.; Craig, L.C., Proceedings of the Conference on Long-Term Stabilities of Liquid Fuels, Israel Institute of Petroleum and Energy: Tel Aviv, Israel, 1983, No. B132.
3. Love, B.E.; Hatchett, K.A.; Peat, A.E., "Fuel-Related Problems in Engine Fuel Systems," SAE Trans. 1967, 75, pp. 441-463.
4. Fodor, G.E.; Naegeli, D.W.; Kohl, K.B.; Cuellar, J.P., Jr., Interim Report BFLRF No. 199, AD A163590, Belvoir Fuels and Lubricants Research Facility, Southwest Research Institute, San Antonio, TX, June 1985.
5. Fodor, G.E.; Naegeli, D.W., Proceedings of the 2nd International Conference on Long-Term Storage Stabilities of Liquid Fuels, Southwest Research Institute, San Antonio, TX, 1986, pp. 632-645.
6. Fodor, G.E.; Naegeli, D.W.; Kohl, K.B.; Cuellar, J.P., Jr., Interim Report BFLRF No. 243, AD A189293, Belvoir Fuels and Lubricants Research Facility, Southwest Research Institute, San Antonio, TX, June 1987.
7. Fodor, G.E.; Naegeli, D.W.; Kohl, K.B., "Peroxide Formation in Jet Fuels," Energy & Fuels, 1988, 2, pp. 729-734.
8. Watkins, J.M., Jr.; Mushrush, G.W.; Hazlett, R.N., Prepr. Pap.--Am. Chem. Soc., Div. Fuel Chem. 1967, 32(1), pp. 513-521.
9. Walling, C., Free Radicals in Solution, John Wiley, New York, 1957, Chapter 9.
10. Standard Test Method for Distillate Fuel Storage Stability at 43°C (110°F), ASTM D 4625.
11. Frost, A.A.; Pearson, R.G., Kinetics and Mechanism, Wiley: New York, 1961, pp. 248-251.
12. Hall, J.M.; Hazlett R.N., Results of the Third CRC Cooperative Test Program on Hydroperoxide Potential of Jet Fuels, May 21, 1987.
13. Nixon, A.C., In Autoxidation and Antioxidants, Lundberg, W.O., Ed., Interscience: New York, London, 1962, Chapter 17.
14. Rubio, F.C.; Rodríguez, F.D.; Gonzalez, F.F.; and Jimenez, V.M., Anales de Quimica. Serie A: Quimica Fisica y Quimica Technica., 1980, 76(2), pp. 261-264.
15. Betts, J., Quart. Rev. 1971, 5, pp. 265-288.
16. Szwarc, M.; Buckley, R.P.; Gresser, J., Prepr. Pap.--Am. Chem. Soc., Div. Pet. Chem. 1958, 3(1), pp. 149-159.
17. Korcek, S.; Chenier, J.H.B.; Howard, J.A.; Ingold, K.U., Can. J. Chem. 1972, 50, p. 2285.

Table 1. Model Fuels

Fuel Code	Fuel Type
1	Straight-run, additive-free, salt-dried, clay-treated kerosene
2	Hydrocracked kerosene, alumina treated
3	Hydrocracked kerosene
4	Fuel 3, alumina treated
5	Hydrofined kerosene
6	Hydrocracked kerosene
7	Hydroprocessed kerosene
8	Hydroprocessed kerosene
9	Hydrocracked kerosene
10	Hydrocracked kerosene
11	Dodecane, distilled
12	Ethyl benzene, distilled
13	Tetralin, distilled and alumina treated

Table 2. Mechanism of Hydrocarbon Oxidation

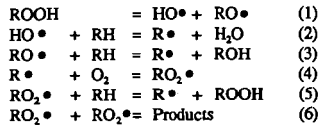


Table 3. Linear Regression Analysis of the Arrhenius Plots Based on $\ln k = \ln A - E_a/RT$

Fuel Code	Period	Range T, °C	E _a kcal/mol	ln A	R ²
1	Unknown	43-120	19.4	23.5	0.963
2	Unknown	43-120	21.6	29.4	0.998
3	Unknown	43-120	29.4	40.3	0.985
4	Unknown	43-120	22.0	30.5	0.998
5	IP	65-120	23.0	30.5	0.999
5	PIP	65-120	21.3	28.8	0.999
6	IP	65-120	21.9	28.2	0.969
6	PIP	65-120	21.5	28.8	0.997
7	IP	43-120	28.4	38.7	0.990
7	PIP	43-120	23.3	32.4	0.988
8	IP	43-120	23.0	30.0	0.994
8	PIP	43-120	23.0	31.9	0.990
9	IP	80-120	22.9	29.3	0.999
9	PIP	80-120	20.7	29.0	0.944
10	IP	80-120	24.4	31.4	0.999
10	PIP	80-120	24.1	32.8	0.984

Notes: IP = Induction Period; PIP = Post-Induction Period.

Table 4. Global Rate Constants for Model Compounds at 80 °C

Compound	Global Rate Constant, (mol/L) ^{1/2} /s × 10 ⁶
Dodecane	0.058
Ethyl benzene	3.9
Tetralin	18.3

Figure 1

PEROXIDE FORMATION
DURING 43 °C BOTTLE STORAGE

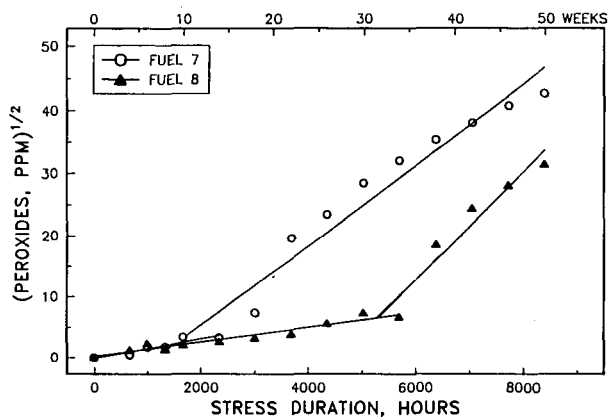


Figure 2

OXIDATION OF FUEL 7
AT 80, 100, AND 120 °C

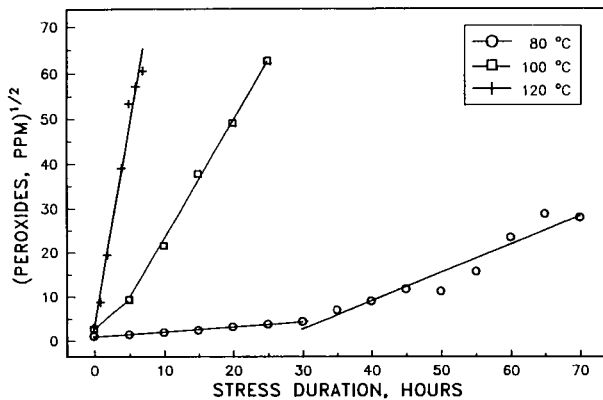


Figure 3

OXIDATION OF FUEL 8
AT 80, 100, AND 120 °C

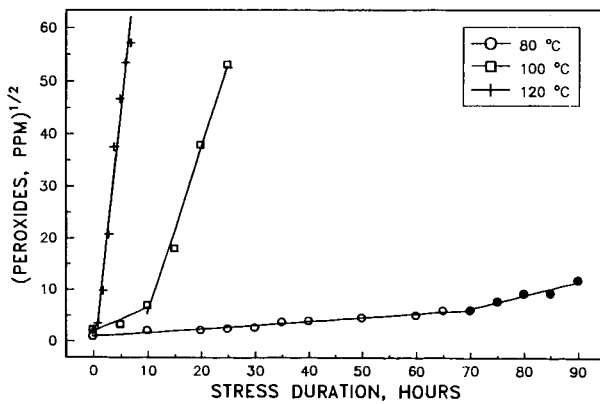


Figure 4
ARRHENIUS PLOT OF OXIDATION
FUELS 7 & 8

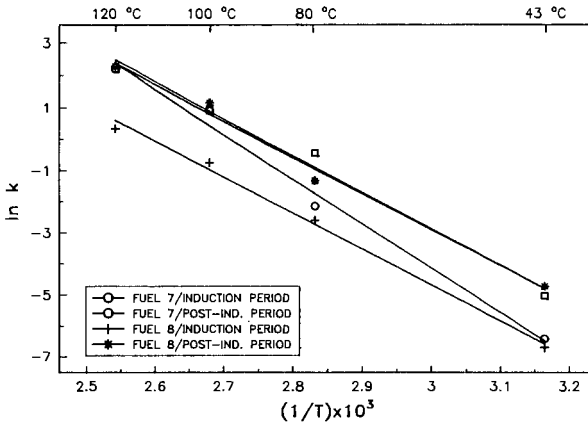


Figure 5
OXIDATION OF FUEL 9
AT 80, 100, AND 120 °C

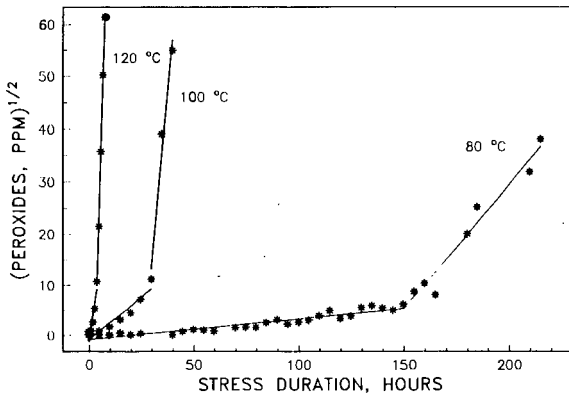


Figure 6
 OXIDATION OF FUEL 10
 AT 80, 100, AND 120 °C

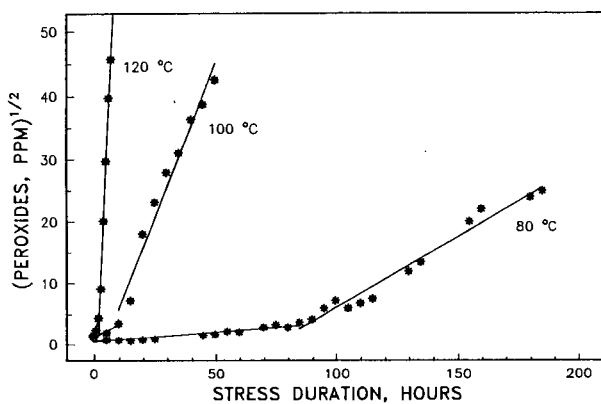
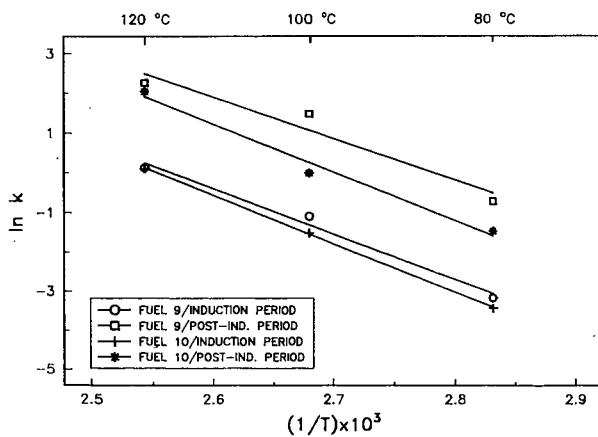


Figure 7
 ARRHENIUS PLOT OF OXIDATION
 FUELS 9 AND 10



**ACCELERATED PEROXIDE FORMATION IN JET FUEL USING
CONVENTIONAL AND OXYGEN OVERPRESSURE METHODS**

Bruce H. Black
GEO-Centers, Inc., Ft. Washington, MD 20744
Dennis R. Hardy and Erna J. Beal
Navy Technology Center for Safety and Survivability
CODE 6181, Naval Research Laboratory, Washington, DC 20375-5000

INTRODUCTION

In recent years the quality of petroleum feedstocks used by refineries has decreased. This has necessitated the use of more severe refinery processes in order to produce jet fuels of higher thermal stability and cleanliness. Unfortunately, these processes remove species that inhibit the formation of hydroperoxides during storage. As a result the storage stability of some jet fuel products, as measured by hydroperoxide formation, has decreased.

Hydroperoxides in jet fuel have a deleterious effect on elastomers in aircraft fuel systems. (1-3) This problem was first recognized in the early 1960s when an unusually large number of flexible fuel manifold hose failures occurred in aircraft operating in the Far East.

(4) To investigate the cause for these failures, a rubber immersion test was developed to distinguish between good and bad fuels. Rubber samples were immersed in jet fuel at 100±1°C and their rate of deterioration, from visual inspection, was recorded. Peroxides, which were known to cause rapid deterioration of elastomers, were monitored during the immersion test. The peroxides in a fuel as received were designated existent peroxides. The peroxides that formed after the fuel was heated to 100°C for 100 hours were designated potential peroxides. In general, as the concentration of potential peroxides in a fuel increased, the failure time for a rubber sample decreased. (4)

During the 1970s and 1980s, additional hydroperoxide induced elastomer failures in aircraft fuel systems occurred. In one instance the failure resulted in the loss of an aircraft. As a result of these failures, a cooperative program was initiated to develop a method to predict a jet fuel's tendency to form hydroperoxides during storage. Six laboratories participated and seven fuels, some of which contained a phenolic antioxidant, were included in the first Coordinating Research Council, Inc., (CRC) cooperative interlaboratory testing (round robin).

A procedure similar to the rubber immersion test was used. Fuel samples were stressed in capped brown borosilicate glass bottles at 100°C for up to 168 hours. The fuel samples were periodically analyzed for hydroperoxide concentration at intermediate intervals by ASTM D3703-78. (5) The results indicated that this procedure had fair repeatability and poor reproducibility. The participants concluded that additional work was needed to achieve better values.

Prior to further developmental work, it was suggested that testing at 100°C may not be indicative of peroxidation at ambient conditions. To verify this possibility, an experiment was performed in which four

fuels from the first round robin were stressed at 43°C, 65°C, and 80°C. Aliquots of the fuels were periodically removed for peroxide analysis. Peroxidation rates at these temperatures were compared to the rates obtained at 100°C in the first interlaboratory round robin.

The fuel samples were, unfortunately, stressed in capped bottles. This limited the amount of oxygen available to the samples. At higher temperatures, 80°C and 100°C for instance, the frequency at which aliquots were removed allowed for more frequent replenishment of atmospheric oxygen. At the lower temperatures where aliquot removal was less frequent, oxygen starvation led to a decrease in the peroxidation rate. This suppression of peroxidation rate in turn led to the erroneous conclusion that peroxidation occurs by a different mechanism at elevated temperatures. In further studies, therefore, the temperature at which fuels were stressed was limited to 65°C.

Two additional interlaboratory round robins were performed. This work culminated in a set of standard test conditions that are useful in research studies. (6) These conditions, however, have serious limitations for fuel quality use. These include the duration, 4 weeks, and the limitation as a Go/No Go (pass/fail) test. The use of a pass/fail criterion does not allow fuels to be ranked relative to each other. Furthermore, under these conditions antioxidant additives cannot be easily or quickly tested for their relative effectiveness. Clearly a more rapid and meaningful test must be developed.

This paper describes experiments that compare fuels stressed at 65°C in capped and vented bottles. Also described is a method for distinguishing between various antioxidant additives using a serial dilution technique.

EXPERIMENTAL

Five fuels were used in this study and included: Three JP-5 blending stocks; coded Fuel #1, #2, and #3; Shale II, a finished JP-5 jet fuel; and n-dodecane. The n-dodecane was treated with silica gel to remove polar species that may have influenced peroxidation rate. This was done by adding 250g of 100-200 mesh activated silica gel to two liters of n-dodecane. The mixture was magnetically stirred for six hours. Two liters of each sample were prefiltered through a pair Gelman type A/E glass fiber filters prior to accelerated aging.

Two sets of each sample were prepared. The first set remained exposed to atmospheric oxygen, and the second set remained tightly capped for the duration of the test. For each anticipated hydroperoxide analysis period, two 125mL brown borosilicate glass bottles each containing a 100mL sample were prepared. The duplicate samples were initially to be analyzed for hydroperoxide concentration in duplicate every two weeks for eight weeks. This was later modified and single samples were analyzed in duplicate for up to twelve weeks. The samples were stressed in an oven at 65°C for the duration of the test.

Phenolic antioxidant experiments were performed using a serial dilution technique. Two pure compounds, 2,6-di-t-butyl-4-methyl phenol (26dtb4mp) and 2,4-di-t-butyl phenol (24dtbp), were used in this study.

Stock solutions were prepared by dissolving 24mg of an additive in 1.0L Fuel #1. This is the maximum concentration allowed in JP-5 jet fuel by MIL-T-5624N. (7) Aliquots of the stock solution were diluted to 100mL, with an appropriate volume of neat Fuel #1, in 125mL brown borosilicate glass bottles. A series of samples for each additive were produced with concentrations between 24.0mg/L and 0.3mg/L.

An entire sample set of either additive, including a 100mL additive-free Fuel #1 aliquot, was simultaneously stressed in a low pressure reactor (LPR) at 100°C and an oxygen overpressure of 793kPa. (8) After 24 hours under these conditions, the samples were removed and analyzed for peroxide concentration.

A Mettler DL20 automatic titrator was used for peroxide determinations. Analyses were performed according to ASTM D3703-85: the Standard Test Method for Peroxide Number of Aviation Turbine Fuels. (5)

RESULTS

The results of accelerated aging at 65°C in capped bottles are shown in Figure 1a. It can be seen that four of the samples approached hydroperoxide concentrations of approximately 90ppm. The fifth sample, Shale II JP-5, continued slow peroxidation for the duration of the test. The results of accelerated aging at 65°C in vented bottles is shown in Figure 1b. It can be seen that three samples, Fuels #1, #2, and #3, produced extremely high concentrations of hydroperoxides under these conditions. In Figure 1c the peroxidation of n-dodecane and Shale II JP-5 in vented bottles is shown with an expanded ordinate.

Comparison of Figures 1a and 1b shows that peroxidation rate in the capped bottles is significantly reduced. This is a result of the limitation of atmospheric oxygen. Although not apparent from these figures, the hydroperoxide concentration in the two sets of fuels significantly differed at two weeks. At four weeks Fuel #3 had the highest hydroperoxide concentration in both sets of fuels. It can be seen, however, that the concentration in the vented sample was nearly eight times that of the capped sample. After four weeks, the hydroperoxide concentration in Fuel #3 continued to increase in the vented bottle. In the capped bottle, however, the concentration of hydroperoxides remained relatively constant. This indicates that oxygen starvation has occurred.

In Figure 1b it can be seen that Fuels #1 and #2 also exhibited a tendency to form high concentrations of hydroperoxides. Both of these fuels undergo a relatively slow rate of peroxidation for six weeks. After six weeks, both fuels rapidly form hydroperoxides. In the vented bottle, Fuel #1 undergoes peroxidation at a linear rate until ten weeks. In the capped bottle, however, Fuel #1 peroxidizes at much slower rate. Unlike Fuel #3, Fuel #1 slowly approaches what appears to be a limit of approximately 100ppm.

Similar characteristics are exhibited by Fuel #2. In the vented bottle this fuel undergoes a rapid rate of peroxidation after six weeks. The peroxide concentration continues to increase for the duration of the test. In the capped bottle, however, Fuel #2

peroxidizes at a much slower rate finally reaching a concentration limit similar to that of Fuels #1 and #3. These results indicate that accelerated aging in capped bottles not only limits the amount of hydroperoxides formed, but reduces the rate at which peroxidation occurs.

Figure 1c shows the rate of peroxidation for n-dodecane and Shale II JP-5 in vented bottles. Both fuels exhibited a relatively slow and linear peroxidation rate. When compared to Figure 1a, it can be seen that Shale II exhibited similar characteristics in capped bottles. The Shale II sample reached a maximum hydroperoxide concentration of 28ppm in the vented bottle. In the capped bottle the maximum concentration formed is approximately 18ppm. In general, the rate of hydroperoxide formation in the capped bottles was approximately $68.6 \pm 7.8\%$ of the rate in vented bottles for the Shale fuel. This again shows that accelerated aging in capped bottles reduces peroxidation rate.

The rate of hydroperoxide formation in n-dodecane in capped bottles seemed to exhibit a periodicity. This was much less apparent in the vented samples. The maximum concentration of hydroperoxides formed was similar in both sets of samples. It is expected that after twelve weeks the hydroperoxide concentration in the capped n-dodecane sample would remain constant.

A cursory examination of phenolic antioxidant effects at 100°C and 793kPa oxygen for 24 hours was also performed. It is well known that hindered phenols significantly reduce liquid phase free-radical autoxidation of hydrocarbon fluids. (9-11) The relative effectiveness of these compounds has been shown to be structure dependent. (9) In general, the presence of a t-butyl group in the 2-position or both the 2- and 6-position increases its effectiveness as an antioxidant. The presence of an alkyl group in the 4-position also leads to an increase in its antioxidant properties. If the alkyl group in the 4-position possesses α -branching, such as a t-butyl or an isopropyl group, however, the additive's antioxidant characteristics are diminished. (9)

Figure 2a shows the effect of 26dtb4mp in Fuel #1 using the serial dilution technique. It can be seen that this additive exhibits an antioxidant effect to concentrations as low as 0.3mg/L. Figure 2b shows the effect of 24dtbp in Fuel #1. It can be clearly seen that under these conditions, 24dtbp is a significantly less effective antioxidant than 26dtb4mp as would be expected.

Figure 2c is a side-by-side comparison of the effect of the two additives. This shows that 26dtb4mp is approximately 20 times more effective than 24dtbp at various concentrations, e.g., 0.3mg of 26dtb4mp is as effective as 6.0mg of 24dtbp; 0.6mg of 26dtb4mp is as effective as 12.0mg of 24dtbp, etc. These results show that under these conditions it is possible to evaluate the effect of various antioxidants relative to each other.

SUMMARY

In the past additive-free fuels have been ranked relative to each other by the length of their induction period. This period is

characterized by slow peroxidation until a readily discernible change in rate occurs, i.e., the "breakpoint". Antioxidants have also been compared by their ability to increase the induction period in a particular fuel. Unfortunately at higher temperatures the induction period for additive-free fuels is either minimal or non-existent. This renders its measurement quite subjective. Furthermore, the end of the induction period, or breakpoint, often occurs at hydroperoxide concentrations higher than are allowed by MIL-T-5624N. (7) The use of the breakpoint as a criterion for ranking fuels or additives is, therefore, not appropriate.

The rate at which a fuel approaches the military specification peroxide limit, 8ppm, would be more useful. For example, a fuel with a longer induction period than another fuel is not necessarily better. If the first fuel's induction period rate is greater, it will reach the specification limit sooner. Unfortunately, the use of induction period rate also presents problems. At lower temperatures the induction period for additive-free fuels is long enough to objectively measure an induction period rate. At higher temperatures, 100°C and 120°C for instance, the induction period rate measurement, like its length, is too subjective.

If more objective measurements of induction period rates are desired, it is necessary to remove and titrate samples for hydroperoxide concentration at very frequent intervals. At 100°C and 120°C, it may be necessary to analyze fuel samples every 30 minutes, or less. For additive-free fuels, or fuel samples obtained from field activities, these labor intensive induction period rate measurements are necessary.

For antioxidant evaluations, the use of the serial dilution technique has advantages over induction period rate and length measurements. First, it is not a subjective test. All samples of a particular fuel and additive combination are stressed under exactly the same conditions. The technique is not concerned with either the length or rate of the induction period. It simply compares the concentration effect of various antioxidants on peroxidation in a given fuel. Second, the technique is far less labor intensive. These advantages make this technique useful for further antioxidant evaluations.

REFERENCES

1. Shertzler, R.H.; "Aircraft Systems Fleet Support/Organic Peroxides in JP-5 Investigation," Final Report NAPC-LR-78-20, Naval Air Propulsion Center, Trenton, NJ, 27 September 1978.
2. Hazlett, R.N., Hall, J.M., Nowack, C.J., Turner, L.; "Hydroperoxide Formation in Jet Fuels," Proceedings of the Conference on Long Term Stabilities of Liquid Fuels; Israel Institute of Petroleum and Energy, Tel Aviv, Israel, December 1983, pp. B132-B148.
3. Nadler, C.; "Effect of Oxidizing Fuels on Aircraft Fuel System Elastomers and Sealants," Final Report NADC-80076-60, Naval Air Development Center, Warminster, PA, 20 May 1980.

4. Smith, M.; "Aviation Fuels," G.T. Foulis & Co. Ltd., Henley-on-Thames, Oxfordshire, UK, 1970.
5. Standard Test Method for Peroxide Number of Aviation Turbine Fuels; ASTM D3703-85; American Society for Testing and Materials; Philadelphia, PA, 1989.
6. Hall, J.M., Hazlett, R.N.; "Results of the Third CRC Cooperative Test Program on Hydroperoxide Potential of Jet Fuels," NRL Memorandum Report 5985, Naval Research Laboratory, Washington, DC, 21 May 1987.
7. Military Specification, MIL-T-5624N, "Turbine Fuel, Aviation, Grades JP-4, JP-5 and JP-5/JP-8 ST," ASD/ENES, Wright-Patterson AFB, OH, 10 February 1989.
8. Hardy, D.R., Hazlett, R.N., Beal, E.J., Burnett, J.C.; Energy & Fuels 1989, 3, 20-24.
9. Scott, G.; "Atmospheric Oxidation and Antioxidants," Elsevier Publishing Company, New York, NY, 1965.
10. Bamford, C.H., Tipper, C.F.H., Eds.; "Chemical Kinetics," Volume 16: Liquid-Phase Oxidation; Elsevier Scientific Publishing Company, New York, NY, 1980.
11. Pospisil, J., Klemchuk, P.P., Eds.; "Oxidation Inhibition in Organic Materials," Volume 2; CRC Press, Inc., Boca Raton, FL, 1990.

**ACCELERATED PEROXIDE FORMATION
12 Wks @ 65C & Atm. Air (Capped Bottle)**

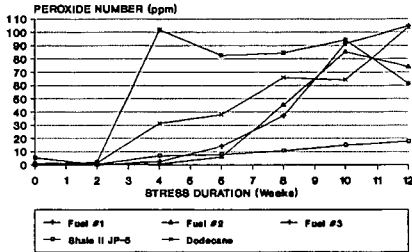


FIGURE 1a

**ACCELERATED PEROXIDE FORMATION
12 Wks @ 65C & Atm. Air (Vented Bottle)**

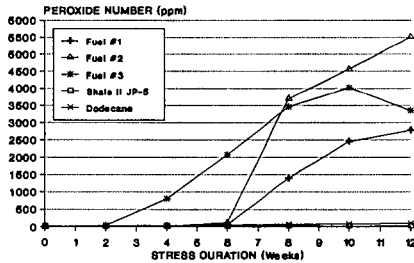


FIGURE 1b

**ACCELERATED PEROXIDE FORMATION
12 Wks @ 65C & Atm. Air (Vented Bottle)**

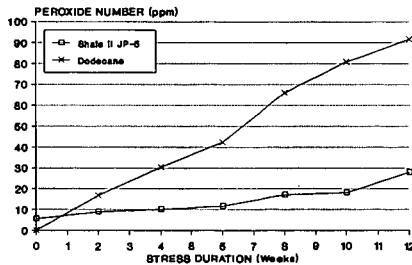


FIGURE 1c

2,6-di-t-Butyl-4-Methyl Phenol
LPR @ 100C & 793kPa Oxygen

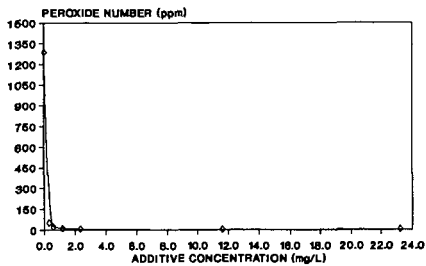


FIGURE 2a

2,4-di-t-Butyl Phenol
LPR @ 100C & 793kPa Oxygen

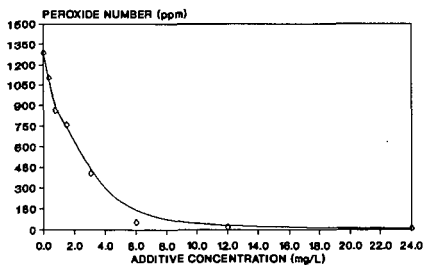


FIGURE 2b

PHENOLIC ANTIOXIDANT EFFECT
LPR @ 100C & 793kPa Oxygen

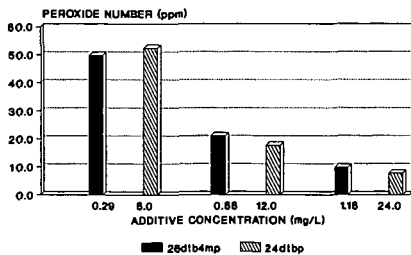


FIGURE 2c

SYMPOSIUM ON STABILITY AND OXIDATION OF MIDDLE-DISTILLATE FUELS
PRESENTED BEFORE THE DIVISION OF PETROLEUM CHEMISTRY, INC.

AND
THE DIVISION OF FUEL CHEMISTRY
AMERICAN CHEMICAL SOCIETY
WASHINGTON, D.C. MEETING, AUGUST 26-31, 1990

ANALYSIS OF SOLIDS FORMED DURING THERMAL- AND
STORAGE-STABILITY TESTING OF JET FUELS
DERIVED FROM PETROLEUM AND FROM COAL

By

R. D. Grigsby, G. P. Sturm, Jr., J. W. Goetzinger,
J. B. Green, and R. P. Anderson

IIT Research Institute
National Institute for Petroleum and Energy Research,
P.O. Box 2128, Bartlesville, OK 74005

INTRODUCTION

Recently, the Department of Energy and the Air Force began a program to investigate the production of jet fuel and other commercial products from the gasification of lignite at the Great Plains Gasification Plant (GPGP), Beulah, North Dakota. This project was undertaken to increase the economic viability of the plant and, at the same time, to create a reliable source of jet fuel for Air Force bases in the northern great plains area (1). In cooperation with DOE and the Air Force, the National Institute for Petroleum and Energy Research (NIPER), has investigated the thermal and storage stability properties of a JP-8 jet fuel produced from GPGP liquid by-products and compared these properties with those of a conventional JP-8 fuel derived from petroleum.

Several decades of investigations on fuel stability have increased our knowledge of the chemistry involved in fuel degradation. Most of these studies have been focused on trace heteroatomic components in fuels (2-16). In the past, ambient storage stability and high temperature thermal stability have been viewed as two separate issues, especially when trace contaminants have been considered. However, our recent findings on petroleum-derived jet fuels indicate that hydrocarbons in neutral fractions from relatively clean fuels are susceptible to oxidative degradation at high temperatures and under ambient storage conditions (10).

Hydrocarbon types that seem to be emerging as important in fuel degradation are the cycloalkylaromatics, such as indans and tetralins (11). These types are abundant in many coal liquids, including the hydrotreated tar-oil distillates from GPGP. In this respect, determination of the thermal and storage stabilities of jet fuel produced from lignite or coal is significant.

Perhaps the most undesirable consequence of fuel degradation is the formation of solids. Thus, a logical approach in studying degradation is to investigate the compositions of the solids formed under ambient storage conditions and at high temperatures to which the fuel might be subjected in a turbine engine. We have used separation procedures and identification methods, particularly HPLC and mass spectrometry, to analyze solids formed under simulated-storage and high-temperature conditions (11,17-21). Two fuels were studied in the present investigation: a coal-derived fuel and a conventional fuel from petroleum. A comparison of results from these two fuels is reported.

EXPERIMENTAL

The two fuels studied were a JP-8 (NIPER No. 2987) produced from GPGP liquid by-products (No. 89-WEH-157) and a petroleum-derived reference JP-8 (NIPER No. 2955).

The storage stability of both fuels was determined by two different methods. In the first, samples were aged at 80° C under 100 psig oxygen for 1, 2, 3, and 4 weeks. In the second, aging was performed by ASTM method D 2274, in which oxygen was bubbled through the samples for 16 and 40 hours at 95° C.

The sediment produced by aging the coal-derived fuel at 80° C was characterized by separation into six fractions using an HPLC acid-fractionation method developed at NIPER in other investigations (17,18). Compound types were separated into fractions of increasing acidity.

Both fuels were subjected to thermal-stability testing in a jet fuel thermal oxidation tester (ALCOR, Inc., San Antonio, TX) using ASTM method D 3241 (JFTOT test). Breakpoints were also determined for each fuel. The fuels were then stressed for extended periods of time at 10° C above the breakpoint to generate sufficient solids on the heated tube and on a downstream filter to permit mass-spectral analysis (20,21).

For extended runs, the fuel-flow system of the JFTOT apparatus was modified so that the fuel passed from the heated test section through a 25 mm diameter membrane filter to a variable-speed pump and then to a spent-fuel reservoir. A fuel-flow rate of 1 mL/min was used (20,21).

In the first extended test with the 2955 reference fuel, a nylon filter with a pore size of 0.45 μm was used to collect the filterable solids. The tube temperature was 280° C. After seven hours, the filter plugged and the experiment was stopped. For the second extended run with the same fuel, a glass-fiber filter, type GF/F, with a 0.7 μm pore size was used. A ten-hour run gave no detectable plugging. However, when the apparatus was disassembled, the filter was found to be partially disintegrated. In the extended JFTOT run with the coal-derived fuel (2987), the tube temperature was 310° C. A nylon filter with a pore size of 0.45 μm was used, and after 17 hours it became plugged. The JFTOT tubes and filters from the experiments with both fuels were saved for analysis by mass spectrometry.

The mass-spectrometric method used in the analyses of the JFTOT tube deposits and filterable sediments was developed previously as part of a similar investigation on fuel stability (19,20). Probe microdistillation/mass spectrometry (PMD/MS) was used to provide high resolution mass spectra of the solids, and the data were analyzed to produce curves of ion intensity vs. temperature or time (elimination curves) for ions identified with specific elemental formulas (19).

Deposits on the JFTOT tubes were sampled by machining their surfaces in a lathe using a cleaned tool bit (20). Turnings containing each deposit were then placed in a temperature-programmed quartz probe for introduction under PMD/MS conditions into a Kratos MS-50 high resolution mass spectrometer (Kratos Analytical Instruments, Manchester, U.K.). Probe temperature was increased linearly at 10° C/min. Twenty to thirty spectra were recorded at a resolving power of 10,000 to 20,000 over a temperature range from ambient to greater than 400° C. Seventy eV electron impact was used for ionization to maximize the signal-to-noise ratio on mass-spectral peaks being formed from a limited amount of sample. Mass spectra were not recorded below m/z 70.

Sediments on the filters used with the JFTOT apparatus were sampled by cutting small filter strips for introduction by probe into the mass spectrometer (20). Using this approach, spectra of the filterable sediments were recorded under the same conditions as given for the tube deposits, except that 25 eV electron impact was used for ionization of the sediment from fuel 2955. The lower-energy ionization was selected to suppress intensities of fragment-ion peaks, but this method did not appear to offer any advantage over 70 eV electron impact and was not used with the other samples. To avoid thermal decomposition of the nylon filter used with fuel 2987, the probe temperature was limited to approximately 300° C.

RESULTS AND DISCUSSION

Initial Fuel Characterization. Results from the initial characterization of both fuels are shown in Table I. The coal-derived fuel (No. 2987) showed a very slight color that may have been caused by suspended clay. This also explains the relatively long filtration time for the fuel. Both fuels easily met the viscosity specification, and both passed the simulated distillation test (results not shown), except for slightly exceeding the maximum value for the endpoint temperature. The simulated distillation also showed that the coal-derived fuel contained more low-boiling components than the reference fuel. No peroxides were detected in the reference, but the coal-derived fuel showed a trace (0.5 ppm).

Storage Stability. Table II summarizes results from the storage stability experiments. The coal-derived fuel (2987) showed lower sediment formation through three weeks of storage at 80° C under 100 psig oxygen. However, the peroxide content in 2987 was consistently higher than in the reference fuel (2955) and reached a maximum at approximately three weeks. Between three and four weeks, the coal-derived fuel deteriorated significantly. A large quantity of sediment was formed and the fuel darkened. After three weeks, the peroxide content in 2987 decreased somewhat, as has been observed in storage-stability testing with other fuels.

The oxidation-stability test (ASTM D 2274) on the two fuels gave similar results (not shown) to those obtained from the storage stability test. Through 40 hours, the coal-derived fuel showed less sediment formation and color than the reference fuel. Peroxide values were somewhat higher in the coal-derived fuel.

Fractionation by HPLC of Sediment Formed During Storage-Stability Testing of Coal-derived Fuel. The sediment produced by aging the coal-derived fuel for four weeks at 80° C under 100 psig oxygen was characterized by separation into six fractions using an HPLC acid-fractionation method (17,18). Yields of the fractions, which are separated according to increasing acidity, are given in Table III along with compound types typically present in each fraction. Any neutral or basic compounds would be expected in fraction 1 together with very weak acids. The relatively low recovery of 78.74% is attributed to loss of material in the work-up of fraction 6 and possible retention of very polar substances on the HPLC column. The yield data show that the bulk of the sediment was separated into fractions 5 and 6, which typically contain carboxylic acids and difunctional acids, respectively.

Thermal Stability. Results from the JFTOT test (ASTM D 3241) of the reference fuel (2955) and coal-derived fuel (2987) are given in Table IV. Both fuels easily met the specifications. Fuel 2987 was stable to a higher temperature than fuel 2955, as determined by the breakpoint temperatures of 295° C and 275° C, respectively.

Mass-Spectral Analysis of JFTOT Tube Deposits and Filterable Sediments. To make a reasonable comparison of results obtained from a large amount of mass-spectral data, abbreviation in tabulated form is used to discuss compound types identified in the solids formed during fuel degradation. Each table lists ions detected in homologous series corresponding to a particular elemental formula. For example, ions arising from hydrocarbons are classified as having C_nH_{2n+Z} formulas where Z ranges from +2 to -23. Thus, molecular ions for alkylbenzenes (C_nH_{2n-6}) are listed under a Z number of -6. Major fragment ions are given along with molecular ions. These occur in series having a Z number one less than the number for molecular ions. For alkylbenzenes, fragment ions thus occur in the C_nH_{2n-7} series (Z number of -7). No ion intensities are given, but the prominence of homologues in a particular series can be estimated from the number of molecular and fragment ions detected for the series. The molecular mass of the first member of a series is identified with the parent compound, e.g., 78 with benzene in the alkylbenzene series. If the first ion detected in a molecular-ion series has a mass less than the mass listed for the parent compound, the ion may arise by rearrangement or it may belong to a series for another type not identified. In either case, the fact that the ion cannot be a molecular ion in the listed series is mentioned in a footnote to the table.

It is necessary to emphasize that names of compound types given in the first column of the tables are intended to be suggestions only. Undoubtedly, many of the ions having the specified elemental formulas do arise from the type indicated; however, others may originate from types not identified. In the discussion that follows, names are restricted to those given in the tables with the understanding that ions in the series can originate from other compound types, as well.

Analysis of Filterable Sediment and Tube Deposit from Coal-Derived Fuel. Numerous compound types were detected in the solids formed during thermal stressing of the jet fuel from coal, including those containing only carbon and hydrogen as well as heteroatomic types containing oxygen and nitrogen. Only traces of compounds containing sulfur were found.

In Table V identification of hydrocarbons in the filterable sediment and tube deposit is presented for the thermal degradation of fuel 2987. A broad range of aliphatic and alicyclic compound types was found in both solids. No molecular ions for alkanes were identified (nor were they expected), but fragment ions corresponding to alkyl groups were found over a mass range extending to m/z 155 in the spectra from the sediment and to m/z 183 in the spectra from the tube deposit. These fragments may have arisen from alkanes or from other compound types having alkyl side chains. Numerous molecular and fragment ions were recorded for olefins, dienes, cycloalkanes, cycloalkenes, and bicycloalkanes. These compound types were distributed rather uniformly between the tube deposit and the filterable sediment. For example, molecular ions for dienes, cycloalkenes, and bicycloalkanes were detected from m/z 68 to m/z 194 in the spectra from both solids. The ions appeared in the spectra over a broad range of probe temperatures, indicating that they arose from surface desorption and by covalent bond rupture, i.e., by pyrolysis.

Many molecular and fragment ions from aromatic hydrocarbons were detected in the spectra from the filterable sediment and tube deposit. Alkylbenzene homologues were identified in the sediment to 190 amu and in the tube deposit to 162 amu. Indans and tetralins were found in both solids with molecular masses extending to 188 amu. Aromatics with a greater degree of unsaturation were evident in both sets of spectra. Six members of the naphthalene series (Z number of -12) were identified in the sediment spectra and five members in the spectra from the tube deposit. The most highly aromatic types identified in either set of spectra were the fluoranthenes and pyrenes (Z number of -22). One member of the series, the parent compound at m/z 202, was identified in the spectra of the sediment, and three members (m/z 202, 216, and 244) were found in the tube-deposit spectra.

A number of molecular and fragment ions containing one oxygen were identified in the spectra from the filterable sediment and tube deposit. These are seen in Table VI. Molecular ions for aliphatic and alicyclic types (e.g., tetrahydrofurans) were almost nonexistent in the spectra, and they were not expected based on the known fragmentation of these compounds. However, a number of fragment ions for aliphatic and alicyclic oxygen-containing types were detected, as noted in the table.

Aromatics containing one oxygen were readily detected in both sets of spectra. Several phenols were identified, as well as a number of more unsaturated types, including naphthols and dibenzofurans. Compounds with a greater degree of unsaturation appeared to be partitioned more toward the filterable sediment than toward the tube deposit. As an illustration, four fluorenones and phenalenones (parent mass of 180) were detected in the sediment, but none were found in the tube deposit.

Compound types containing two oxygens were identified in the spectra of the filterable sediment and tube deposit, including nonaromatic and aromatic carboxylic acids and dihydroxyaromatics (results not shown). The aromatics were decidedly partitioned more toward the sediment. For example, six benzoic acids and benzodioxoles were found in the spectra of the sediment ranging from the parent compound (m/z 122) to homologues having five alkyl carbons attached (m/z 192). On the other hand, in the spectra of the tube deposit only one fragment ion attributable to these compound types was detected (m/z 149). Although molecular ions containing two oxygens were detected in Z series as negative as -18 in the spectra of the sediment, no molecular ions in series more negative than -4 were detected in the tube-deposit spectra.

Table VII shows ions detected in homologous series for compounds containing three oxygens. Because of the more complex nature of these types, names are omitted except to note that the ions are attributable to multifunctional compounds. Phthalates are indicated by m/z 149 in the -11 Z series. These compounds, especially dioctylphthalate, are common artifacts seen in mass spectra.

A very prominent peak appeared in the spectra of the tube deposit at m/z 129, corresponding to a fragment ion of elemental formula $C_6H_9O_3$. It must have arisen from a nonaromatic oxygen-containing compound, such as an alcohol, ether, or peroxide. None of these compound types would produce a significant molecular ion. At first glance, m/z 129 might appear to have an elemental formula of C_9H_7N , corresponding to quinoline or isoquinoline. However, the accurately measured mass of the peak was consistently closer to the value expected for the CHO_3 combination (129.0552) than for the CHN combination (129.0578). Therefore, a formula of C_9H_7N was ruled out. The $C_6H_9O_3$ ion at m/z 129 was much weaker in the spectra of the filterable sediment, showing that the corresponding compound(s) was strongly partitioned toward the tube deposit.

Except for compound(s) producing the m/z 129 peak, types containing three oxygens were partitioned more toward the sediment than toward the tube deposit. This is evident from the larger number of molecular and fragment ions found for the sediment as compared with the number found for the tube deposit. The difference is not easily explainable, but it may result from the relatively low thermal stability of compounds containing alcohol or ether groups; that is, these compounds may have appeared in smaller quantities in the tube deposit because they may have been thermally decomposed on the hot metallic surface of the tube.

A number of compounds containing one nitrogen were identified in the filterable sediment, but only a few were found in the tube deposit, as seen by comparing results in Table VIII. The difference may have been a consequence of thermal decomposition of nitrogenous compounds on the hot tube surface. Compound types prominent in the spectra of the filterable sediment included pyrrolines (molecular ions from m/z 69 to 125 and 153) and aromatic types such as pyridines (or anilines), showing molecular ions from m/z 79 to m/z 149. Indolines, indoles, and quinolines (or isoquinolines) were abundant, as indicated by the number of molecular and fragment ions detected in homologous series for these types.

Analysis of Filterable Sediment and Tube Deposit from Petroleum-derived Fuel. In spite of the different origins of fuel 2987 (coal liquid) and fuel 2955 (petroleum), mass-spectral analyses of solids formed by thermally stressing the two fuels produced surprisingly similar results. Therefore, discussion of the compositions of the filterable sediment and tube deposit from fuel 2955 is limited mainly to differences found between the solids formed from the two fuels.

Numerous hydrocarbons were identified in the filterable sediment and tube deposit from fuel 2955. When these were compared with hydrocarbons from fuel 2987, it became evident that the compositions of the hydrocarbons in the solids from the two fuels were very similar. This observation suggests that the same hydrocarbons were contributing to the formation of the solids in both fuels.

Compound types having one oxygen were identified in the filterable sediment and tube deposit from fuel 2955. When compared with the same types identified in the solids from fuel 2987, only slight differences were seen that may not be significant. For example, only one dibenzofuran (mass 196) was detected in the sediment from fuel 2955, but in the sediment from fuel 2987 four homologues were found (masses 168 to 210), as noted in Table VI. Several fluorenones and phenalenones were detected in the tube deposit from fuel 2955 but not in the sediment from the same fuel. The opposite was found for fuel 2987, i.e., fluorenones and phenalenones were detected in the sediment but not in the tube deposit (Table VI).

Fewer compounds containing two oxygens were found in the filterable sediment from fuel 2955 than in the sediment from fuel 2987. Differences were particularly evident for the more unsaturated species. No types with Z numbers more negative than -12 (coumarins and dihydroxynaphthalenes) were detected in the 2955 sediment, whereas in the sediment from fuel 2987, types with Z numbers as negative as -18 were identified (biphenylene carboxylic acids and hydroxyfluorenones). In contrast, by comparing results from the two tube deposits, it was evident that more types containing two oxygens, especially aromatics, were detected in the tube deposit from fuel 2955 than in the 2987 deposit.

A very similar distribution of compound types containing three oxygens was found between the filterable sediments from the two fuels as well as between their tube deposits. As mentioned previously, a very strong m/z 129 peak of elemental formula $C_6H_9O_3$ was found in the spectra of the tube deposit from fuel 2987 (Table VII). This same peak was present in the spectra of the 2955 tube deposit although its intensity was not as strong as in the 2987 spectra. The $C_6H_9O_3$ ion was also detected in the spectra of the filterable sediment from fuel 2955; however, its intensity was much weaker than in the spectra of the tube deposit from the same fuel.

Ions containing one nitrogen were identified in the spectra of the filterable sediment and tube deposit from fuel 2955. The corresponding compound types were seen to be distributed more toward the sediment than toward the tube deposit. This same observation was noted in the discussion of solids formed during thermal stressing of fuel 2987 (Table VIII). Although the compositions with respect to nitrogen-containing compounds were similar in the sediments from the two fuels, fewer highly aromatic types were detected in the spectra of the sediment from fuel 2955. For example, only one homologue

for acridines and phenanthridines (mass 193) was identified in the 2955 spectra, but three were found in the spectra of the 2987 sediment (masses 179, 193, and 221), as noted in Table VIII. A few nitrogen-containing species were detected in the tube deposit from fuel 2955 as compared to virtually none in the spectra of the 2987 deposit (Table VIII). In this respect, several quinolines (or isoquinolines) were identified in the tube deposit from fuel 2955, but the presence of this compound type in the 2987 deposit was doubtful.

SUMMARY AND CONCLUSIONS

Storage and thermal stabilities of a JP-8 fuel produced from GPGP liquid by-products were compared with those of a conventional petroleum-derived JP-8 fuel. Initial characterization and simulated distillation of the two fuels showed that the coal-derived fuel contained more lower-boiling components, a longer filtration time, and a higher particulate content than the petroleum-derived fuel. Also, the coal-derived fuel possessed a slight color. Nevertheless, for the most part both fuels met JP-8 specifications.

Both fuels exhibited good oxidation stability through 40 hours of aging according to ASTM D 2274, with the coal-derived fuel showing less sediment and color formation but somewhat higher peroxide content than the petroleum-derived fuel. Storage stability (aging at 80° C under 100 psig oxygen) gave approximately the same results for both fuels through three weeks of aging. However, between the third and fourth week, the coal-derived fuel deteriorated rapidly and exceeded the petroleum fuel in sediment and color formation as well as peroxide content.

Fractionation of the 80° C aged sediment from the coal-derived fuel by HPLC indicated that the sediment was composed primarily of carboxylic acids and difunctional acids.

Both fuels easily met thermal-stability specifications with the coal-derived fuel showing a higher breakpoint temperature than the petroleum-derived fuel.

Mass spectra of the filterable sediments and JFTOT-tube deposits formed during thermal stressing of the coal-derived and petroleum-derived fuels were remarkably similar, indicating that the same compound types were responsible for solids formation in both fuels.

When spectra of the filterable sediment from either fuel were compared with those of the tube deposit from the same fuel, a number of similarities were found as well as some significant differences. Both sets of spectra showed molecular- and fragment-ion peaks for aromatic and nonaromatic hydrocarbons and for compounds containing one to three oxygens. Strong peaks were observed in the spectra of the filterable sediment corresponding to aromatic compounds containing one nitrogen. These peaks were much weaker or absent in the spectra from the tube deposit. No spectra of the sediment or tube deposit from either fuel showed more than traces of sulfur-containing compounds.

An intense, nonaromatic fragment ion containing three oxygens was identified in the spectra the tube deposits from both fuels. This ion was also found in the spectra of the filterable sediments from both fuels although its intensity was much weaker. The ion could not be correlated with a

molecular ion from any particular compound type, but it may have originated from an alcohol, ether, or some other type that does not produce a significant molecular ion.

Although structural information obtained through mass-spectral analysis of solids formed during thermal-stressing experiments has not specifically identified precursors responsible for solids formation in either fuel, the results demonstrate the value of the method for identifying compound types associated with fuel degradation under conditions of high temperature, such as those encountered in turbine engines.

ACKNOWLEDGMENTS

Appreciation is expressed to F. L. Tilley, S. K-T. Yu, and M. White for technical assistance. This work was supported by the U.S. Department of Energy under Contract DE-FC22-83FE60149 and by the Pittsburgh Energy Technology Center through Military Interdepartmental Purchase Request FY1455-86-N0657.

LITERATURE CITED

- (1) Farlong, M., Fox, J., and Masin, J., AFWAL-TR-87-2042, Vol. IX, "Production of Jet Fuels from Coal-Derived Liquids, Results of Bench-Scale and Pilot-Plant Testing," AMOCO Oil Company, Naperville, IL, June, 1989.
- (2) Whisman, M. L., Cotton, F. O., Goetzinger, J. W., and Ward, C. C., "Radiotracer Study of Turbine Aircraft Fuel Stability," Bureau of Mines Report of Investigation 7493, Bartlesville, OK, March, 1971.
- (3) Goetzinger, J. W., Thompson, C. J., and Brinkman, D. W., "A Review of Storage Stability Characteristics of Hydrocarbon Fuels, 1952-1982," Report No. DOE/BETC/IC-83/3, Bartlesville Energy Technology Center, Bartlesville, OK, October, 1983.
- (4) Loeffler, M. C. and Li, N. C., Fuel, 64, 1047-1053 (1985).
- (5) Smith, R. O., Udseth, H. R., and Hazlett, R. N., Fuel, 64, 810-815 (1985).
- (6) Mayo, F. R. and Lan, B. Y., Ind. Eng. Chem. Prod. Res. Div., 25, 333-348 (1986).
- (7) Taylor, W. F. and Frankenfeld, J. W., Proceedings, 2nd International Conference on Long-Term Storage Stabilities of Liquid Fuels, ed. by L. L. Stavinoha, Southwest Research Institute, San Antonio, TX, 1986, pp. 496-511.
- (8) Malhotra, R. and St. John, G. A., Proceedings, 2nd International Conference on Long-Term Storage Stabilities of Liquid Fuels, ed. by L. L. Stavinoha, Southwest Research Institute, San Antonio, TX, 1986, pp. 327-335.

- (9) Wright, B. W., Kalinoski, H. T., Udseth, H. R., and Smith, R. D., Proceedings, 2nd International Conference on Long-Term Storage Stabilities of Liquid Fuels, ed. by L. L. Stavinoha, Southwest Research Institute, San Antonio, TX, 1986, pp. 526-539.
- (10) Bhan, O. K., Brinkman, D. W., Green, J. B., and Carley, B., Fuel, 66, 1200-1214 (1987).
- (11) Sutterfield, F. D., Brinkman, D. W., Bhan, O. K., Green, J. B., Goetzinger, J. W., Sturm, G. P., Jr., Speck, G., and Turner, L., Proceedings, 3rd International Conference on Stability and Handling of Liquid Fuels, ed. by R. W. Hiley, R. E. Penfold, and J. F. Pedley, The Institute of Petroleum, London, U.K., 1988, pp. 321-337.
- (12) Brinkman, D. W., Bhan, O. K., Green, J. B., Goetzinger, J. W., Grigsby, R. D., and Kamin, R., Proceedings, 3rd International Conference on Stability and Handling of Liquid Fuels, ed. by R. W. Hiley, R. E. Penfold, and J. F. Pedley, The Institute of Petroleum, London, U.K., 1988, pp. 796-807.
- (13) Mayo, F. R., Stavinoha, L. L., and Lee, G. H., Ind. Eng. Chem. Res., 27, 362-363 (1988).
- (14) Reddy, K. T., Cernansky, M. P., and Cohen, R. S., Energy & Fuels, 2, 205-213 (1988).
- (15) Bhan, O. K., Tang, S. Y., Brinkman, D. W., and Carley, B., Fuel, 67, 227-237 (1988).
- (16) Pedley, J. F., Hiley, R. W., and Hancock, R. A., Fuel, 67, 1124-1130 (1988).
- (17) Green, J. B., J. Chromatogr., 358, 53-75 (1986).
- (18) Green, J. B., Yu, S. K-T., Green, J. A., Doughty, D. A., Vogh, J. W., Grigsby, R. D., Chapter 3 in "Analysis of Heavy Oils: Method Development and Application to Cerro Negro Heavy Petroleum, Final Report," NIPER-452 (Vol. 1) (DE90000200). IIT Research Institute, National Institute for Petroleum and Energy Research, Bartlesville, OK, December, 1989.
- (19) Schronk, L. R., Grigsby, R. D., and Scheppelle, S. E., Anal. Chem., 54, 748-755 (1982).
- (20) Grigsby, R. D., Sturm, G. P., Jr., Green, J. B., Goetzinger, J. W., and Kamin, R. A., PREPRINTS, Div. of Petrol. Chem., ACS, 34 (4), 825-831 (1989).
- (21) Sturm, G. P., Jr., Grigsby, R. D., Goetzinger, J. W., Green, J. B., and Anderson, R. P., AFWAL-TR-87-2042, Vol. XIII, "Production of Jet Fuels from Coal-Derived Liquids, Evaluation of Storage and Thermal Stability of Jet Fuels Derived from Coal Liquids," IIT Research Institute, National Institute for Petroleum and Energy Research, Bartlesville, OK, May, 1990.

TABLE I
 INITIAL CHARACTERIZATION OF JP-8 FUELS DERIVED FROM
 PETROLEUM (2955) AND COAL (2987)

Property	Method	Fuel		Specification maximum
		2955	2987	
Color, Saybolt	D 156	+29	+14	---
Viscosity, -20 oC, cSt	D 445	4.8	4.4	8.0
Particulate, mg/mL	D 2276	0.26	1.2	1.0
Filtration time, min.	MIL-T-83133B, Appendix A	6.5	28	15
Peroxide, ppm	D 3703	0	0.5	---

TABLE II
 STORAGE-STABILITY RESULTS FOR PETROLEUM-DERIVED FUEL (2955)
 AND COAL-DERIVED FUEL (2987)

Aging Time	1 week		2 weeks		3 weeks		4 weeks	
	2955	2987	2955	2987	2955	2987	2955	2987
Fuel								
Property								
Filterable sedi- ment, mg/100 mL	0.8	0.3	1.3	0.5	1.5	1.0	2.7	9.1
Adherent sedi- ment, mg/100 mL	0.5	0.2	0.5	0.1	0.6	0.7	1.1	398
Total sediment, mg/100 mL	1.3	0.5	1.8	0.6	2.1	1.7	3.8	407
Peroxide, ppm (D 3703)	3.5	9.5	6.6	39.0	8.9	757	12.8	334
Color (D 1500)	L1.0	L0.5	L1.0	L0.5	L1.0	L0.5	L1.0	2.5

TABLE III
SEPARATION OF SEDIMENT FROM COAL-DERIVED FUEL (2987) BY HPLC.
YIELDS AND TYPICAL COMPOSITIONS.

Fraction	Yield, wt%	Typical composition
1	0.77	very weak acids, polynuclear aromatic hydrocarbons
2	1.21	2-3 ring pyrrolic benzologs
3	1.21	4-5 ring pyrrolic benzologs and hindered hydroxyaromatics
4	7.84	hydroxyaromatics
5	13.03	carboxylic acids
6	54.68	difunctional acids
Recovery	78.74	

TABLE IV
THERMAL STABILITY RESULTS (ASTM D 3241) FOR
PETROLEUM-DERIVED FUEL (2955) AND COAL-DERIVED FUEL (2987)

Property	Fuel		Specification maximum
	2955	2987	
Tube deposit rating at tube temp. of 260° C	1	1	3
Pressure drop, mm HG	0	0	25
Breakpoint, °C	275	295	---

TABLE V

MASS-SPECTROMETRIC ANALYSIS OF FILTERABLE SEDIMENT AND TUBE DEPOSIT FROM THERMALLY STRESSED FUEL 2987. IDENTIFICATION OF HYDROCARBONS.

Suggested origin ¹	Elemental composition:	Homologous ions detected	
	C_nH_{2n+z}	Filter	Tube
	$z = +2$	---	---
	+1	71-155	71-183
Olefins, cycloalkanes (70)	0	70-140 ²	70-140,168 ²
	-1	69-167	69-153
Dienes, cycloalkenes (68), bicycloalkanes	-2	68-194	68-194
	-3	81-207	81-179
Cyclic dienes (66), tricycloalkanes	-4	80-178	80-192
	-5	79-191	79-205
Alkylbenzenes (78)	-6	92,106,134,148,176,190	78-162
	-7	77-189	77-203
Indans (118), tetralins	-8	76-188 ³	76-188 ³
	-9	75-173	75-187
Indenes (116), dihydronaphthalenes	-10	74-200 ³	74-186 ³
	-11	73-157	87-185,213
Naphthalenes (128)	-12	114-142,170-212 ³	114-184 ³
	-13	113-211	113-197
Acenaphthenes (154), biphenyls	-14	126,154 ³	126,154-196 ³
	-15	125-195	139-195
Acenaphthylenes (152), phenalenes, fluorenes	-16	152-194	152-208
	-17	151-193	151-207
Anthracenes (178), phenanthrenes	-18	150-206 ³	164-220 ³
	-19	163,191,205	163,205
Methylenephenanthrenes (190), phenyl-naphthalenes	-20	176,190 ³	176,204,218 ³
	-21	189,203	133,189-217
Fluoranthenes, pyrenes (202)	-22	202	202,216,244
	-23	215	145,215,229

¹Molecular mass of first member of homologous series in parentheses.

²Series may contain rearrangement ions.

³First members of series may represent rearrangement ions.

TABLE VI

MASS-SPECTROMETRIC ANALYSIS OF FILTERABLE SEDIMENT AND TUBE DEPOSIT
FROM THERMALLY STRESSED FUEL 2987. IDENTIFICATION OF COMPOUNDS
CONTAINING ONE OXYGEN.

Suggested Origin ¹	Elemental Composition:	Homologous Ions Detected	
	$C_nH_{2n+z}O$	Filter	Tube
	$z = +2$	---	---
	+1	73	---
Tetrahydrofurans (72)	0	---	72
	-1	71-113,239	71-127
Dihydrofurans (70)	-2	70-112	70-126
	-3	69-139	69-139
Furans (68)	-4	68-110,138	68-152
	-5	81-151	81-165
Phenols (94)	-6	94-150	94-122
	-7	93-163,191	107-135
Dihydrobenzofurans (120), hydroxyindans	-8	120-162	106-162 ²
	-9	105-175	105-161
Benzofurans (118), indanones	-10	104-188 ²	104-188 ²
	-11	131-201	131-173
Naphthols (144)	-12	130-214 ²	144-200
	-13	143-199	157-185
Acenaphthenols (170)	-14	156-226 ²	184,198
	-15	155-211,253	155-197
Dibenzofurans (168)	-16	168-210	182,196
	-17	181-209	181-209
Fluorenones (180), phenalenones	-18	180-222	---
	-19	207	---

	-22	218, 246	---

¹Molecular mass of first member of homologous series in parentheses.

²First member of series may represent rearrangement ion.

TABLE VII

MASS-SPECTROMETRIC ANALYSIS OF FILTERABLE SEDIMENT AND TUBE DEPOSIT
FROM THERMALLY STRESSED FUEL 2987. IDENTIFICATION OF COMPOUNDS
CONTAINING THREE OXYGENS.

Suggested Origin ²	Elemental	Homologous	
	Composition: $C_nH_{2n+2}O_3$	Ions Detected Filter	Tube
	$z = +2$	78,162	---
	+1	119-147	---
	0	104,146-174	---
	-1	131,145	---
	-2	116-172	242
	-3	129,157	129 ³ ,143, 185,241
	-4	100,128,170	100,128,142
	-5	141-183	127
	-6	154,182	---
	-7	167,181	---
	-8	166,208,222	152
	-9	221,235	151
	-10	150-178,220	---
	-11	149-191	149

¹Peaks overlap with those containing one nitrogen.

²Multifunctional compounds.

³Very strong peak at m/z 129.

TABLE VIII

MASS-SPECTROMETRIC ANALYSIS OF FILTERABLE SEDIMENT AND TUBE DEPOSIT
FROM THERMALLY STRESSED FUEL 2987. IDENTIFICATION OF COMPOUNDS
CONTAINING ONE NITROGEN.

Suggested Origin ²	Elemental Composition: C _n H _{2n+z} N	Homologous Ions Detected	
		Filter	Tube
Aliphatic amines	z = +3	---	---
	+2	72-100	268,296 ⁴
Pyrrolidines (71), piperidines	+1	85	---
	0	70-112	294 ⁴
Pyrrolines (69)	-1	69-125,153	---
	-2	68-152	---
Pyrroles (67)	-3	81,95,123	---
	-4	80-150	---
Pyridines (79), anilines	-5	79-149	---
	-6	78-162	---
Indolines (119)	-7	91-175 ³	---
	-8	76-174	---
Indoles (117)	-9	75,103-173 ³	---
	-10	88-158,228	242 ⁴
Quinolines (129), isoquinolines	-11	129-171	185,241 ⁴
	-12	114-184	---
Phenylpyridines (155)	-13	127-183 ³	---
	-14	140-196	---
Carbazoles (167)	-15	153-181 ³	---
	-16	152,194,208	---
Acridines (179), phenan- thridines	-17	179,193,221	---
	-18	178,220	---
	-19	163-191	---
	-20	162-204,232	---
Aminofluoranthenes (217), aminopyrenes	-21	217	---
	-22	188,216-244	---

¹Peaks overlap with those containing three oxygens.

²Molecular mass of first member of homologous series in parentheses.

³First members of series may represent rearrangement ions.

⁴Ions probably originate from different molecular structure.

TABLE V

MASS-SPECTROMETRIC ANALYSIS OF FILTERABLE SEDIMENT AND TUBE DEPOSIT
FROM THERMALLY STRESSED FUEL 2987. IDENTIFICATION OF HYDROCARBONS.

Suggested origin ¹	Elemental composition: C_nH_z n^2n+z	Homologous ions detected	
		Filter	Tube
	$z = +2$	---	---
	+1	71-155	71-183
Olefins, cycloalkanes (70)	0	70-140 ²	70-140,168 ²
	-1	69-167	69-153
Dienes, cycloalkenes (68), bicycloalkanes	-2	68-194	68-194
	-3	81-207	81-179
Cyclic dienes (66), tricycloalkanes	-4	80-178	80-192
	-5	79-191	79-205
Alkylbenzenes (78)	-6	92,106,134, 148,176,190	78-162
	-7	77-189	77-203
Indans (118), tetralins	-8	76-188 ³	76-188 ³
	-9	75-173	75-187
Indenes (116), dihydronaphthalenes	-10	74-200 ³	74-186 ³
	-11	73-157	87-185,213
Naphthalenes (128)	-12	114-142, 170-212 ³	114-184 ³
	-13	113-211	113-197
Acenaphthenes (154), biphenyls	-14	126,154 ³	126,154-196 ³
	-15	125-195	139-195
Acenaphthylenes (152), phenalenes, fluorenes	-16	152-194	152-208
	-17	151-193	151-207
Anthracenes (178), phenanthrenes	-18	150-206 ³	164-220 ³
	-19	163,191,205	163,205
Methylenephenanthrenes (190), phenylnaphthalenes	-20	176,190 ³	176,204,218 ³
	-21	189,203	133,189-217
Fluoranthenes, pyrenes (202)	-22	202	202,216,244
	-23	215	145,215,229

¹Molecular mass of first member of homologous series in parentheses.

²Series may contain rearrangement ions.

³First members of series may represent rearrangement ions.

SYMPOSIUM ON THE STABILITY AND OXIDATION CHEMISTRY OF MIDDLE DISTILLATE
FUELS, DIVISION OF FUEL AND PETROLEUM CHEMISTRY, AMERICAN CHEMICAL
SOCIETY, WASHINGTON D.C. MEETING, AUGUST 1990

THE THERMAL DEGRADATION OF AVIATION FUELS IN JET ENGINE INJECTOR FEED-ARMS:
RESULTS FROM A HALF-SCALE RIG

By

R.H. Clark* and P.A. Stevenson

Shell Research Ltd., Thornton Research Centre, P.O. Box 1, Chester CH1 3SH

INTRODUCTION

Aviation kerosine undergoes significant heating within the fuel system of an aviation gas turbine. Heating occurs because, firstly, fuel is used as a coolant for the engine lubricating oil and for other heat exchanger systems (e.g. avionics, air conditioning, etc.) and, secondly, because certain regions have a high intrinsic temperature (e.g. injector feed-arms). The feed-arms, which pass fuel directly into the combustor, represent the most severe fuel system environment in that the combination of high fuel inlet temperatures and very hot metal surface can promote a very high degree of thermal degradation. In this event, the small apertures within the fuel atomisers can become obstructed, causing flow restriction or fuel spray pattern distortion, and leading ultimately to engine malfunction. Thus, the thermal stability of aviation fuels within the feed-arm environment is crucial for the safe operation of gas turbine engines.

Whilst the thermal degradation of aviation fuels is well documented¹, relatively few researchers have addressed the specific problem of deposition within burner feed-arms²⁻⁴. Two such investigations were collaborative projects³⁻⁴ between Shell Research and Rolls-Royce plc., Derby. A full-scale rig simulation⁵, the IFAR (Injector Feed-Arm Rig), was used to look at the effects on fouling of fuel flow rate and fuel pressure, the addition of additives, and rig repeatability. However, the large appetite of the rig (50,000 litres of fuel per test) prevented a more detailed examination of the contribution of fuel chemistry to the fouling.

The study reported here used a half-scale rig, the MIFAR (Mini Injector Feed-Arm Rig), which is similar in design to the IFAR and operates at identical temperatures. The use of this scaled-down rig with its significantly decreased fuel appetite - a reduction from 50,000 litres to 2,000 litres/test - has enabled the effects of fuel processing and chemistry on feed-arm fouling to be evaluated for a wide range of fuels. In addition, it has permitted correlations to be drawn between the MIFAR and other thermal stability rigs.

The objectives of the research program were as follows:

- To make a direct comparison of fuel performance in large- and small-scale injector feed-arm rigs, and thence to pursue the initial findings about the feed-arm deposition process.

- To relate a fuel's deposition tendency to its chemical composition and to correlate the MIFAR with other predictors of fuel thermal stability, in particular to the JFTOT (Jet Fuel Thermal Oxidation Tester).
- To gain greater insight into the action of one additive, the approved metal deactivator, Du Pont's MDA, specifically to confirm related findings⁵ on its dual action as metal chelator and metal passivator.

EXPERIMENTAL

Mini Injector Feed-Arm Rig (MIFAR)

The philosophy underlying the aviation fuel thermal stability testing pursued at Shell Research Ltd has been always to construct simulation rigs, using actual engine components where possible, and to measure fuel deposition quantitatively at well characterised temperatures. The MIFAR, illustrated in Figure 1, is a realistic, half-scale simulation of an aircraft fuel system. Fuel is supplied from external storage tanks via a 0.45 μm filter to a glass reservoir (to simulate a wing tank); in the current programme, the reservoir was left unheated to simulate the absence of fuel recirculation in civil aviation practice. On leaving the reservoir, the fuel is pressurised to 250 psi by a Lucas high-pressure piston pump and supplied to a fuel line heater, comprising two stainless-steel sheathed electrical cartridge heaters in series; the heaters simulate the avionic and engine cooling components of a gas turbine engine. The hot (165°C), pressurised fuel is then fed to a model feed-arm mounted in a fluidised sandbath, which simulates the hot compressor discharge air environment. Thereafter, the fuel passes through filters, is cooled and dumped to waste. A DEC micro PDP-11 computer provides automatic control of the rig operating conditions via process control software; the same software also provides data logging and reporting functions.

At Shell Research the model feed-arms are designed to simulate the burner stems that lead to the nozzle assemblies and are plain, thick-walled steel tubes (0.25" O.D. x 0.090" I.D.), corresponding to a half-scale system. The tubes are instrumented with thermocouples mounted in grooves along the arms to allow the temperature of the inner wall (TIW) to be measured. Only the central 10 cm of the arm (corresponding to 7.2 cm^2) are immersed in the sandbath. Bulk fuel temperatures at the inlet and outlet of the arm are determined by the associated thermocouples.

Deposition Monitoring

The deposition process is monitored "on-line" during a test by measuring the rise in the inner wall temperature (ΔTIW) of the feed-arm; this rise occurs because of the deposit's insulating effect on heat transfer. After a test has been completed, the deposit mass is calculated from the amount of carbon (W_c) recovered as carbon dioxide from the controlled combustion of the deposit. Empirical data have shown that the weight of carbon recovered is 70% of the original deposit weight; this allows W_c values to be converted into deposit weight (W_d) values, thus providing an "off-line" reference of fouling rate.

Test conditions

As with the IFAR⁴, the tests were targetted to reflect severe thermal conditions; therefore a bulk fuel inlet temperature of 165°C and an inner wall temperature of 300°C were selected. The fuel pressure was 250 psi, and a flowrate of 300 ml/min was chosen to give a turbulent flow regime (Reynold's Number, Re = 8000).

The 300°C TIW was achieved by adjusting the temperature of the fluidised sandbath within the range 410°-450°C at the start of each test; thereafter the sand bath was maintained at a constant temperature.

Test fuels

The ten fuels studied included examples of the three main process types: sweetening, hydrotreating and hydrocracking. Most were Jet A/A-1 type fuels meeting the DERD 2494/ASTM D1655 specifications, but some were chosen because of their poor/borderline stability. The fuels and their inspection properties are listed in Table 1. The fuels encompass a wide range of sulphur contents and responses in the JFTOT specification thermal stability test. These fuels were used in a series of 16 tests (detailed in Table 2).

RELATED THERMAL STABILITY TESTS/RESULTS

Fuel performance within the MIFAR was not considered in isolation; the wide range of thermal stability tests available at Shell Research enabled fuel performance in the MIFAR to be compared with other measures of stability. From these data, two complementary pieces of information were derived: firstly, the ability of other tests to predict fuel performance - as determined in a realistic environment; secondly, the prediction of fuel performance from more fundamental compositional information.

The IFAR

The IFAR was built as part of a programme undertaken jointly by Shell Research and Rolls-Royce to study injector feed-arm fouling⁴. The rig, whilst similar in principle to the MIFAR, is essentially a full-scale simulation. The operating principles, test temperatures and measurements made are directly comparable and essentially identical to those of the MIFAR. Insights gained from the IFAR into feed-arm fouling have been published in the literature^{4,5}.

The single tube heat transfer rig (STHTR)

The STHTR realistically simulates fuel degradation within an oil-cooler⁶. It is Shell's principal benchmark of fuel thermal stability in service, insofar as it duplicates the dimensions, fuel flow rates and metallurgy of an oil-cooler. In the rig, the fuel undergoes three stages of heating to simulate those heat sources encountered in an aircraft fuel system:

- Fuel tank heating (aerodynamic heating, fuel transfer/recirculation)
- Heating from hydraulics/avionics/environmental system heat exchangers
- The engine oil-cooler (i.e., that component simulated by the test heat-exchanger)

Fuel degradation is monitored via the reduction in heat-transfer coefficient of the test element.

JFTOT testing

For commercial purposes, the thermal stability of aviation fuels is generally assessed in the Jet Fuel Thermal Oxidation Tester⁷ (JFTOT, ASTM method D3241) at a defined temperature. In essence, fuel is passed over a heated metal tube and then through a filter; the fuel is rated on a go/no go basis by the tube lacquer or the blockage of the filter. For research purposes this is not very informative. Accordingly, in the current work, fuels were ranked using the breakpoint temperature (i.e., the highest temperature sustainable without causing the fuel to fail on the tube lacquer or filter blockage criterion.) In addition, the degree of carbon deposition in the tests carried out at a 350°C tube temperature was also determined.

Flask oxidation studies

The flask oxidation test (FOT) is an in-house method of measuring the liquid phase oxidation rate of fuels and thereby determining their other oxidation characteristics⁸. Perturbing the system with a radical initiator (t-butyl peroxide) enables a fuel's intrinsic radical initiation rate to be determined. This rate has been found to be a good predictor of a fuel's deposition tendency within our oil-cooler simulation.

MIFAR RESULTS: DEPOSITION RATES

The raw MIFAR test results comprise two types of measurement:

- (i) The tube wall temperature, TIW, recorded as a function of time throughout the test;
- (ii) The total weight of deposit formed on the feed-arm wall, W_D , at the end of test.

By plotting, in log-log form, the end-of-test increase in wall temperatures, ΔTIW , against the weight of deposit, W_D , for each test, an empirical linear relationship between the two parameters has been identified:

$$W_D = Y(\Delta TIW)^Z \quad \dots (1)$$

The value of Y is 1.82 and that of Z is 1.0, resulting in a linear relationship. This compares with the near quadratic form of relationship (i.e. $W_D \propto (\Delta TIW)^{2.2}$) found in the full-scale IFAR. The reason

for the differing exponents in the expression is obscure. One supposition is that the lower sandbath temperature of the MIFAR (400°C versus 540°C) has resulted in different heat-transfer characteristics between the sandbath and the feed-arm. However, there could well be other consequences of reducing scale.

The relationship has been used to convert the ATIW recorded during the test to the equivalent W_0 , so generating a picture of the build-up of deposit as a function of duration (Figures 2 - 4). Now, assuming that deposition occurs only on the directly heated surface of 7.2cm² area, deposition rates have been calculated for each test (Table 2).

The main points are as follows:

- (1) The form of the curves confirms our earlier findings as to the nature of the deposition process; namely, it comprises three distinct phases:
 - A finite, variable-duration "induction period", during which no significant deposition occurs.
 - A period of near-constant deposition rate.
 - In some tests, a decrease in deposition rate towards the end of test.
- (2) Deposition rates span a factor of 25. The sweetened fuels (excluding off-grade Fuel A) encompass the range 0.1 - 0.5 mg cm⁻²h⁻¹ and the hydrotreated fuels are all less than 0.05 mg cm⁻²h⁻¹.
- (3) The highest deposition rate was that of the off-grade Fuel A, which was consistent with its high metal content. However, addition of MDA restored this high rate to that more typical for a sweetened fuel.

DISCUSSION

The nature of the deposition process

The graphs of the temporal evolution of deposits on the feed arms (Figure 2 - 4) show features identical to those in the IFAR study⁴, i.e. the three main phases in the deposition process noted above,

- Finite hold-up or induction period, during which little or no deposition is detected. This corresponds to the low deposition rate on a clean steel surface.

Followed by:

- A higher constant rate of deposition on a fouled surface.

Ultimately

- A reduction in deposition rate due to the insulating effect of the cumulative deposit.

However, the current studies, with the large suite of fuels, have given a much clearer insight into the deposition process. Examination of the data reveals an obvious link between the length of the induction period (r_{ip}) and the post-induction deposition rate (r_p); i.e. the less stable a fuel is, the shorter its induction period and the higher its deposition rate. In fact, it is reasonable that there should be a relationship between these two parameters; the reciprocal induction period ($1/r_{ip}$) is a measure of fuel deposition rate on a clean metal surface, whereas the post-induction rate is a measure of deposition rate on a fouled surface. In Figure 5, the plotting of deposition rate versus $1/r_{ip}$ yields a straight line passing through the origin, illustrating the relationship between two measures of deposition. The data can be interpreted further, by making certain assumptions. Examination of the W_p versus duration plots suggests that the induction period is the time taken for 5 mg of deposit to build up. From this, an estimation can be made of the relative fuel deposition rates on a clean surface versus those on a lacquered one; the ratio obtained is 1:4.

The influence of MDA

The mechanism by which the metal deactivator additive (MDA) affects fuel performance can be resolved into two components:

- Metal chelation, the claimed role of the additive, whereby dissolved metals within the fuel are rendered catalytically inactive. In this mode, bulk fuel reactivity is affected, thus increased chelation is manifested as a decrease in deposition rate.
- Metal passivation, in which the MDA adsorbs onto and, thereby, modifies a clean metal surface, thus inhibiting formation of the first layer of deposit. Increased passivation is evident from an increase in induction periods.

These feed-arm studies have provided an excellent illustration of the above mechanisms. Consider the test sequence 1 - 4 (Figure 2 - 4), in which an off-grade fuel (Fuel A) contaminated with catalytic metal is progressively doped with higher concentrations of the MDA additive (0, 5.7 and 12 mg l⁻¹). (i) The base fuel gave the highest deposition rate 1.1 mg cm⁻² h⁻¹ and the shortest induction period of 3 hours. (ii) At 5.7 mg l⁻¹, MDA is present in excess relative to the metal contamination (0.25 mg l⁻¹ of MDA would be required). Thus, all metals are chelated and the deposition rate decreases to 0.3 mg cm⁻² h⁻¹ via the chelation mechanism. However, in tandem, the induction period increases from 3 to 8 hours via the passivation mechanism. (iii) At 12 mg l⁻¹ there can be no extra benefit from chelation over and above that seen at the 5.7 mg l⁻¹ level, which was already an excess of MDA. In consequence, the deposition rate remains essentially unaffected. However, this additional MDA can affect the passivation mechanism and increase the induction period from 8 to 20 hours.

From our previous work⁴ using metal-free fuel to avoid the chelation mechanism, it can be estimated from the induction period data that deposition rates on a clean steel surface are reduced by two-thirds by the MDA passivation associated with the 5.7 mg l⁻¹ doping level.

Comparing the MIFAR with other measures of thermal stability

A major aim of the research programme was to predict fuel performance within the MIFAR from compositional data, and to relate the performance to other thermal stability rigs. Six potential predictors of fuel thermal stability were considered:

- (1) Radical initiation rate (FOT)
- (2) JFTOT breakpoint
- (3) JFTOT carbon deposit determination
- (4) Oil-cooler rig (i.e. STHTR) data
- (5) Fuel sulphur content
- (6) Total acid content (TAC) via ion-exchange

Accordingly, MIFAR test results in the form of deposition rates were correlated with these other measures. The resultant statistical information is illustrated in Table 3 and the correlation graphs in Figures 6 and 7.

Two striking features can be observed from the statistics:

- (1) The lack of a significant correlation between the oil-cooler rig and the MIFAR (correlation confidence is well below the significant level of 95%)
- (ii) The superiority of all the analytically derived predictors (i.e. sulphur, R_1 and TAC), when compared to rig-based tests, in forecasting MIFAR deposition rates.

In fact these two points are probably related. The MIFAR, in its current configuration, simulates a fuel system that is not subject to wing tank heating. Thus, the fuel is not resident in any heated component for any length of time, and as a consequence one would expect deposition to be influenced by fuel chemistry in a straightforward manner, i.e. oxidation followed by reaction of intermediates with fuel polar species (acids and sulphur compounds). It is seen that the statistical data are in accord with such a mechanism. The poor correlation with the STHTR may well relate to the more complex chemistry associated with the multi-stage heating system of the rig whereby the fuel is pre-heated in a simulated wing tank for a comparatively long residence time (ca. 1 hour) before encountering the test section.

The poor correlation of the MIFAR with either JFTOT measure could result from the JFTOTs' lack of realism in utilising a laminar fuel flow condition and thus not responding solely to fuel chemistry⁷.

Overall, the best prediction of fuel thermal stability in both the large-scale rigs, i.e. the MIFAR and STHTR, is given by total acid content (TAC) via ion-exchange chromatography⁸.

CONCLUSIONS

- A half-scale injector feed-arm fouling rig, the MIFAR, provides clear confirmation of the deposition mechanisms first observed in full-scale

rig (i.e. the IFAR) measurements, namely, the three distinct deposition phases of induction, constant rate deposition and tail-off. However, working with a large suite of fuels enables the mechanism to be resolved at a greater level of detail. In particular, relationships have been drawn up between fuel deposition on a clean steel surface (estimated from the induction period length) and deposition on a fouled surface (post induction).

- MIFAR data provide an excellent illustration of the mode of action of the two mechanisms by which the approved thermal-stability-enhancing additive MDA affects fuel-deposition tendency: metal chelation and metal passivation. Chelation is measured as a change in the post-induction deposition rate, whereas passivation is measured in terms of the length of the induction period.
- Simple chemical composition parameters are superior to other measures for predicting the thermal stability performance of fuels in the MIFAR. These three parameters, radical initiation rate, fuel total sulphur and total acid content (TAC), are in accord with our current understanding of the chemistry of the degradation mechanism. TAC by ion-exchange chromatography is considered the best measure.
- The poor MIFAR/STHTR correlation suggests that the more complex heating stages within the STHTR have a significant effect on the chemistry of the decomposition process.

ACKNOWLEDGEMENTS

The authors thank Mr. G. Houlbrook and Mrs L. Smith for their assistance in the experimental work and Dr. D.R. Kendall for helpful discussions.

REFERENCES

1. CRC Report No. 509, April 1979, CRC, Boca Raton, Fl.
2. C.A. Moses, M.W. Shayeson and P.A. Karpovich, ASME Paper 86-GT-94.
3. A.E. Peat, ASME Paper 82-GT-27.
4. D.R. Kendall, G. Houlbrook, R.H. Clark, S.P. Bullock and C. Lewis, Injector Feed Arm Fouling - Part 1 Results from a Full-scale Rig, presented at the 30th International Gas Turbine Congress Tokyo, Oct 1987.
5. R.H. Clark, Paper #47, p283, presented at the 3rd International Conference on the Stability and Handling of Liquid Fuels, London, Sept 1988, Institute of Petroleum (1989).
6. J.S. Mills and D.R. Kendall, ASME paper 85-GT-33.
7. R.H. Clark and L. Thomas, SAE Paper 881533.
8. D.R. Kendall and J.S. Mills, Ind. Eng. Chem. Prod. Res. Dev., Vol 25, June 1986, pp 360-366.
9. R.H. Clark and L. Smith, Paper #46, p268, presented at the 3rd International Conference on the Stability and Handling of Liquid Fuels, London, Sept 1988, Institute of Petroleum (1989).

Table 1
Inspection properties of fuels used in the MIFAR fouling studies

FUEL	A	B	C	D	E	F	G	H	I	J
PROCESS TYPE	SWEETENED	MERX SWEETENED	MERX SWEETENED	-50/50 STRAIGHT RUN/ HYDROCRACKED	MERX SWEETENED (TUEL 7) +12v UNTREATED LCCO	MERX SWEETENED	MERX SWEETENED	HYDROCRACKED PRODUCT	HYDROTREATED	HYDROTREATED
AROMATICS, Iv	18.9	19.2	19.2	18.4	27.7	17.5	17.4	8.6	16.0	14.7
OLEFINS, Iv	0.7	0.3	0.8	0.2	0.4	0.5	0.3	0.4	<1	0.4
MERCAPTAN SULPHUR, Iv	0.0002	0.0003	0.0005	0.0004	0.0008	0.0017	0.0002	0.0001	-	0.0001
TOTAL SULPHUR, Iv	0.14	0.03	0.10	0.01	0.30	0.21	0.133	0.013	0.002	0.004
ACTIVITY, mgKOH g ⁻¹	0.001	0.001	<0.001	0.007	0.005	0.003	0.001	0.001	0.004	0.001
*Total Acids, mg l ⁻¹	-	190	123	112	273	153	281	27	47	16
Distillation										
IBP, °C	163	151	148	153	154	141	147	171	155	160
50%, °C	186	203	190	197	223	184	180	210	200	190
FDB, °C	265	250	252	256	350	260	259	278	259	263
Density, kg l ⁻¹	0.8078	0.8110	0.7909	0.8032	0.8214	0.7960	0.7878	0.8033	0.7960	0.8016
Copper, µg l ⁻¹	47	2	7	<2	53	16	<2	2	2	<2
Antioxidant, mg l ⁻¹	#11	#11	#11	18	#11	#11	#11	20	20	20
JFTOT Breakpoint, °C	250	285	265	280	245	250	285	305	285	285

* Total Acid Content, TAC, extracted by ion exchange chromatography

Table 2
Comparison between MIFAR deposition rates and some other thermal stability indices

MIFAR Test no.	Fuel	MIFAR deposition rate mg cm ⁻² h ⁻¹	IFAR deposition rate mg cm ⁻² h ⁻¹	Single tube rig ΔHTC, I h ⁻¹	JFTOT breakpoint, °C	JFTOT carbon deposit, µg	Radical initiation rate mol l ⁻¹ s ⁻¹ x 10 ⁷
1, 2	A	1.04, 1.18	-	0.33	250	-	26.9
3, 4	A + MDA 5.7 ppm, 12 ppm	0.31, 0.50	-	-	-	-	-
5, 6	B	0.29, 0.37	0.43	1.3	285	143	2.5
7, 8	C	0.18, 0.36	0.43	0.6	265	138	5.8
9	D	0.15	0.47	1.9	290	71	4.9
10	E	0.41	0.63	12.3	245	553	4.9
11, 12	F	0.11, 0.10	-	1.3	250	307	6.3
13	G	0.22	-	5.4	285	87	0.5
14	H	0.046	-	0.2	305	59	0.70
15	I	0.049	-	0.19	285	54	0.93
16	J	0.046	-	0.002	285	25	0.76

Table 3

The correlation of MIFAR deposition rates with some other thermal stability indices

Test	Correlation Confidence, %	R	MSE*	Gradient [§]	Intercept [§]
$R_i, 10^{-7} \text{ mole l}^{-1} \text{ s}^{-1}$	99.7	0.730	0.106	$0.62 \pm 27\%$	$-1.0 \pm 12\%$
JFTOT, B.P., °C	95.5	0.542	0.160	$-7.9 \pm 45\%$	$1.8 \pm 46\%$
STHTR, $\Delta HTC, \% \text{ h}^{-1}$	85.4	0.409	0.189	$0.21 \pm 64\%$	$-0.66 \pm 18\%$
S, % M	48.2	0.620	0.140	$0.41 \pm 37\%$	$-0.16 \pm 19\%$
# JFTOT, C.D. μg	96.3	0.601	0.090	$0.58 \pm 41\%$	$-2.0 \pm 25\%$
# TAC, mg l^{-1}	99.9	0.843	0.049	$0.77 \pm 20\%$	$-2.39 \pm 13\%$

+ MSE: Mean square error, |R| : Correlation Coefficient

§ Values in the expression

$$\log_{10} (\text{MIFAR}) = \text{Intercept} + \text{Gradient} * \log_{10} (\text{Test index})$$

Data set for these indices comprise 12 measurements. All others 14 measurements

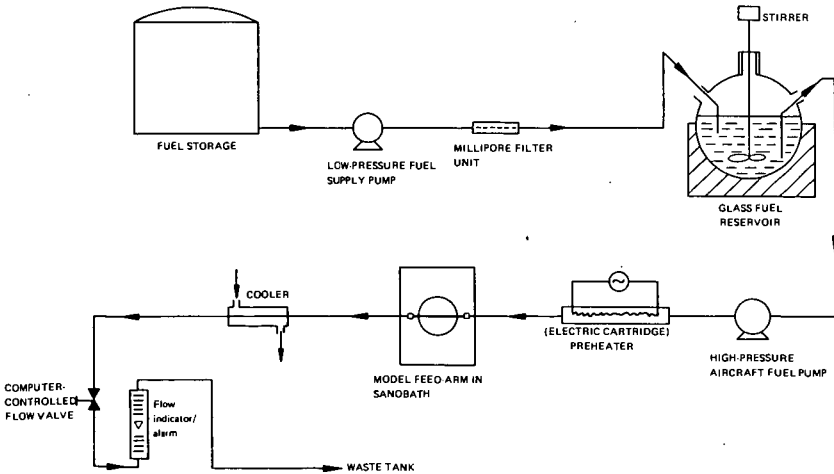


FIG. 1 - Schematic diagram of the Mini Injector Feed-Arm Rig (MIFAR)

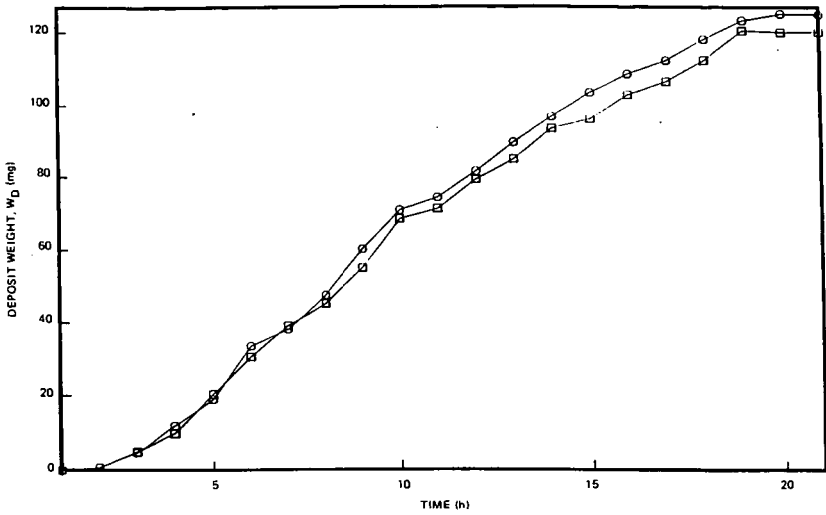


FIG. 2 - The evolution of feed-arm deposition for Fuel A, Test 2

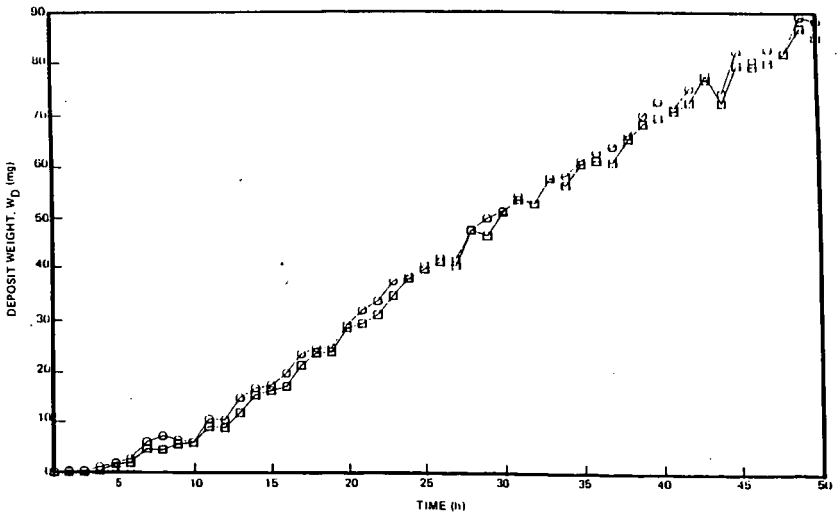


FIG. 3 - The evolution of feed-arm deposition for Fuel A + 5.7 mg l⁻¹ MDA

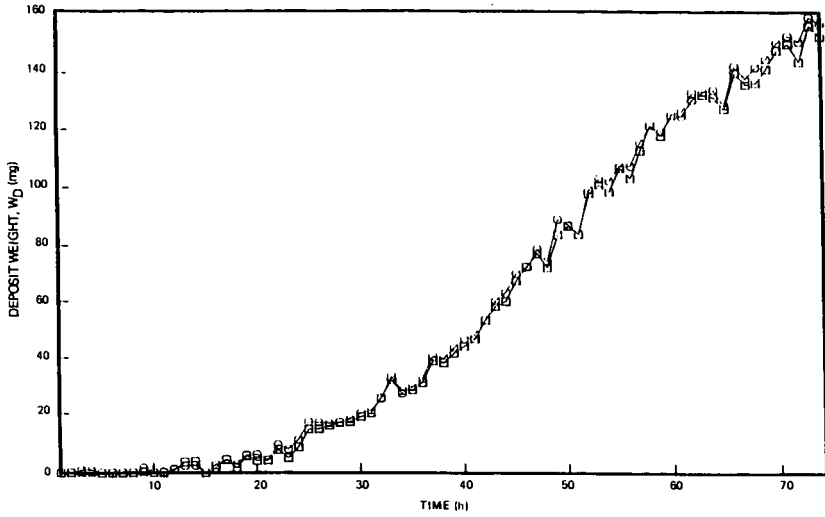


FIG. 4 - The evolution of feed-arm deposition for Fuel A + 12 mg l⁻¹ MDA

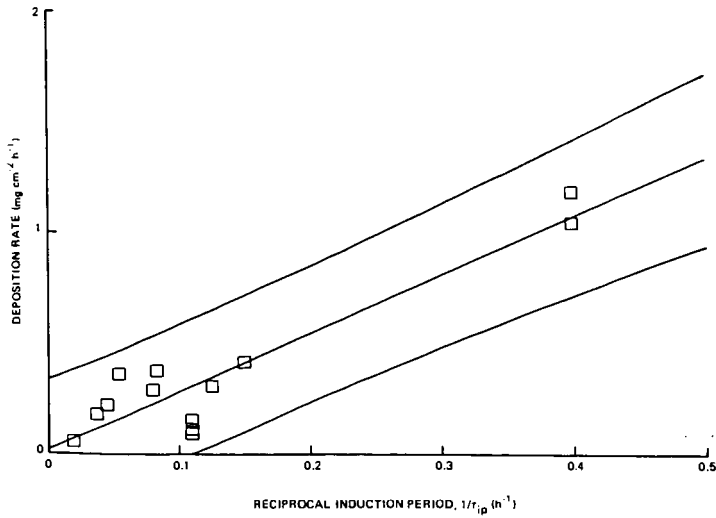


FIG. 5 - The relationship between feed-arm deposition rate and induction period

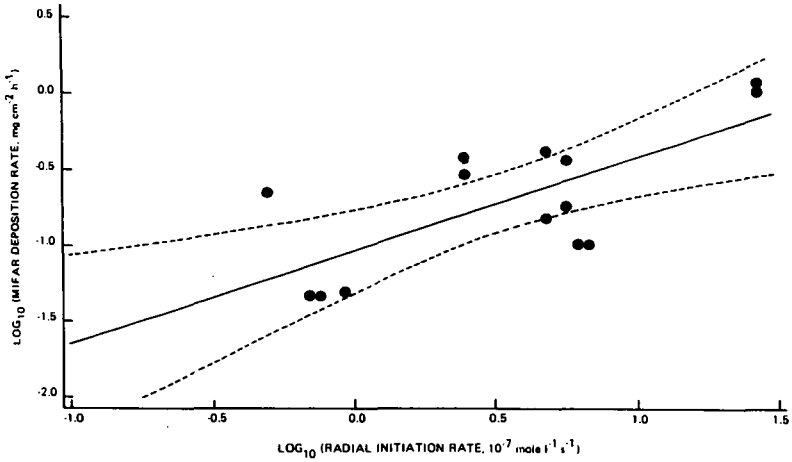


FIG. 6 - The correlation between feed-arm deposition rate in the MIFAR and fuel radical initiation rate

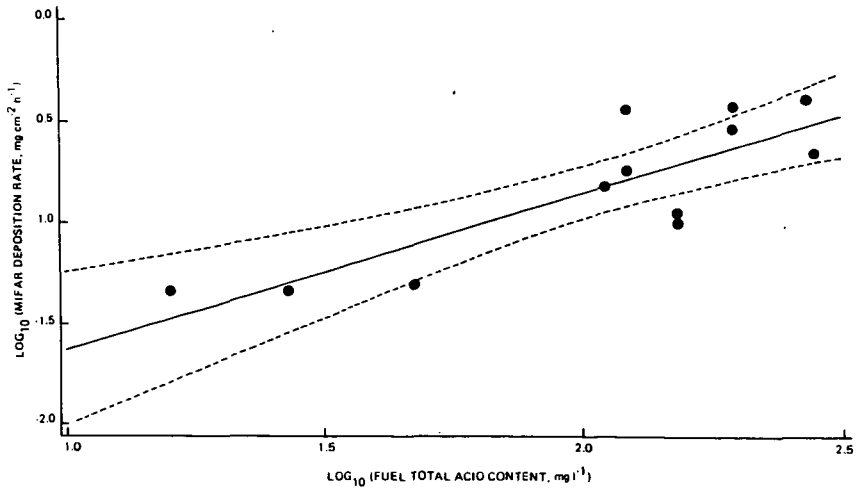


FIG. 7 - The correlation between feed-arm deposition rate in the MIFAR and fuel total acid content

THE ROLE OF SURFACE COMPOSITION IN FUEL DEPOSITION

L.L. Stavinoha, D.W. Naegeli and L. McInnis
Belvoir Fuels and Lubricants Research Facility
Southwest Research Institute
San Antonio, Texas 78238

Keywords: Thermal stability, JFTOT, deposit, metal catalyst

Abstract: Experiments were performed in a Hot Liquid Process Simulator (HLPS) configured and operated such that it performed under conditions similar to Jet Fuel Thermal Oxidation Tester (JFTOT) ASTM D 3241 requirements. The JFTOT heater tubes used were 316 stainless steel (SS), 304 SS, and 304 SS tubes coated with aluminum, magnesium, gold, and copper. A low sulfur Jet A fuel with a breakpoint temperature of 254°C was used to create deposits on the heater tubes at temperatures of 300°, 340°, and 380°C. Deposit thickness was measured by dielectric breakdown voltage and Auger ion milling. Auger ion milling of the deposits showed the order of deposition to be copper > magnesium = 316 SS > gold > aluminum. The dielectric strength method indicated that 316 SS > 304 SS > gold > magnesium = aluminum = copper. The pronounced differences between the deposit thickness measuring techniques suggest that the dielectric strength of the deposit is strongly affected by metal ions that become included in the bulk of the deposit. The results show that the surface temperature and composition play an important role in deposition.

Introduction: The effect of fuel system metallurgy on fuel stability is an important concern in the development of high efficiency/advanced engine technology such as adiabatic, low heat rejection engines and hypergolic injection systems. Several studies have shown that trace metals adversely affect the thermal stability of hydrocarbon fuels.(1,2) Metal concentrations as low as 15 ppb of copper, 25 ppb of iron, 100 ppb of zinc, and about 200 ppb of lead have been found to cause significant change in the thermal stability of jet fuels. These studies suggest that the slightest metallic contamination could cause a significant change in the thermal oxidative stability of hydrocarbon fuels. In fact, the theory has been advanced that all hydrocarbon autoxidations are trace metal catalyzed.(3)

Recent work (4), in which only limited data are available, suggests that aluminum tubes with magnesium-enriched surfaces tend to have lower deposit buildups than the standard aluminum tubes. If such minor changes in surface metallurgy cause significant changes in the rate of deposit formation, major changes in surface composition could dramatically effect processes such as deposit adherence and oxidation catalysis.(5) Experiments with metal deactivator in dodecane using JFTOT equipment suggest that the effect on deposit reduction may be a consequence of interactions in the liquid-phase rather than a reduced adherence to the hot metal surface.(6)

One measure of the thermal stability of aviation fuels is the quantity of deposits formed on heated metal surfaces.(7) In accelerated stability tests conducted in accordance with the JFTOT procedure (ASTM D 3241) (8), the rating methods currently employed involve either visual comparisons or measurements of reflected light by the tube deposit rater (TDR), both of which are sensitive to deposit color and surface texture. In the research reported in reference 7, deposits formed on stainless-steel JFTOT heater tubes were examined by the TDR, a gravimetric carbon combustion method, and two new nondestructive techniques for determining deposit volumes based on measurements of dielectric strength and optical interference. Measurements of total carbon content by combustion were used as a reference. It was found that the dielectric and interference methods correlated well with the combustion analyses and each other, while the total TDR often yielded misleading results. The purpose of the present study was to investigate the role of JFTOT metal surface composition in deposit formation.

Experimental: Experiments were performed in an Alcor model HLPS300 Hot Liquid Process Simulator (HLPS), which is a modular version of the JFTOT apparatus used for the ASTM D 3241 method. The HLPS was operated to give conditions equivalent to D 3241 requirements except that Triton-treated fuel prefilers were not used. In the development of the experimental technique, there was a desire to achieve a more isothermal temperature profile over the length of the tube so that greater accuracy could be achieved in the measurement of rate parameters such

as activation energies for deposit formation. In the first attempt to broaden the hot zone over the tube, a "heated line transformer with line clips" was used to preheat the fuel. Figure 1 shows the result of fuel preheating on the longitudinal temperature profile of the JFTOT heater tube. In Figure 1, station 0 in the fuel inlet and station 60 is where the fuel leaves the JFTOT heater tube jacket. Preheating the fuel to 150°F (66°C) and 200°F (93°C) at heater tube temperatures of 300° and 340°C did not demonstrate any significant hot zone broadening advantages over fuel at room temperature. Figure 2 shows the results of a second approach to broadening the temperature profile using a reverse fuel flow by the JFTOT heater tube. The reverse flow approach did, in fact, achieve a much higher degree of isothermal tube temperature behavior, but because it was less standard and could possibly hinder comparisons with other studies, it was not used in the experiments reported here.

Procedure for Coating Heater Tubes. Aluminum, gold, carbon, magnesium, and copper were deposited on sets of three each 304 SS heater tubes. Basically, the objective was to make coatings on the heater tubes thick enough to cover the surface completely yet thin enough to minimize possible effects of both electrical and thermal conductivity. The coatings were accomplished with a Denton model DV-502 vacuum deposition apparatus that was set up to produce a thin layer of the test element onto standard 304 SS JFTOT heater tubes. In developing the procedure for coating the tubes, it was found that the success of the method depended greatly on the cleanliness of the heater tube surface. Quality adherence of the coatings was achieved when the heater tubes were cleaned with trichloroethane in a sonic bath for about two minutes and dried in a laboratory specimen dryer.

Deposit Measurement Device. The deposit thickness measurement device (DMD) determines the thickness of a deposit on a conductive surface by applying a voltage across the deposit while measuring the dielectric breakdown of the layer at various points.(9) The DMD used in this work was first reported in reference.(10) The DMD voltage measurements were shown to relate thickness of deposits with 350 volts equal to 1 micrometer.(10) Methods for calculating deposit volume on JFTOT heater tubes were also discussed in reference.(10) This procedure was used to develop DMD data correlations to carbon burn-off values reported in reference 7.

Auger Milling Technique. The raw data from Auger ion milling are given in units of time. To determine thickness repeatably, it is necessary to make the appropriate calibration. For the deposit thickness measurements, a piece of tantalum foil with a layer of tantalum oxide of known thickness was ion-milled at a given rate until the oxide was removed. For a given milling rate, it was then possible to measure thickness in terms of time. JFTOT deposit thicknesses were determined assuming that the rates of material removal from the deposit and the tantalum oxide standard were equivalent. However, it was expected that the deposit would mill at a somewhat faster rate since it is primarily carbon and hydrogen, i.e., lighter elements than the oxygen and tantalum. Since the mass removal rate for the deposit could be faster than that of the standard, the actual deposit thicknesses may have been somewhat larger than those reported in this paper.

Test Fuel. The objective in choosing a test fuel was to find one that could provide assessable deposits on 304 SS heater tubes at test temperatures of 300°, 340° and 380°C. After evaluating several fuels, a West Coast Jet A fuel was found to give measurable levels of deposit on 304 SS heater tubes at all three of the chosen test temperatures. This fuel met ASTM D 1655 specification at the time of manufacture; it had a code 3 breakpoint temperature of 254°C when the work was started.

Test Procedure. Stainless steel (304) tubes were evaluated using the West Coast Jet A fuel and test durations of 0.5, 1.0, 1.5 and 2.5 hours at maximum heater tube temperatures of 300°, 340°, and 380°C. These data are summarized in Table 1. The 1.5-hour test period was selected for use in the metal surface evaluations because it produced a deposit that was relatively nascent, yet assessable by the DMD and Auger measuring techniques.

Results and Discussion: The results in Figure 3 show the longitudinal temperature profile of the heater tubes at controlled maximum temperatures of 300°, 340°, and 380°C. These data were used as a reference to determine the temperature at a particular heater tube station. Figures 4 through 9 summarize the deposit thickness by DMD for the West Coast Jet A using the 316 SS heater tube, the 304 SS heater tube, and the 304 SS heater tubes coated with aluminum, magnesium, gold, and copper. Auger milling measurements of deposit thickness were made at

several of the heater tube stations for the various surfaces as shown in Figures 4 through 9. Note that Auger results were not available for the 304 stainless steel.

All the DMD deposit profiles were consistent in that they each exhibited a shift toward the fuel inlet (station 0) as the maximum heater tube temperature was raised. General comparison of Auger milling values to DMD thickness values suggest:

- * Auger milling gives much greater thicknesses for deposits formed on copper coated tubes. The two methods give similar deposit profiles and locations of maximum thickness.
- Magnesium coated tube deposit values by Auger were increasingly higher than DMD values at higher heater tube temperatures.
- 316 SS tube deposit values by Auger were increasingly higher than DMD values at higher heater tube temperatures.
- Aluminum coated tube deposit thickness by Auger was approximately one-half of that by DMD.
- * Gold coated tube deposit thickness by Auger milling was essentially equal to DMD measured values.

Auger ion milling of the deposits showed the order of deposition to be copper > magnesium = 316 SS > gold > aluminum. The dielectric strength method indicated that 316 SS > 304 SS > gold > magnesium = aluminum = copper.

The pronounced differences between the deposit thickness measuring techniques suggest that the dielectric strength of the deposit is strongly affected by metal ions that become included in the bulk of the deposit. The results show that the surface temperature as well as composition plays an important role in deposition. Other than for variation in the thickness of deposits formed during 1.5-hour tests using various metal surfaces, the most dramatic effect observed was that the bulk of deposits moved to lower tube temperature as the maximum tube temperature was increased from 300° to 380°C. These data suggest that this fuel is unique in that it deposits over a relatively narrow temperature range; compared to the other surface materials, copper tends to shift this temperature to somewhat lower limits (See Table 2).

Basically, there are two theories on the role of metals in fuel stability. When fuels are exposed to hot metal surfaces, it is believed that naphthenic acids react with surface oxides and produce fuel-soluble metal naphthenates. In solution, the trace metals may either initiate autoxidation reactions or enhance reaction rates by decomposing hydroperoxides and producing more reactive free radicals. The other theory is that gums formed in the autoxidation process have different affinities for surface materials and thus adhere to some surfaces more than others. If it is simply the adherence of gums to the surface that matters, the effect would be expected to be important only in the formation of nascent deposits, and the composition of the deposit would not be changed by the metal. If the mechanism is based solely on the dissolution of metals by acidic constituents in the fuel, one would not anticipate a change in the rate of deposition as the deposit builds up. Also, metal ions would probably become incorporated homogeneously in the deposit since metals tend to form chelates with the relatively polar gum molecules in the fuel.

In ASTM D 3241-88a, note 8 states: "Heater tubes should not be reused. Tests indicate that magnesium migrates to the heater tube surface under normal test conditions. The enriched magnesium surface may reduce adhesion of deposits to re-used heater tubes." The topography of the deposit formed on the magnesium surface was found to be somewhat different than that of the other metal surfaces. A cursory examination of photographs taken with the scanning electron microscope (SEM) at magnifications of 1000X and 2000X showed hemispherical deposits on the magnesium surface and flat platelet-type deposits on the other metal surfaces. Before the tests, the magnesium coatings showed no apparent abnormalities; all of the metal coatings were made with essentially the same thickness. After the test, the deposit thickness profiles appeared to be similar to those formed on the other metal surfaces. The results indicate either adhesion of agglomerated insolubles or the formation of deposits from soluble gums at particular sites on the magnesium surface. The adhesion of agglomerated insolubles seems to be a more likely candidate because the Auger deposit thickness measurements were higher than those with the DMD and the difference tended to increase with rising temperature. The results indicate that greater amounts of

magnesium become incorporated into the structure of the deposit as the temperature is raised. This suggests, as mentioned above, that magnesium dissolution is an important process as the fuel is prestressed on its journey to the hot section of the heater tube. Perhaps the dissolved magnesium initiates nucleation of soluble gums and causes agglomerates to form which then deposit (adhere) on the surface.

Conclusion: Under JFTOT D 3241 test conditions thickness profiles of deposits formed on a variety of surfaces, 316 SS, 304 SS, Al, Mg, Cu and Au, were compared using the DMD (dielectric breakdown voltage) and Auger milling. Except for gold and aluminum, the deposit thicknesses measured by DMD were substantially lower than those measured by Auger milling, and the disparity in the two methods seemed to grow with increased deposit thickness. Some deposits, especially those on the copper coated tubes, gave particularly low DMD thickness values compared to Auger milling values. Metal dissolution and subsequent inclusion into the deposit is thought to be responsible for the increased conductivity of the deposit, an effect which becomes more pronounced at higher tube temperatures. Aside from variations in the thickness of deposits due to metallurgy, the most dramatic effect observed was that the bulk of deposits moved to tube locations of lower temperature as the maximum temperature of the tube was increased from 300° to 380°C. These results suggest that the fuel used in this study forms its deposit over a relatively narrow temperature range; compared to the other surfaces this effect was observed at lower temperatures on the copper coated tubes. A cursory examination of photographs taken with the scanning electron microscope (SEM) showed hemispherical deposits on the magnesium surface and flat platelet type deposits on the other metal surfaces. Deposit morphology will be further studied and new experiments are planned using heater tube surfaces under more isothermal conditions with fuel flow across the tube (as opposed to longitudinal flow).

Acknowledgement: This work was conducted under DOD Contract No. DAAK70-87-C-0043, administered by the Fuels and Lubricants Division of the Materials, Fuels, and Lubricants Laboratory, U.S. Army Belvoir Research, Development and Engineering Center, Fort Belvoir, Virginia 22060-5606, with Mr. T.C. Bowen, STRBE-VF, serving as contracting officer's representative and Mr. M.E. LePera, STRBE-VF, serving as technical monitor. Approved for publication, this paper represents only the views of the authors.

References

- (1) Cuellar, Jr., J.P., Russell, J.A., "Additive Depletion and Thermal Stability Degradation of JP-5 Fuel Shipboard Samples," Report No. NACP-PE-141C.
- (2) CRC Literature Survey on the Thermal Oxidation Stability of Jet Fuel, CRC Report NO.509, April 1979.
- (3) Uri, N.; ACS Advances in Chemistry Series, #36, Chapt.10, p. 102, 1962.
- (4) Hazell, L.B., Baker, C., David, P., and Fackereel, A.D., "An AES Depth Profiling Study of the Deposits on Aluminum During the Jet Fuel Thermal Oxidation Test," Surface and Interface Analysis 1, pp. 507-513, 1986.
- (5) Clark, R.H., "The Role of a Metal Deactivator in Improving the Thermal Stability of Aviation Kerosines," 3rd International Conference on Stability and Handling of Liquid Fuels, London, UK, 13-16 September 1988.
- (6) Schreifels, J.A., Morris, R.E., Turner, N.H., and Mowery, R.L., "The Interaction of a Metal Deactivator With Metal Surfaces," American Chemical Society, Division of Fuel Chemistry, Preprints, 35, No.2, pp. 555-562, 22-27 April, 1990.
- (7) Morris, R.E. and Hazlett, R.N., "Methods for Quantifying JFTOT Heater Tube Deposits Produced From Jet Fuels," Energy and Fuels, Vol. 3, No. 2, pp. 263-267, 1989.
- (8) ASTM Thermal Oxidation Stability of Aviation Turbine Fuels (JFTOT Procedure). In Annual Book of ASTM Standards; ASTM: Philadelphia, PA, 1989; Part 5.02, ASTM D 3241-88a.
- (9) U.S. Patent No. 4,791,811, "Deposit Thickness Measurement," J.G. Barbee, Southwest Research Institute, Granted Dec. 20, 1988.
- (10) Stavinocha, L.L., Barbee, J.G., and Buckingham, J.P., "Thermal Stability Deposit Measuring Device," Proceedings of 2nd International Conference on Long-Term Storage Stabilities of Liquid Fuels, San Antonio, TX, 29 July - August 1986.

TABLE 1. Summary of Deposit Measuring Device (DMD) Evaluation of JFTOT Tubes Along With Standard ASTM D 3241 Ratings

Test No.	Tube Metal	Total Test Time, hr	Prefilter	Temp, °C	Pressure Drop, mm of Hg at Time	TDR Spin Rating at Station, mm	Visual Rating	DMD, Max. Thickness, cm x 10 ⁷ at Station, mm	DMD, Vol. of Deposit, cm ³ x 10 ⁷
253-H	304 SS	2.5	No	300	125 at 46.5 min	50+ at 44-58	>4 Peacock	2394 at 54	3785
254-H	304 SS	2.5	No	340	125 at 38.1 min	50+ at 32-50	>4 Peacock	2277 at 40	2999
255-H	304 SS	2.5	No	380	125 at 52.1 min	50+ at 26-58	>4 Peacock	2005 at 32	3226
157-T	Al	2.5	Yes	260	2 at 148.7 min	12 at 38-45	<4	42 at 54	54
256-H	304 SS	1.5	No	340	125 at 36.0 min	50+ at 34-58	>4 Peacock	1862 at 40	2282
257-H	304 SS	1.5	No	300	125 at 31.2 min	50+ at 45-58	>4 Peacock	1968 at 50	2255
258-H	304 SS	3.5	No	300	125 at 63.3 min	50+ at 40-58	>4 Peacock	2742 at 54	2742
259-H	304 SS	0.5	No	300	5.3 at 30.0 min	47 at 50-52	4	345 at 54	439
260-H	304 SS	1.0	No	300	125 at 56.1 min	50+ at 45-58	>4	1811 at 54	1835
261-H	304 SS	0.5	No	340	19.5 at 30.0 min	50 at 38-42	>4	591 at 42	651
262-H	304 SS	1.0	No	340	125 at 48.0 min	50+ at 36-49	>4	1845 at 42	2091
257-H	304 SS	1.5	No	300	125 at 31.2 min	50+ at 45-58	>4 Peacock	1968 at 50	2255
263-H	Al/304 SS	1.5	No	300	125 at 56.0 min	36 at 54	4 Peacock	1168 at 52	1256
264-H	Au/304 SS	1.5	No	300	125 at 66.3 min	50+ at 50-56	>4 Peacock	1411 at 52	1294
266-H	Mg/304 SS	1.5	No	300	125 at 52.1 min	Too Dark to Rate	4	1082 at 54	1558
267-H	Cu/304 SS	1.5	No	300	125 at 18.5 min	50+ at 38-58	4 Peacock	862 at 46	1164
279-H	316 SS	1.5	No	300	125 at 58.2 min	50+ at 28-58	>4 Peacock	2211 at 54	2669
256-H	304 SS	1.5	No	340	125 at 36.0 min	50+ at 34-58	>4 Peacock	1862 at 40	2282
268-H	Al/304 SS	1.5	No	340	125 at 33.5 min	50+ at 40-45	>4 Peacock	1200 at 42	1649
269-H	Au/304 SS	1.5	No	340	125 at 31.5 min	50+ at 40-45	>4 Peacock	1917 at 42	2048
270-H	Mg/304 SS	1.5	No	340	125 at 40.5 min	Too Dark to Rate	>4	1297 at 42	1944
271-H	Cu/304 SS	1.5	No	340	125 at 30.0 min	50+ at 29-58	>4 Peacock	751 at 36	682
278-H	316 SS	1.5	No	340	125 at 40.9 min	50+ at 24-56	>4 Peacock	2668 at 40	2440
272-H	304 SS	1.5	No	380	125 at 52.4 min	50+ at 30-40, 49-54	>4 Peacock	2137 at 34	2191
273-H	Al/304 SS	1.5	No	380	125 at 48.1 min	50+ at 32-36	>4 Peacock	1805 at 34	1633
274-H	Au/304 SS	1.5	No	380	125 at 56.9 min	50+ at 32-36	>4 Peacock	2248 at 34	1824
275-H	Mg/304 SS	1.5	No	380	125 at 58.3 min	Too Dark to Rate	>4	1237 at 36	1782
276-H	Cu/304 SS	1.5	No	380	125 at 31.2 min	50+ at 24-58	>4	1148 at 30	812
277-H	316 SS	1.5	No	380	125 at 35.5 min	50+ at 18-58	>4 Peacock	2477 at 34	1757

(L.A.M.F.)

Table 2. Tube Locations of Maximum Deposit For Three Control Temperatures

Tube control temp. = <u>Metal Surface</u>	Deposit Peak Locations, mm		
	<u>300°C</u>	<u>340°C</u>	<u>380°C</u>
316 SS	52	40	32
Mg/304 SS	52	40	34
Cu/304 SS	46 (301°C)*	36 (325°C)*	30 (340°C)*
Au/304 SS	52	40	32
Al/304 SS	52	44	34
304 SS	50 (298°C)*	40 (335°C)*	34 (345°C)*

* Approximate Tube Temperature, °C, at location, estimated from Figure 3.

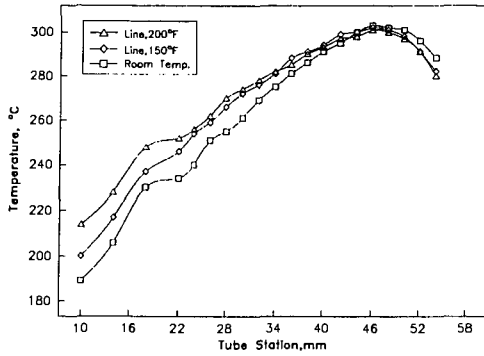


Figure 1. HLPS temperature profiles at 300°C

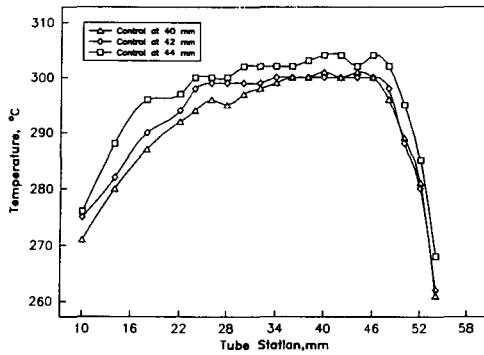


Figure 2. HLPS temperature profile with fuel flow through top of the 304 stainless steel heater tube at 300°C

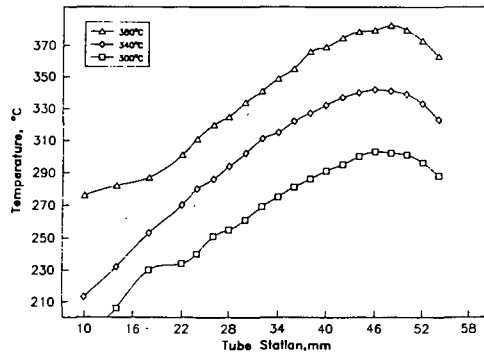


Figure 3. HLPS temperature profile of three temperatures using 304 stainless steel heater tubes

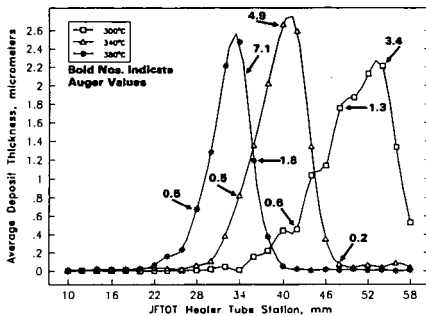


Figure 4. Deposit thickness on 316 stainless steel heater tube run at 300°C, 340°C, and 380°C

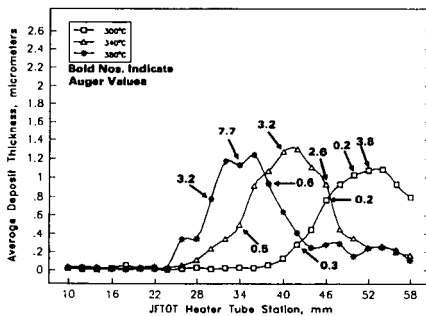


Figure 5. Deposit thickness on magnesium plated heater tube run at 300°C, 340°C, and 380°C

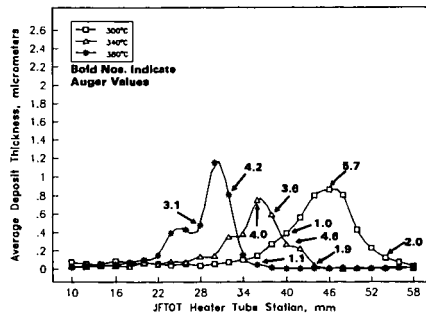


Figure 6. Deposit thickness on copper plated heater tube run at 300°C, 340°C, and 380°C

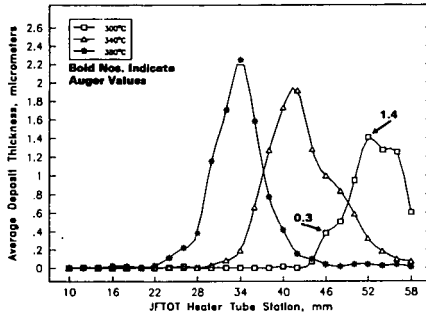


Figure 7. Deposit thickness on gold plated heater tube run at 300°C, 340°C, and 380°C

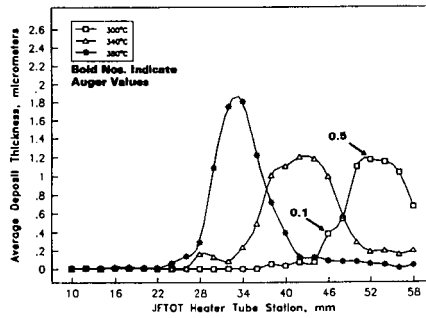


Figure 8. Deposit thickness on aluminum plated heater tube run at 300°C, 340°C, and 380°C

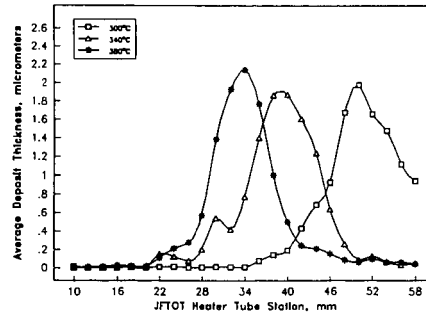


Figure 9. Deposit thickness on 304 stainless steel heater tube run at 300°C, 340°C, and 380°C

HIGH TEMPERATURE GAS PHASE PYROLYSIS OF JP-8

by

Jeffrey L. Moler^{*†}, Ellen M. Steward[†], and Philip H. Taylor[‡]

[†]Aero Propulsion and Power Laboratory (WRDC/POSF), Aeronautical Systems Division, Air Force Systems Command, United States Air Force, Wright-Patterson Air Force Base OH 45433-6563 (U.S.A.)

[‡]University of Dayton Research Institute, Dayton OH 45469 (U.S.A.)

Gas phase pyrolysis of JP-8 (NATO designation F-34), neat and with a thermal stability additive (JFA-5) is reported. Experiments were conducted in a quartz test cell to minimize catalytic effects. Data were collected isothermally at 50 degree intervals from 350°C (662°F) to 850°C (1562°F) and at mean residence times in the range of 0.3 to 3.0 seconds. Products were analyzed using gas chromatography with mass selective and flame ionization detectors, GC/MS and GC/FID, respectively. The low molecular weight decomposition products, from C₁ to C₇, are identified. The onset of decomposition and formation of decomposition products were observed under these conditions. The products of thermal decomposition and the time and temperature relationship of the decompositions are discussed and compared to the decomposition products of pure compounds. The results obtained from the jet fuel thermal oxidation tester (JFTOT) for the same fuels are also discussed. The JFA-5 additive had almost no effect on the thermal decomposition over this temperature range.

INTRODUCTION

The chemical composition of aviation fuels determines the thermal stability of the fuel. The temperatures and times required for a fuel to degrade determine the limits of aircraft performance and how much of the advantage gained from more efficient engines can actually be achieved. Thermal stability and thermal decomposition products of aviation fuels will play an important role in the design of future aircraft systems.

The thermal stability of aviation turbine fuels was first recognized as a problem in the 1950's. In conventional turbine engines, aviation fuels encountered high temperatures in the lubrication oil heat exchanger and the combustor manifold and nozzles[1]. Exposure of the fuel to these high temperatures resulted in the thermal degradation of the fuel and formation of deposits on critical engine parts.

With the development of high-Mach aircraft and more efficient engines, thermal stability of fuels has become even more crucial. The fuel in these aircraft and systems may reach temperatures of 538°C (1000°F), or higher[2]. This increased thermal stress may increase the thermal degradation and the deposits formed on critical engine parts and in fuel systems. Therefore, a better understanding of the thermal stability characteristics of current United States Air Force and NATO jet fuels is needed.

Previously, the pyrolysis of several alkanes, branched alkanes, and alkylated cycloalkanes within a carbon number range of 8 to 14 was reported[3]. These classes were chosen for study because they number among the major components of a typical JP-8. Comparison of individual component pyrolysis behavior with the pyrolysis behavior of JP-8 will yield a better understanding of JP-8 thermal stability.

A systematic study of the thermal decomposition of JP-8 (NATO designation F-34) from 600°C to 1000°C has been accomplished. JP-8 is typically a petroleum distillate cut from 177°C to 266°C (kerosenes) and commonly contains certain classes of compounds that may lower thermal stability. The rates at which individual components decompose and products form, *i.e.*, the temperatures and times necessary for pyrolysis to occur, are important factors in understanding the general thermal stability of a jet fuel.

EXPERIMENTAL

Apparatus

The system for thermal diagnostic studies (STDS)[4], developed at the University of Dayton Research Institute, is a continuous system consisting of three in-line units: the thermal decomposition unit, an analytical gas chromatograph (GC) for separation of parent compounds and pyrolysis products, and hydrogen flame ionization and mass selective detectors (FID and MSD, respectively)[5][6].

The thermal decomposition unit has a test-cell control module and an interchangeable test-cell assembly. The test-cell assembly has a quartz reaction cell heated by a hinged tube furnace (Linberg) over a temperature range of 250°C to 1150°C. The test-cell assembly is housed in a GC oven (Hewlett-Packard 5890A) for temperature control of the transfer lines, e.g., -100°C to +400°C.

Chromatographic separation was performed in a GC (Hewlett-Packard 5890A) with two separate chromatographic columns. Initial experiments were performed on a 30-meter Hewlett-Packard Ultra-5 column that was fed from the reactor cell assembly to the MSD (Hewlett-Packard 5970B). The Hewlett-Packard Ultra-5 column was then replaced with a 12-meter Hewlett-Packard Ultra-1 column that was fed from the reactor cell assembly to the FID. Ultra-high purity helium (99.999%) was used in the reactor cell assembly and as the carrier gas for chromatographic analysis.

Reagents

Thermal stability enhanced JP-8 was prepared from a WRDC/POSF standard JP-8 and 30 mg/l of JFA-5, obtained from the DuPont Company. Standard mixtures of C₂ to C₆ alkenes and C₁ to C₆ normal alkanes were obtained from Scott Specialty Gases for identification standards and quantitation.

Procedure

A 0.03 μl sample was injected into the test-cell assembly resulting in a gas-phase concentration of 1.78 × 10⁻⁴ moles/l. Both a neat JP-8 and a JP-8 standard containing 30 mg/l of JFA-5 were tested. The reaction temperature was governed by the tube furnace temperature. Temperatures were monitored before, within, and after the reaction zone using chromel/alumel thermocouples. The sample was held at 200°C before and after isothermal exposure (±1°C) to the experimental temperature in the reactor. Residence time at temperature was controlled by changing the mass flow. Unreacted sample and decomposition products were swept through a heated transfer line—to prevent condensation—after emerging from the test-cell and were captured at the head of the analytical chromatographic column, held at -60°C. During the first 6 minutes, separation of the C₁ to C₄ products occurred on the column. After the initial 6 minutes, the analytical GC was temperature programmed at 15°C/min to 285°C to allow for chromatographic separation of the remaining decomposition products and the jet fuel sample. The GC eluents were detected qualitatively by the MSD and quantitatively by the FID.

RESULTS AND DISCUSSION

JP-8 is composed of thousands of compounds, among which normal alkanes, branched alkanes, and alkylated cycloalkanes have the largest concentration, with smaller amounts of aromatic and unsaturated compounds. Trace components, such as nitrogen-, sulfur-, and oxygen-containing species and dissolved oxygen and metals, are present in the fuel and may act as initiators in free radical decomposition of the fuel components[7][8]. Thermal decomposition of JP-8 was not observed at temperatures below 650°C. Thermal decomposition of alkanes at high temperatures (500°C or higher)[9] occurs via a radical-chain mechanism[10]. Other pyrolysis experiments with low molecular weight alkanes at 660°C[11][12] produced the same products as JP-8, but the higher molecular weight hydrocarbons in JP-8 require higher temperatures to produce similar decompositions[13]. This is supported by the trends observed for individual component decomposition[3].

JP-8 was subjected to pyrolysis to determine its overall thermal decomposition and the thermal decomposition characteristics of individual components in a complex mixture at various mean residence times. In Table 1, the reactor residence times necessary for one, five, ten, fifteen, and twenty percent decomposition of neat JP-8 have been calculated from the experimental data for temperatures from 600°C to 1000°C. In Figure 1, the gas chromatograms of the neat JP-8, subjected to temperatures from 500°C to 1000°C with a mean residence time of 1 second, illustrate typical behavior observed from the thermal decomposition. Additional chromatograms showing similar behavior were collected at reactor residence times between 0.3 and 3.0 seconds.

While data were collected over a range of residence times, 0.3 to 3.0 seconds, within the temperature range of 500°C to 1000°C, the typical patterns of formation and decomposition observed are shown in Figures 2 through 9, using a residence time of 1.0 second. The C₁ to C₆ compounds in Figures 2 to 5 are not present in the unstressed JP-8. The C₇ and higher carbon number compounds in Figures 5 to 9 are present at differing

concentrations in the unstressed JP-8. The concentrations of the decomposition products relative to the initial JP-8 concentration are also given in Figures 2 through 9.

Inspection of Figures 2 through 4 indicates that for temperatures less than 750°C, the lighter hydrocarbons (C₁ through C₄) are the principal products. At higher temperatures, the rate of decomposition for C₂ and higher carbon number compounds competes with their rate of formation until the formation of methane dominates above ~900°C. Higher molecular weight aromatic compounds are observed chromatographically, but were not quantitatively measured. These higher molecular weight compounds include alkylated benzenes, naphthalenes, and multiple-aromatic-ring compounds identified by the MSD.

Methane and ethene increase in concentration up to 800°C, where the rate of formation no longer increases with temperature (Figure 2). Propene and propyne each reach a maximum at 800°C and 900°C, respectively, and then fall off in concentration (Figure 3). 1,3-Butadiene and 1-butene reach maxima at 750°C and 800°C, respectively, before decreasing in concentration (Figure 4). Finally, the two primary aromatic species formed are benzene and methylbenzene (Figure 5). These aromatic species reach their maxima at 750°C and 825°C, respectively. Their formation is a potential indicator of deposit precursor formation[14], and may provide a link to the degradation kinetics.

The normal and branched alkanes found in JP-8 show similar behavior in most cases. Nonane and decane can be formed through pyrolysis of higher molecular weight alkanes, and therefore show maxima before rapidly decreasing at 650°C (Figure 6). Slightly higher in molecular weight and thermal stability, the concentrations of undecane and dodecane are fairly constant until they reach a breakpoint after which their concentration decreases (Figure 7). The branched alkanes shown in Figure 8 have very different behavior resulting from their formation from the decomposition of higher molecular weight species. 2-Methyldodecane behaves similar to nonane and decane, with a maximum at 650°C. At 800°C, 2-methylundecane coeludes with naphthalene, which begins to dominate as a more favorable by-product of decomposition and addition reactions at higher temperatures, because the naphthalene concentration increases up to 1000°C. The concentrations of tetradecane and pentadecane decrease linearly in concentration as temperature increases (Figure 9).

The addition of 30 mg/l of the JFA-5 additive into JP-8 increased the JFTOT breakpoint temperature from 280°C to 360°C using a 2.5 hour duration test[15]. Comparisons of 1.0 second residence time data within the 650°C to 1000°C temperature range show a slightly greater decomposition occurring for the JP-8 with additive compared to the neat JP-8 (Figure 10). Other thermal oxidative inhibitors have been reported to enhance thermal stability at moderate temperatures and decrease stability at much higher temperatures[16]; inhibiting radical formation at moderate temperatures and acting as a radical initiator at much higher temperatures. Additional tests above 650°C with varied amounts of the radical-inhibitor JFA-5 will be needed to determine its effectiveness for extremely high temperatures.

Although the STDS contained an oxygen-free environment, as noted previously, oxygen was most likely present as small amounts of dissolved oxygen and oxygenated species, approximately 55 ppm. This results in an oxygen concentration of approximately 1.65 ppb in the reactor. The presence of oxygen affects the pyrolysis behavior; oxygen readily supports the formation of radical species that are important in the decomposition of hydrocarbon compounds. Even so, the typical behavior of an average JP-8 at these temperatures was observed. The kinetics of thermal decomposition of JP-8 are complex, and remain unresolved.

CONCLUSIONS

The maximum temperature and minimum times at various temperatures, at which a fuel will resist thermal degradation in the presence of small amounts of oxygen, have been approximately determined. To obtain a ten percent decomposition using reactor residence times of 0.3 to 3.0 seconds, temperatures from 680°C to 600°C, respectively, were required. For a one second residence time, a temperature of 636°C was needed for ten percent decomposition of JP-8. The addition of 30 mg/l of the JFA-5 additive did not change the temperature required for equivalent decomposition in the neat JP-8. This information will provide the basis for determining the limits of thermal stability and developing methods that will be used to enhance thermal stability of future jet fuels[17].

The major components of JP-8 are normal and branched alkanes. The majority of other components have alkyl groups attached to them. The decomposition products are formed by the cracking of alkanes and

cleaving alkyl groups. Additionally, dehydrogenation and isomerization occurs at temperatures above 850°C and reformed products undergo further cracking and cleavage. The major low molecular weight products formed from 600°C to 1000°C are the methane, ethene, propene, propyne, and the butenes. From 600°C to 700°C, terminal alkenes are formed preferentially. From 700°C to 850°C, alkylated cycloalkanes and alkenes dominate the higher molecular weight products. Above 850°C, the major products become alkylated benzenes, naphthalenes, and multiple-aromatic-ring compounds.

Further work needs to be accomplished before the kinetics can be resolved. The pyrolysis studies of more single components and simple mixtures of these single components are required before the mechanisms and kinetics will be understood. Pure compound studies are planned to attempt to unravel the kinetic complexity of JP-8 decomposition.

The JFA-5 additive had the effect of increasing the thermal oxidative stability at lower temperatures (up to 350°C); yet, it had almost no effect on the thermal stability of JP-8 from 600°C to 1000°C at a residence time of 1.0 second.

LITERATURE CITED

1. S. M. Cohen, *Aircraft Research and Technology for Future Fuels Symposium*, NASA Conf. Pub. 2146, april 16-17, 1980.
2. A. C. Nixon, Performance Report Battelle Subcontract No. F-4186(8827)-484 under U. S. Air Force Contract No. F33615-84-C-2410, January, 1986.
3. J. L. Moler and E. M. Steward, *ACS, Div. Pet. Chem., PREPRINTS*, **34**, (4), 837 (1989).
4. W. R. Rubey and R. A. Grant, *Rev. Sci. Instrum.*, **59**, (2), 265 (1988).
5. H. S. Hertz and S. N. Chesler, *Trace Organic Analysis: A New Frontier in Analytical Chemistry*, (NBS, Washington, 1979).
6. W. A. Rubey and R. A. Carnes, *Rev. Sci. Instrum.*, **56**, 1795 (1985).
7. E. W. Pitzer and E. M. Steward, AFWAL-TR-86-2043, 1986. (Available through NTIS.)
8. C. Martel, WRDC-TR-89-2021, 1989. (Available through NTIS.)
9. F. O. Rice, *J. Am. Chem. Soc.*, **55**, (7), 3035-3040 (1933).
10. A. Kossiakoff and F. O. Rice, *J. Am. Chem. Soc.*, **65**, (4), 590-595 (1943).
11. A. N. Rumyantsev and E. Yu. Oganosova, *Kimiya i Tekhnologiya Topliv i Masel*, No. 1, 29-30, January, 1987.
12. A. N. Rumyantsev and E. Yu. Oganosova, *Kimiya i Tekhnologiya Topliv i Masel*, No. 3, 29-31, March, 1987.
13. B. M. Fabuss, J. O. Smith, and C. N. Satterfield, *Advances in Petroleum Chemistry and Refining*, (Interscience, New York, Vol IX, Chapter 4, 1964).
14. I. C. Lewis, E. M. Dickinson, D. J. Miller, and J. Amos, *ACS, Div. Pet. Chem., PREPRINTS*, **33**, (3), 404 (1988).
15. P. D. Liberio and M. R. Swensen, Unpublished Data, June, 1989.
16. R. E. Morris and R. N. Hazlett, *ACS, Div. Pet. Chem., PREPRINTS*, **33**, (2), 364 (1988).
17. A. C. Nixon, G. H. Ackerman, R. D. Haawthorn, H. T. Henderson, and A. W. Ritchie, Technical Documentary Report No. APL TDR-64-100, Part II, September, 1966.

Table 1. Temperature Versus Reactor Residence Time Required for One, Five, Ten, Fifteen, and Twenty Percent Decomposition of Neat JP-8.

T (°C)	t _(1%)	t _(5%)	t _(10%)	t _(15%)	t _(20%)
600	0.56	1.64	2.38	2.64	2.75
650	0.06	0.37	0.71	0.92	1.13
700	<0.01	0.02	0.21	0.32	0.47
750	<0.01	<0.01	0.06	0.11	0.19
800	<0.01	<0.01	0.02	0.04	0.08

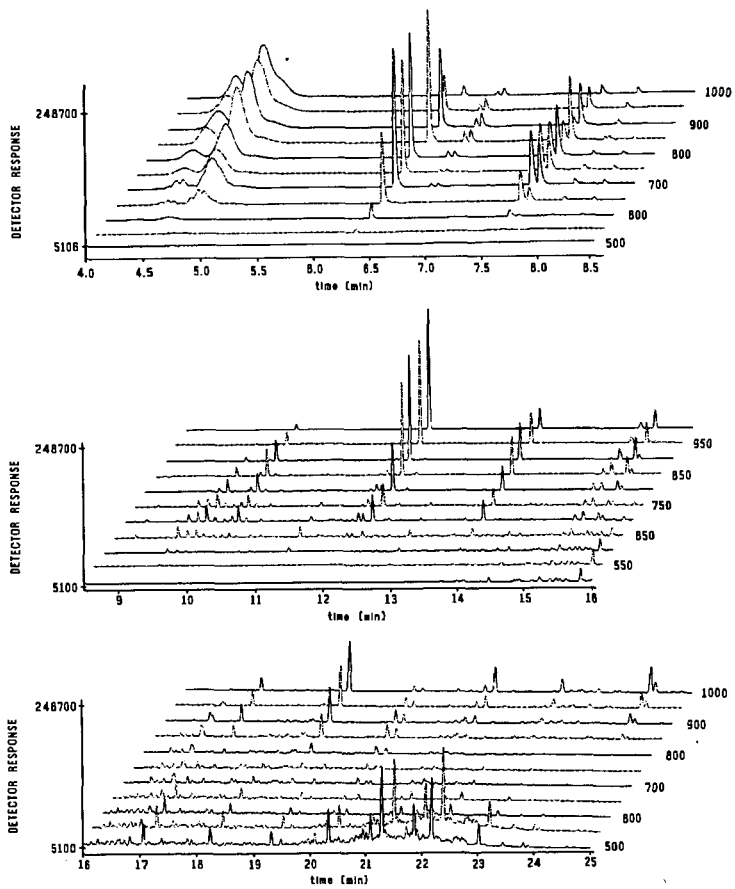


Figure 1. Gas Chromatograms of JP-8 from 500°C to 1000°C with a 1 Second Residence Time.

Compounds not initially present in JP-8.

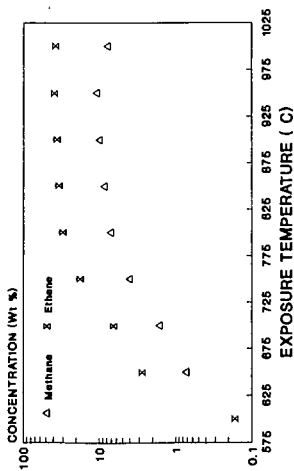


Figure 2. Formation of CH4 and C2H4.

Compounds not initially present in JP-8.

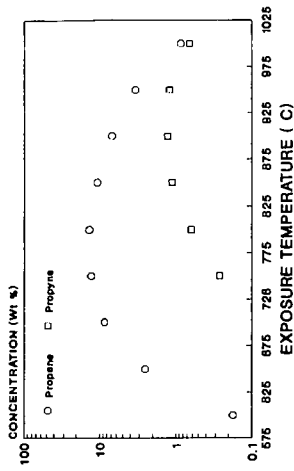


Figure 3. Formation of C3 Species.

Compounds not initially present in JP-8.

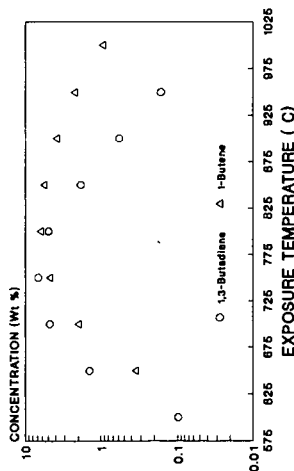


Figure 4. Formation of C4 Species.

Benzene is not initially present in JP-8.

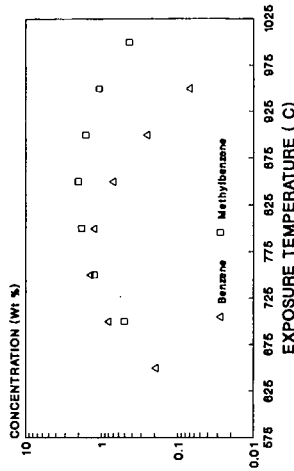


Figure 5. Formation of C6-C7 Aromatics.

Changes in amounts present in JP-8.

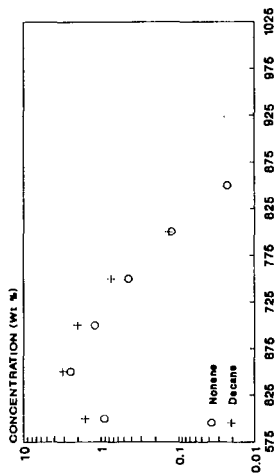


Figure 6. Decomposition of C9 and C10.

Changes in amounts present in JP-8.

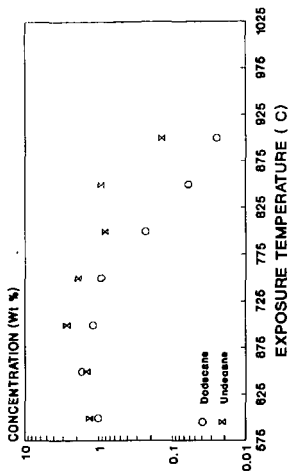


Figure 7. Decomposition of C11 and C12.

Changes in amounts present in JP-8.

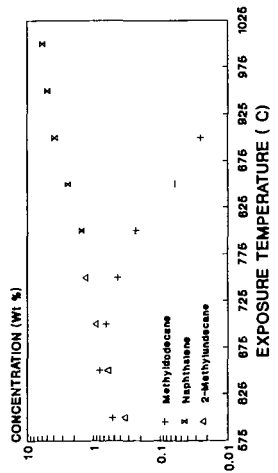


Figure 8. Behavior of Branched Alkanes and Formation of Naphthalene.

Changes in amounts present in JP-8.

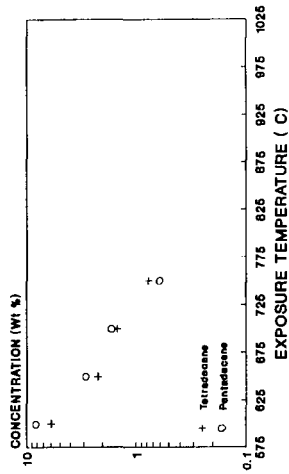


Figure 9. Decomposition of C14 and C15.

Samples run at 1 second residence time.

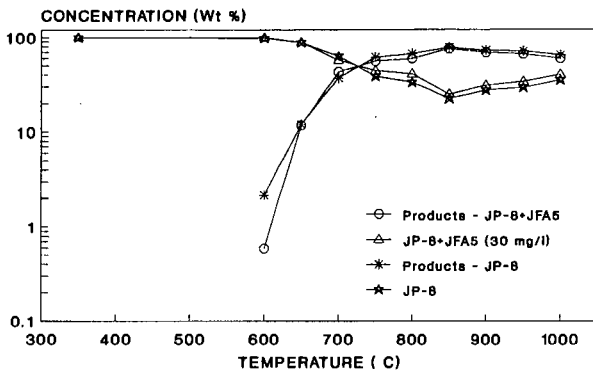


Figure 10. JP-8 versus JP-8 + JFA-5.

SYMPOSIUM ON THE STABILITY AND OXIDATION CHEMISTRY
OF MIDDLE DISTILLATE FUELS
PRESENTED BEFORE THE DIVISIONS OF FUEL
AND PETROLEUM CHEMISTRY, INC.
AMERICAN CHEMICAL SOCIETY
WASHINGTON MEETING, AUGUST 26-31, 1990

A THREE-DIMENSIONAL ANALYSIS OF THE FLOW AND TEMPERATURE
DISTRIBUTIONS IN THE JFTOT

By

J. A. Pearce and W. M. Roquemore
WRDC Aero Propulsion and Power Laboratory, Wright-Patterson AFB, Ohio, 45433

and

C. H. Oh, B. J. Merrill, and R. P. Wadkins
Idaho National Engineering Laboratory, P. O. Box 1625, Idaho Falls, Idaho 83415

ABSTRACT

This paper provides an insight into the detailed flow and temperature distributions in the Jet Fuel Thermal Oxidation Tester (JFTOT), a test device that has been used for many years to quantify the thermal stability of aircraft fuels. Though the JFTOT has found wide application as a qualification test device, very little is known about the many intricacies and nuances of the JFTOT flow field. Of particular interest is the possibility that variations in the flow field could be manifested in terms of changes in deposition on the JFTOT heater tube. To quantify the flow and temperature distributions, a three-dimensional numerical analysis is applied using the KIVA code. Also included in the analysis is a simplified model for jet fuel thermal degradation. Due to the limited amount of quantitative data available from JFTOT experiments, the deposition model used in the study is a global type Arrhenius equation with "calibration" data derived from tests with the Fiber Optic Modified JFTOT (FOM-JFTOT).

NOMENCLATURE

a_i constants in temperature curve fit
 A_d Arrhenius preexponential factor
 A_e exit flow area
 A_i inlet flow area
 D characteristic diameter

E_d	Arrhenius activation energy
i	grid representation of r
j	grid representation of θ
k	grid representation of z
K	deposit thermal conductivity
l	starting length
r	radial direction
r_i	inner radius
r_o	outer radius
Δr	$r_o - r_i$; channel width
Re_D	Reynolds number based on hydraulic diameter
t	time
T	temperature
u_r	radial velocity component
u_z	axial velocity component
u_θ	azimuthal velocity component
z	axial direction
θ	azimuthal direction
τ	deposit thickness

INTRODUCTION

Thermal stability of jet fuels is a research area which has received significant attention for more than 30 years. Current interest in the field is high due to the prospects for future thermal stability challenges. These challenges arise primarily from the practice of using fuel to cool critical on-board aircraft systems. Large thermal stresses on the fuel are the consequence of this practice, and this condition is expected to worsen with increasingly sophisticated aircraft design. To further aggravate the problem, crude stock quality is expected to decrease in the future with possible deleterious effects on fuel thermal stability (1). At this juncture it has become critical to better understand the mechanisms that affect a fuel's thermal stability. The consequences of failing to gain a better understanding of thermal stability could include limiting aircraft performance envelopes for lack of suitably stable fuels.

A long standing tool of the thermal stability researcher is the Jet Fuel Thermal Oxidation Tester (JFTOT). This device has long been used by laboratories in the qualification of jet fuel thermal stability. Full details on the test procedures are not

necessary for the current discussion but can be found in the literature (2,3). A qualification test for a typical aviation fuel such as JP-4, JP-5, or JP-8 consists of flowing the given fuel around an electrically heated tube for a period of 150 minutes at a peak heater tube temperature of 260°C. The test is evaluated by comparing the color of the deposit on the heated tube to a standard reference. A numerical value or rating is assigned to the test results based on the tube coloration. Based on this rating a fuel either "passes" or "fails" the test. Unfortunately, the qualification test yields little or no data which can be used to better understand the various detailed mechanisms contributing to the degradation of fuel within the device.

In an attempt to try to increase the research value of JFTOT testing, variations on the standard qualification test have been devised (4). A common practice is to run tests at progressively higher tube temperatures until a "failure" is recorded. The temperature at which a fuel "fails" the test has been designated as the *Breakpoint Temperature*. Though this type of test certainly has more value than the qualification test, it still provides little information which could be valuable in the study of detailed degradation mechanisms.

Recent attempts have been made to try to quantify the results of JFTOT tests in terms which are more valuable to researchers (4-6). These tests have focused on examining the effects that various subprocesses have on the overall deposition process. Among the factors examined in these studies are fuel flow rate, tube temperature, and heater tube metallurgy. One of the more interesting results taken from the tests of Warner and Biddle (4) was a marked azimuthal asymmetry in the deposition on the tube. This trend was repeated in subsequent testing and is believed to be strongly linked to the complex flow field which exists within the JFTOT. Therefore, an exercise which may help to elucidate deposit mechanisms within the JFTOT is a determination of the detailed flow field within the device. The work presented here is focused on obtaining a description of the flow field within the JFTOT.

JFTOT GEOMETRY AND BOUNDARY CONDITIONS

JFTOT Geometry

A thorough understanding of the JFTOT geometry is necessary to comprehend the results which will be subsequently presented. The JFTOT is intended to be a simple flowing device for the qualification of jet fuels; however, a close examination of the flow passage reveals much about the JFTOT flow which is not simple. The Reynolds number at the tube entrance, based on the hydraulic diameter, is $Re_D \approx 13$. This Reynolds number places this flow firmly in the domain of laminar flow. The low Reynolds number is a

product of both the low flow rate through the JFTOT (3 ml/min) and the small annular flow channel ($\Delta r < 1$ mm). A schematic representation of the JFTOT is provided as Figure 1 to aid in demonstrating this point; also, the coordinate system (cylindrical) which is utilized for all subsequent discussions is provided as Figure 2.

The primary flow direction in the JFTOT is the axial (+z) direction; however, the flow is not a simple annular pipe flow as one might expect. Complexities arise in the JFTOT flow which are directly attributable to the orientation of the fuel inlet and exit. The fuel enters the JFTOT in the radial direction; consequently, the entry is normal to the primary flow direction (+z). This orientation of the flow, as it is introduced to the JFTOT, then provides a great deal of complication to the otherwise simple flow field. Also note that the entering flow impinges on a step in the JFTOT tube which further complicates the flow. Therefore, components of velocity in the r and θ directions in the lower region of the tube are introduced by the incoming fuel.

The flow is similarly perturbed by the fuel exit which is again situated normal to the primary flow direction. Since the JFTOT flow is elliptic in nature, the influence of a downstream disturbance will be manifested upstream of the exit; therefore, the effects of the exit orientation should be apparent in the region of the JFTOT upstream from the exit. Also, in a manner similar to the entering flow, the exiting flow must flow past a step on leaving the flow channel.

A further element complicating the JFTOT geometry is the respective orientation of the inlet and exit planes. The fuel is introduced in the $-r$ direction at the location $\theta = 0^\circ$, while the fuel exits in the $+r$ direction at the location $\theta = 90^\circ$. Therefore, there is a 90° rotation in the azimuthal plane from the inlet to the exit and an azimuthal (θ) component of velocity must be introduced to the flow to account for this rotation. In light of the previous discussions, it should now be apparent that the flow in the JFTOT is three-dimensional and quite complex, and the analysis of the flow field is not a trivial problem.

Boundary Conditions

One aspect critical to the determination of the JFTOT flow field is the application of proper boundary conditions. The primary quantities of interest are the velocity components and the fuel temperature. The following boundary conditions apply at the tube inlet:

$$\begin{aligned} r &= r_o = 2.3125 \times 10^{-3} \text{ m}; \theta = 0^\circ; z = 0 \\ u_r &= -0.01 \text{ m/s}; u_\theta = 0; u_z = 0 \\ T &= T_{amb} = 300 \text{ K} \end{aligned}$$

1)

Conditions at the tube exit ($r = r_o$, $\theta = 90^\circ$, $z = 0.06$ m) are determined by the code and are unspecified at the outset. However, there is a constraint that the exiting velocity be in the $+r$ direction.

At the outer radius of the tube (excepting the inlet and exit), the following conditions apply:

$$\begin{aligned} r &= r_o = 2.3125 \times 10^{-3} \text{ m} \\ u_r &= u_\theta = u_z = 0 \\ T &= T_{amb} = 300 \text{ K} \end{aligned} \quad 2)$$

Admittedly, the temperature boundary condition at the outer radius is likely incorrect. In reality, the outer surface is exposed to ambient air, but it is certainly heated by both conduction through the test apparatus and convection from the heated fuel. However, since no reliable measurements of the outer housing temperature were available, the boundary was fixed at the ambient air temperature.

Finally, at the inner radius (JFTOT heater tube outer surface) the following conditions apply:

$$\begin{aligned} r &= r_i = 1.40 \times 10^{-3} \text{ m} \\ u_r &= u_\theta = u_z = 0 \\ T &\text{ (see (3))} \end{aligned} \quad 3)$$

Note that the ASTM (3) description of the JFTOT test provides axial temperature profiles along the heater tube. There is no azimuthal variation in these prescribed temperature profiles. For the particular case modeled in this study (maximum heater tube temperature of 550°F), a curve fit of the heater tube temperature profile was employed with the following form:

$$T(\text{K}) = a_1 + a_2 z + a_3 z^2 + a_4 z^3 \quad 4)$$

where z is in mm and the constants a_i are

$$\begin{aligned} a_1 &= 519.6 \text{ K} \\ a_2 &= -3.676 \text{ K/mm} \\ a_3 &= 0.2718 \text{ K/mm}^2 \\ a_4 &= -0.003857 \text{ K/mm}^3 \end{aligned}$$

NUMERICAL MODEL

Computational Fluid Dynamics

The fluid flow in the JFTOT was modeled using the KIVA code developed at the Los Alamos National Laboratory. The partial differential equations solved in the KIVA code are the Navier-Stokes, conservation of mass, and internal energy equations. The code is both three-dimensional and transient. For these calculations, JP-5 fuel was the fluid of interest; consequently, temperature dependent curve fits of the fluid properties were derived from existing data (7) and implemented into the code. Details of the numerical scheme employed in the code can be found in the literature (8-12), and their inclusion here is unnecessary.

The computational grid applied to the given problem is shown in Figures 3 and 4. Figure 3 shows a three-dimensional representation of the grid which consists of 8 radial cells, 24 azimuthal cells, and 24 axial cells (4,608 total cells). The coordinate orientations are supplied in the figure, as are the general locations of the fuel inlet and exit. Figure 4, which depicts an $r-\theta$ plane of the grid, further clarifies the geometry. Fuel is inlet in the azimuthal (j) cells between $j = 3$ and $j = 7$. The fuel exits between cells $j = 9$ and $j = 13$. Logically, the inlet is at the bottom of the computational grid at axial (k) cells $k = 1$ and $k = 2$, and the exit is at the top of the computational grid at $k = 24$ and $k = 25$. All fuel enters and exits the flow domain at the outer radius which corresponds to the radial (i) location $i = 9$. By specifying the inlet and exit regions in this manner, the correct flow areas of $A_i = A_e = 4.91 \times 10^{-6} \text{ m}^2$ are preserved in the model.

Jet Fuel Thermal Degradation

The calculation of jet fuel thermal degradation, in terms of a deposit thickness on the JFTOT heater tube, was accomplished separately from the KIVA code. A number of assumptions were made regarding the deposition on the heater tube; primarily that the deposition was solely a function of the temperature at the deposit/fuel interface and that the local flow field had *no* effect on the deposition. Due to a severe lack of quantitative deposition data from the JFTOT, a simple global Arrhenius expression was used to model the accumulation of deposits on the heater tube. The expression governing deposit growth is given by

$$\frac{d\tau}{dt} = A_d \exp\left(\frac{-E_d}{T}\right) \quad 5)$$

The preexponential factor (A_d) and activation energy (E_d) were determined from data provided by Warner and Biddle (4) with the Fiber Optic Modified JFTOT (FOM-JFTOT). From this data the following constants for the preexponential factor and activation energy were determined:

$$\begin{aligned} A_d &= 155,970 \text{ m/s} \\ E_d &= 19,920 \text{ K} \end{aligned}$$

The temperature used in Equation 5 is the temperature at the fuel/deposit interface. This temperature is determined by analyzing the following energy equation for heat transfer in the deposit layer:

$$\left[\frac{1}{r} \frac{\partial}{\partial r} \left(Kr \frac{\partial T}{\partial r} \right) + \frac{1}{r^2} \frac{\partial}{\partial \theta} \left(K \frac{\partial T}{\partial \theta} \right) \right] = 0 \quad (6)$$

The boundary conditions for this equation, which is solved separately from KIVA, are taken from the KIVA temperature field for a given time step in the calculation.

RESULTS

JFTOT Flow Field

Though the KIVA code calculates the flow field in a transient sense, all of the velocity vectors and temperature contours displayed are for an instant in time subsequent to the system achieving a steady state. The first depiction of the flow field is provided as Figure 5. On the left are contours of the fluid temperature and on the right are velocity vectors. The three slices of the flow field shown are r - θ planes at the bottom ($z = 0$), mid-height ($z = 0.03 \text{ m}$), and top ($z = 0.06 \text{ m}$) of the flow domain. Note the orientation of the inlet and exit with respect to the plots which are shown (refer to Figures 3 and 4).

First considering the plots of the isotherms, note that for each plot the minimum and maximum temperatures are given below the figure and the contours are evenly spaced throughout the given temperature range. At the bottom of the domain note how the contour lines are bunched near the surface of the tube on the side corresponding to the fluid inlet. This bunching indicates steep thermal gradients and is a consequence of the entering fluid. On the side of the tube opposite from the inlet, note how the contour lines are much more widely spaced indicating the penetration of thermal energy into the flow. This is a consequence of the nearly stagnant flow in this region of the domain.

The temperature contours at the mid-height appear to be evenly distributed both radially and azimuthally. This is apparently because the thermal energy has sufficiently penetrated the fuel to eliminate any significant radial or azimuthal variations in the temperature field which were caused by the inlet. Furthermore, at this plane the flow is farthest from any of the influences which tend to perturb the flow (i. e., the inlet and exit). Moving to the exit, the contours are evenly spaced excepting the region where the fuel is exiting. At the exit, the contours appear to be stretched by the influence of the exiting flow.

Before discussing the velocity vectors depicted in Figure 5, some explanatory notes are necessary. First, since these depictions are $r-\theta$ planes, no axial velocity component is visible in these plots. Second, the plot routine scales the vectors independently for each plot; therefore, the length of the vectors is an indicator of velocity magnitude only for a given plot. The magnitudes of vectors *are not* directly related from plot to plot.

In the plot at the bottom of the domain, the influence of the incoming fluid can clearly be seen. There is an expected high radial component of velocity near the inlet, and there is also a high azimuthal velocity away from the inlet. However, on the side of the tube opposite the inlet the radial and azimuthal velocity components are very small. Moving to the mid-height, the flow is considerably more complex. Even at the mid-height, the influence of the exit can already be seen in terms of an outward radial component of velocity. However, note that the magnitude of these vectors is approaching the limits of the code's numerical accuracy. Directly opposite the azimuthal location of the exit, the azimuthal velocity component is again very small. Away from this location in both directions is a large azimuthal component of velocity. In some regions, there is also evidence of recirculation.

Finally, moving to the tube exit, the flow appears to be much more well ordered. There is a strong outward radial component of velocity at the exit, and there is also a significant azimuthal component of velocity on the side of the tube corresponding to the exit. However, on the opposite side of the tube, both the radial and azimuthal velocity components appear to be minute.

Moving to another view of the flow field, Figure 6 depicts radial profiles of temperature and axial velocity at the same axial locations used in Figure 5. Note that each of the plots in Figure 6 is at the azimuthal location corresponding to the fuel exit ($\theta = 90^\circ$). In the three temperature plots, the penetration of thermal energy can be seen progressively as one moves up the tube. At the bottom of the tube, there is a large radial gradient in temperature near the heater tube surface, and this effect is diminishing at the mid-height. At the tube exit, the slope is in fact very shallow, indicating a low rate of heat transfer to the fluid.

The velocity plots show basically an expected result. Note that the influences of radial and azimuthal velocity components are not present in this figure. At both the bottom of the tube and the mid-height, the velocity profiles are basically parabolic. This is the type of behavior that would be expected in a developed laminar pipe flow. Note that for laminar pipe flows, the length required for a flow to develop is approximately

$$l = 0.058 Re_D D \quad 7)$$

which for $Re_D \cong 13$ equates to approximately $0.75D$ (13). Assuming D is the hydraulic diameter, the entire length of the JFTOT is approximately $160D$. This implies that the flow becomes developed a short distance from the inlet. Admittedly, the geometry of the JFTOT is not the specific geometry to which this relationship applies; however, even if this relationship were in error by two orders of magnitude, the flow would still be developed at the tube mid-height. Finally, the profile at the top of the domain appears to have an anomaly at the outer radius where the velocity is not zero. This is simply due to the presence of the fuel exit.

The final figure of the flow field is given as Figure 7. This plot depicts the velocity vectors in an r - z plane of the flow domain. The plot on the left represents the azimuthal positions corresponding to the exit ($\theta = 90^\circ$ and 270°) and the plot on the right represents the positions corresponding to the inlet ($\theta = 0^\circ$ and 180°). At the inlet ($\theta = 0^\circ$), the influence of the entering fluid can clearly be seen, as can the flow stagnation in all other regions. Through the middle section of the tube there is little to note. Due to the great magnitude of the axial velocity with respect to the radial velocity ($u_z/u_r \gg 1$) in most regions of the flow field, the influence of the radial velocity is not apparent. Finally, at the exit ($\theta = 90^\circ$) the influence of the exiting flow is evident, and the flow is basically stagnant in all other regions.

Jet Fuel Thermal Degradation

The results of the calculation of deposit thickness on the JFTOT heater tube are given in Figure 8. Axial profiles of both the deposit thickness and wall temperature are shown. The results clearly show that the growth of the deposit layer follows the increase in wall temperature along the tube length. One would certainly expect this when considering that the model for deposit growth is based solely on the temperature of the fuel/deposit interface (Equation 5). The maximum deposit occurs at the location of the maximum temperature, and the maximum deposit thickness of $0.13 \mu\text{m}$ compares favorably with the measured value of $0.14 \mu\text{m}$ (4). It appears that this deposition model does a reasonable job of

approximating the JFTOT deposition for the specific case for which it was devised. However, its applicability to any other thermal stability experiments is questionable, and further studies would have to be accomplished to make any determination.

The premise that the local fluid flow has no influence on the deposition process is most certainly incorrect. Though many experiments have substantiated the significant role that surface temperature plays in the deposition process, it is not the sole contributing factor in jet fuel degradation. Some models have recently been presented that have addressed the issue of including multiple reaction steps in the degradation chemistry and allowing for the influence of fluid flow and bulk fuel temperature on the overall deposition process (14-16). However, the complexity of these models was beyond the scope of the current modeling effort, which was primarily focused on a determination of the JFTOT flow field.

CONCLUSIONS AND RECOMMENDATIONS

The results presented here have clearly demonstrated that the flow field in the JFTOT is quite complex. Due to the orientation of the flow inlet and exit, elements of flow in the radial and azimuthal directions are evident throughout the entire flow field. If one assumes that the flow field has some bearing on the deposition process, this complication of the flow could have a significant effect on the deposition observed on the JFTOT heater tube. However, the effects that the radial and azimuthal flow disturbances have on the deposition are not clear.

Further experimental efforts are necessary to elucidate the various mechanisms of fuel thermal degradation. Both the complex degradation chemistry and the effects of fluid mechanics and heat transfer must be addressed to better understand the overall deposition process. The most difficult task appears to be designing experiments that can isolate particular chemical and transport processes. Clearly the JFTOT is not such a device. Even though the JFTOT has been of great value in the qualification of fuel thermal stability, its use as a research tool is of questionable value.

ACKNOWLEDGEMENTS

This effort was jointly supported by the WRDC Aero Propulsion and Power Laboratory and the Department of Energy (DOE) Pittsburgh Energy Technology Center. The authors wish to thank Dr. Nand K. Narain, the DOE-Pittsburgh Program Manager, and William E. Harrison III, the U. S. Air Force Program Manager, for their guidance in this effort.

LITERATURE CITED

- (1) TeVelde, J. A. , and Glickstein, M. R. , United Technologies/Pratt & Whitney, NAPC-PE-87C (1983).
- (2) Alcor, Inc., Report No. 75-167 (1975).
- (3) ASTM D 3241-82, *1985 Annual Book of ASTM Standards: Petroleum Products, Lubricants, and Fossil Fuels*, Volume 05.03, 150-172 (1985).
- (4) Warner, P. A. and Biddle, T. B., United Technologies/Pratt & Whitney, Report No. FR 19032-11 (1988).
- (5) Clark, R. H. and Thomas, L., "An Investigation of the Physical and Chemical Factors Affecting the Performance of Fuels in the JFTOT," SAE Aerospace Technology Conference and Exposition (1988).
- (6) Kendall, D. R. and Mills, J. S., SAE Paper 851871 (1985).
- (7) Nixon, A. C., Ackerman, G. H., Faith, L. E., Henderson, H. T., Ritchie, A. W., Ryland, L. B. , and Shryne, T. M., Shell Development Company, AFAPL-TR-67-114, Pt. III, Vol. II (1970).
- (8) Amsden, A. A., Ramshaw, J. D., O'Rourke, P. J., and Dukowicz, J. K., Los Alamos National Laboratory, LA-10245-MS (1985).
- (9) Amsden, A. A., Ramshaw, J. D., Cloutman, L. D., and O'Rourke, P. J., Los Alamos National Laboratory, LA-10534-MS (1985).
- (10) O'Rourke, P. J. and Amsden, A. A., Los Alamos National Laboratory, LA-10849-MS (1986).
- (11) Amsden, A. A., O'Rourke, P. J., and Butler, T. D., Los Alamos National Laboratory, LA-11560-MS (1989).
- (12) Oh, C. H., Merrill, B. J., and Wadkins, R. P., Idaho National Engineering Laboratory, WRDC-TR-89-2138 (1989).
- (13) Shames, Irving H., *Mechanics of Fluids*, New York, McGraw-Hill Book Company, 270 (1982).
- (14) Roquemore, W. M., Pearce, J. A., Harrison, W. E., III, Krazinski, J. L. , and Vanka, S. P., *Preprints - Division of Petroleum Chemistry* 34 (4), 841-849 (1989).
- (15) Deshpande, G. V., Serio, M. A., Solomon, P. R., and Malhotra, R., "Modeling of the Thermal Stability of Aviation Fuels," Symposium on the Chemical Aspects of Hypersonic Propulsion, 198th National Meeting of the ACS, Miami, FL (1989).
- (16) Krazinski, J. L., Vanka, S. P., Pearce, J. A. , and Roquemore, W. M., ASME Paper No. 90-GT-33 (1990).

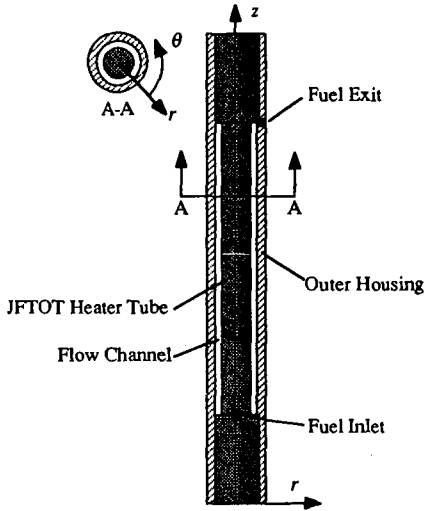


Figure 1: Schematic Representation of the JFTOT (Not to Scale)

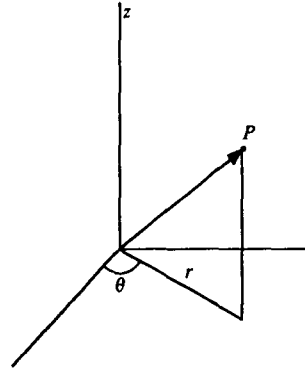


Figure 2: Cylindrical Coordinate System Used in KIVA Calculations

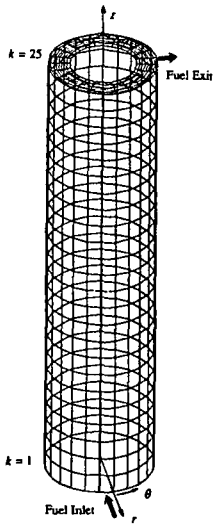


Figure 3: Three-Dimensional View of 8 x 24 x 24 Computational Grid

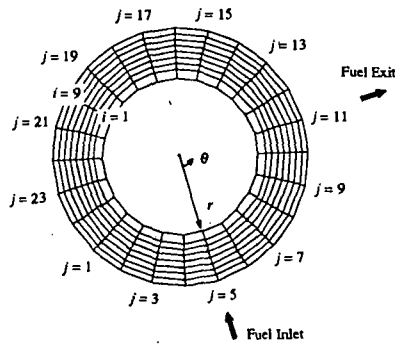


Figure 4: Top View of Computational Grid

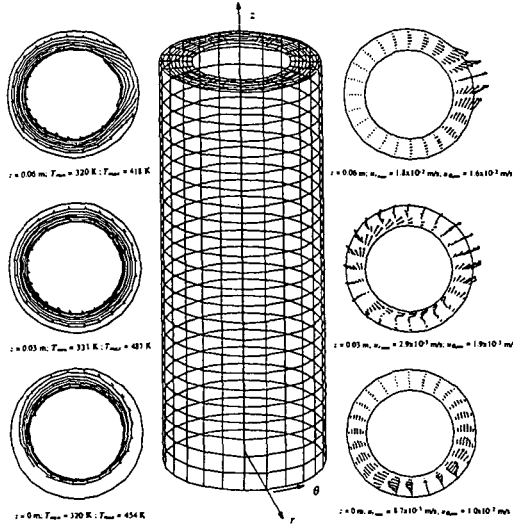


Figure 5: Calculated Temperature Contours and Velocity Vectors at the Bottom, Mid-Height, and Top of the JFTOT

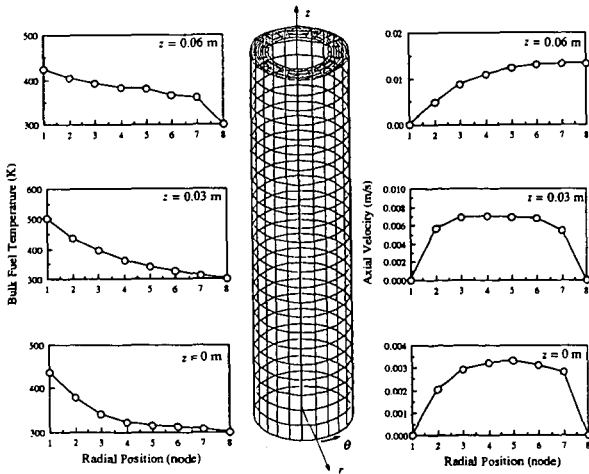


Figure 6: Calculate Radial Temperature and Axial Velocity Profiles at the Bottom, Mid-Height, and Top of the JFTOT

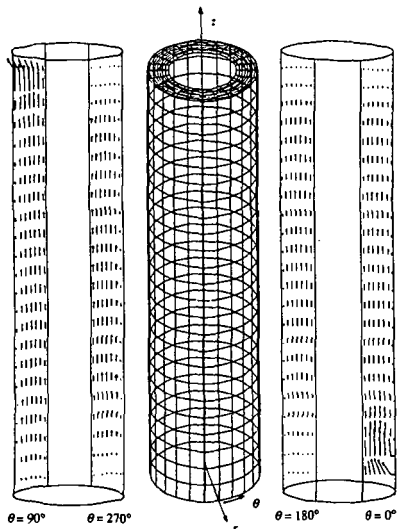


Figure 7: Calculated Velocity Vectors in the r-z Plane for Azimuthal Positions Corresponding to the Fuel Inlet and Exit

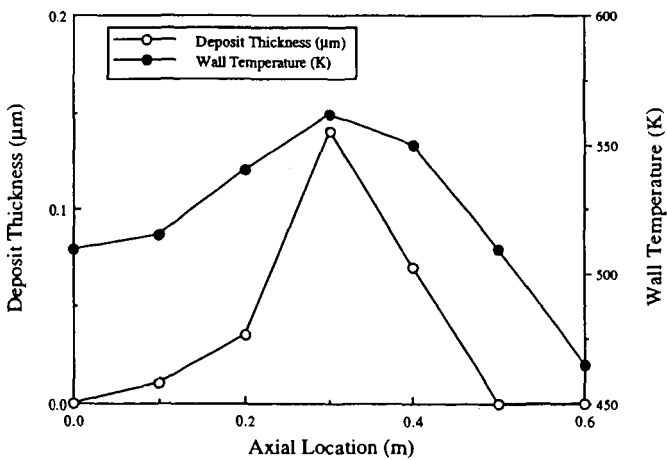


Figure 8: Predicted Axial Profiles of Deposit Thickness and Wall Temperature in the JFTOT

SYMPOSIUM ON THE STABILITY AND OXIDATION CHEMISTRY
OF MIDDLE DISTILLATE FUELS
PRESENTED BEFORE THE DIVISIONS OF FUEL
AND PETROLEUM CHEMISTRY, INC.
AMERICAN CHEMICAL SOCIETY
WASHINGTON MEETING, AUGUST 26-31, 1990

**A TIME-DEPENDENT MODEL WITH GLOBAL CHEMISTRY
FOR DECOMPOSITION AND DEPOSITION OF AIRCRAFT FUELS**

By

K. V. Reddy and W. M. Roquemore
WRDC/Aero Propulsion and Power Laboratory,
Wright-Patterson Air Force Base, OH 45433-6563

Abstract

The complicated decomposition processes of a thermally stressed aircraft fuel are mathematically treated using a computational fluid dynamics (CFD) base model with global chemistry. Recently Krazinski et al. (6) proposed a time-averaged CFD model with global chemistry for predicting the deposition rate of jet fuel. This model has proven to give reasonable results when calculations are compared to heated tube experiments lasting 25 hours or less. However, longer duration heated tube experiments have shown that the deposition rate increases with test time. This cannot be adequately treated by the time-average model since it assumes that the deposition rate is independent of time. This paper presents a time-dependent CFD model with global chemistry that directly accounts for deposit build-up and the impact this has on the fuel velocity and heat transfer rate and, thus their effect on deposition rate. The time-dependent incompressible Navier-Stokes equations along with the species continuity and energy equations are solved in an uncoupled manner using a fully implicit scheme. The model uses the global chemistry model proposed by Krazinski et al., but also assumes that the surface deposition reaction rate increases as a power of the deposit thickness. Comparisons of predictions with data from long duration tests, show that the model gives reasonable results for test durations of 150 hours or less but begins to deviate substantially for longer test times. Future improvements to the chemistry in the model are needed to correctly account for the effects of very long test times on deposition rate.

Introduction

The thermal stability of future jet fuels and the processes that result in fouling of fuel system components are of increasing concern. Thermal stability refers to the potential of a fuel to thermally decompose into insoluble products that can adhere to solid surfaces. Exceeding the thermal stability limit of a fuel in an aircraft fuel system can result in sticking of fuel control valves, poor performance of heat exchangers, clogging of fuel nozzles and hot streaks in the combustor due to an alteration of fuel nozzle spray pattern (1). Although these fouling problems occur sporadically in today's engines, they are expected to be more serious in future high performance aircraft due to the higher heat loads that the fuel will experience as it is used to cool the engine lube oil, avionics, environmental systems, and the fuel controls (2).

The thermal stability of jet fuels has been studied for many years. Quality control methods and empirical design information for hot fuel system components such as heat exchangers and fuel nozzles have resulted from these studies (1). Also, a considerable quantity of data have been collected for different experimental conditions and test apparatus. However, the overall complexity and a lack of fundamental understanding of the processes leading to fouling has hindered the development of a general theoretical framework that can be used to interpret or predict different experimental results. Two empirically based fouling models with similar global kinetics for fuel decomposition chemistry have been developed (3,4). One of the models (4) contains heat and mass transport expressions, which makes it potentially applicable to many engineering problems. However, the empirically based models do not provide, in a fundamental way, the general mathematical framework necessary for predicting the thermal deposition of different jet fuels for radically different experimental apparatus with a wide range of operating conditions. Thus, they do not have the general theoretical framework needed to interpret and predict the results for many different types of experiments. On the other hand, recently proposed computational fluid dynamics based models with global chemistry (CFDC) (5,6) do have the potential of being generally applicable for different test section geometries and a wide range of test conditions. Furthermore, the CFDC models can serve as an aid in designing meaningful experiments, interpreting experimental results in terms of fundamental processes, evaluating theories, providing insights into coupled processes, and estimating the relative sensitivity of parameters associated with fouling.

This paper extends the CFDC thermal stability modeling approach by solving the time-dependent Navier-Stokes equations instead of the Reynolds or time-averaged equations as done in Refs. 5 and 6. The model takes into account the build-up of deposits with time and the impact this has on the fluid velocity and heat transfer rate at the fuel/solid interface. The global chemistry model of Krazinski (6) is used in the present analysis along with the preexponential and activation energies determined therein. These global kinetic parameters were determined by curve fitting procedures using data from short duration tests of 25 hours or less.

Effects of Long Duration Testing on Deposition Rate

The importance of time on the deposition rate was demonstrated in long duration tests conducted by Giovanetti and Szetela (4) and Marteny (7). The average deposition rate at 500 hours is a factor of approximately two greater than that at 400 hours and is approximately four times that at 100 hours (7). This increase is larger at lower wall temperatures than at higher wall temperatures. Since clean fuel is always entering the test section, these changes in deposition rate with exposure time suggest that changes in surface reactivity and changes in fluid dynamics and heat transfer due to deposit blockage might be important factors. A microscopic analysis of deposit surfaces revealed that they are highly irregular and granular (7). The surface irregularity and the structure of the cavities depend mainly on the fluid velocity and the deposit thickness. This rough surface might affect the deposit growth rate by trapping fuel in the cavities and altering the surface sticking properties. Because of the constant heat flux used in heating the fuel, the trapped fuel may experience higher temperatures and residence times than the surrounding flowing fuel thereby, yielding more deposits. Blockage of the tube also becomes significant for long duration tests. At a fuel velocity of 0.076 m/s, Marteny (7) observed only a 43 percent open area after 50 hours of testing. This dropped to 16 percent after 150 hours. The blockage is not evenly distributed along the length of the tube because of the way the deposition rate depends on temperature. The large blockage with uneven distribution of deposits alters the fuel velocity and the heat transfer rate which can, in turn, change the deposition rate. These factors are considered in the time-dependent CFDC thermal stability model.

Mathematical Approach

The time dependent Navier-Stokes equations along with the turbulent energy and species conservation equations are used to describe the fuel motion in a long thin circular tube that is heated electrically with a constant heat flux. To advance the calculations with large time steps (to complete the hundreds of hours of real time within a few minutes of computational time), the governing equations are discretized into finite-difference equations and then are integrated using a fully implicit scheme. At each time step, the oxygen and precursor conservation equations are solved simultaneously with the other governing equations in an uncoupled manner.

The present formulation allows the deposit to grow on the wall surface with test time. In other words, after every time step, the geometry of the fuel/deposit interface, is allowed to change as part of the solution procedure. The computational domain is bounded between the axis of symmetry and the fuel-deposit interface and the grid system is reconstructed after every time-step for the changes in the boundary shape.

The mass, momentum and energy transport equations of the governing equations contain several coefficients related to molecular diffusion, viscosity, and thermal conductivity, respectively. Since a wide range of temperatures exists within the test section, the transport properties of the fuel vary significantly. A fresh JP-5 fuel is used as the fluid in the present calculations and the transport properties, along with the enthalpy and density at the given temperature, are obtained from the curve fits, just as done in Ref. 6.

Chemical Kinetics

Although there is only a limited understanding of the thermal decomposition processes in jet fuels, it is widely believed that they involve oxidation and pyrolysis of hydrocarbon fuel molecules and the formation of radical species (8,9). Autoxidation of the fuel, which is promoted by dissolved oxygen, occurs at temperatures up to about 540 K. Krazinski, et al. (6) used a global kinetics model with two reaction steps to account for the autoxidation reaction. This model did well in predicting the deposition rates in different heated tube experiments and is used in the present analysis. The two reaction steps of this model, which are assumed to occur in the bulk fuel, can be written as follows:



Step 1 generates the important deposit forming precursor species through an autoxidation process. The removal of precursors from the deposition process is assumed to occur at higher temperatures through the second reaction step. A wall reaction, that is similar to the oxidation reaction but, with different reaction rate constants, is also used as a surface reaction mechanism.

To take into account the effects of test duration on the wall reaction, the rate constant for the wall autoxidation reaction is assumed to be a function of both temperature and deposit thickness. Experimental observation (7) indicates that the deposition rate, thickness and granularity of the deposits increase with test duration. This suggests that the number of sites on which the deposit can form increases with time. As a first approximation, the wall reaction rate is assumed to be:

$$\text{Reaction Rate} = k (\Delta h/R)^m \exp(-E_a/R_0T) \quad 1)$$

Here, Δh is the deposit thickness at any given axial location on the tube with initial inner radius R , m is a constant to be determined and k is the pre-exponential constant used in Ref. 6. In the above global reaction model, all the precursors produced on the wall surface and those transported from the bulk fuel to the wall, are assumed to stick to the wall instantaneously and form a deposit. After the $(n+1)$ time-step, the deposit thickness is calculated by updating the deposit geometry at the n th time-step using the expression:

$$\Delta h^{n+1} = \Delta h^n + (\Delta t) P / \text{Density of the Deposit} \quad 2)$$

where P is the rate of generation of precursor particles on the wall surface due to the wall reaction and molecular transport mechanisms.

Results

The time-dependent CFDC model was initially evaluated by repeating the CFDC time averaged calculations presented in Ref. 6. Using the same rate boundary conditions and global reaction model, the time-dependent calculations of wall and fuel temperatures, fuel velocity,

turbulent intensities, deposition rate, and concentrations of precursor and oxygen converged to steady-state values that were in agreement with the time-averaged calculations performed using the model in Ref. 6. For this initial check out of the model the influence of deposit growth on the flow field and heat transfer rate, nor the increase of the surface reaction rate with deposit thickness, these capabilities were not activated. This was necessary to simulate the conditions in the time-average CFDC model.

Marteny (7) conducted a series of experiments to investigate the dependence of deposition rate and deposit morphology on test time duration. The fuel was thermally stressed as it flowed through electrically heated stainless steel tubes with an inner radius of 1.08 mm. A constant heat flux along the 914.4 mm tube length was maintained for the duration of a test. Steady-flow test were conducted from 25 to 500 hours. Tests were run at fuel inlet velocities of 0.0762 m/s and 0.3048 m/s. These test results are used to investigate the capabilities of the time-dependent CFDC model. The ability of the model to correctly determine the dependence of deposition rate and deposit thickness on test duration are of prime interest in the following results.

Figure 1 is presented to demonstrate how the deposit thickness and deposition rate change with wall temperature for test durations of 50 and 150 hours and a fuel velocity of 0.0762 m/s. Two types of calculations are presented. Both have $m = 0$ in the surface deposition rate equation (Eq. 1). In one calculation, the influence of deposit blockage on the fluid dynamics and heat transfer processes is not taken into account. In this case, the time-dependent calculations converged to a steady-state solution shown in Fig. 1. In this case the solution is the same as would be obtained by using the time averaged model in Ref. 6. For the steady-state solution, the total deposition rate is the mass of deposit divided by the test time. By using a deposit density of 0.9 g/cc, as recommended in Ref. 7, this linear relationship can be used to calculate the deposit thickness for the two test times. The deposit thickness results are also shown as steady-state solutions in Fig. 1.

The second type of calculation presented in Fig. 1 considers the influence of deposit blockage as a function of time on the fluid dynamics and the heat transfer processes. These calculations show that the deposition rate is not influenced at the low wall temperatures and only weakly influenced at the higher wall temperatures. The model does, however, give the correct trends. The model predicts that the deposition rate should increase more rapidly at the lower wall temperatures than for the higher wall temperatures, and that after 150 hours the deposition rate reaches a saturation value at a wall temperature of about 550 K. These trends are also observed in the experiments. Figure 1 also shows that the predicted deposit thickness is also only weakly

influenced by the effects of blockage on deposit formation. However, there is a significant discrepancy in the two measured thicknesses and the calculated values.

The experimental deposition rates shown in Fig. 1 for the 50 and 150 hours tests have a larger separation than the calculated rates. This indicates that the deposition rate mechanism is different from that used in the model. In Fig. 2, calculations are presented in which the deposition rate in Eq. 1 is assumed to go as the deposit thickness to a power $m = 0.8$. This assumption appears to improve the agreement between the calculated and measured deposition rates as compared to those in Fig. 1. The deposit thicknesses are also in better agreement but the calculated values are lower than the measured values. This is inconsistent with the fact that the calculated deposition rates are consistently higher than the measured values. The deposit thickness appears to be a sensitive function of deposit density. This opinion was reached by repeating the calculations for different deposit densities. It was determined that with a deposit density of 0.15 g/cc, the deposit thickness would agree with the measured values. However, the value of m had to be limited to 0.8 in order to keep deposition rate from becoming unrealistically high. The sensitivity of deposit thickness to density illustrates the importance of having accurate measurements of deposit density.

Calculations have also been made with the same tube but at a higher inlet fuel velocity (0.3048 m/s) and using a value of $m = 0.8$. At this velocity, the flow inside the tube is transitional. Since the present CFDC code can only simulate either a completely laminar or a fully turbulent flow, two calculations are made at this velocity; one with the assumption that the flow is laminar, and the other with a fully turbulent flow assumption. In the heated-tube section, the laminar flow assumption yields more accurate values of wall temperatures but the predicted bulk temperature is very low compared to the experimental data. On the other hand, the overall temperature distribution is better for the turbulent flow simulation and fairly accurate bulk fuel temperatures are obtained; but, agreement for the wall temperatures is poor near the entrance region up to 500 K. These results are shown in Fig. 3. Since the experimental data for deposition rate are available only up to 500 K, laminar flow simulations are used to predict the deposit growth.

The predicted and measured deposition rates are plotted in Fig. 4 for long duration tests with a fuel velocity of 0.3048 m/s. For test durations up to 300 hours, the predicted deposition rate curves closely follow the experimental data. For very long exposure times and low wall temperatures, however, the computed deposition rates are significantly lower than the measured values and at the higher temperatures the deposition rates undergo rapid increases. This trend is not observed in the experimental results.

Summary and Conclusions

A time-dependent CFDC model for predicting the thermal autoxidation decomposition and deposition characteristics has been developed. This model is used to estimate the effects of long duration tests on deposition rate as measured by Marteny (7). The experimental result that the deposition rate increases significantly with time, suggests that the deposition rate depends in some way on the deposits that are already present. It was assumed in the model that the surface deposition rate increases with deposit thickness. This resulted in fair agreement of deposition rates for test times of less than 150 hours but poor agreement for longer times. The calculated deposit thicknesses were also in poor agreement with measured values for the shorter duration tests. In conclusion, additional work must be performed on the model to better account for the effects of test time duration on deposition rate and deposit thickness.

ACKNOWLEDGMENT

The first author wishes to thank the National Research Council, Washington for supporting him to carry-out this research through the NRC-Air Force Systems Command Research Associateship.

LITERATURE CITED

- (1) Anon: CRC Literature Survey on the Thermal Oxidation Stability of Jet Fuel. CRC Report No. 509, Coordinating Research Council, Inc., Atlanta, GA, April 1979.
- (2) Koff, Bernard L., The Next 50 Years of Jet Propulsion, The Global Anniversary of Jet Powered Flight:1939 -1989, Dayton and Cincinnati AIAA Meeting, Dayton,OH, August 1989.
- (3) Deshpande, G. V., Serio, Michael A., Solomon, Peter R. and Malhotra, Ripudaman, Modeling of the Thermal Stability of Aviation Fuels, ACS Division of Petroleum Chemistry, Inc., Washington D. C., Vol. 34, No. 3, p. 955, Sept. 1989.
- (4) Giovanetti, A. J., and Szetela, E. J., Long Term Deposit Formation in Aviation Turbine Fuel at Elevated Temperature, AIAA Paper 86-0525, 24th Aerospace Sciences Meeting, Reno, January 6-9, 1986
- (5) Roquemore W. M., Pearce, J. A., Harrison III, W. E., Krazinski, J. L., and Vanka, S. P., Fouling in Jet Fuels: A New Approach, Preprints-Symposia in the Structure of Jet Fuels II, ACS Division of Petroleum Chemistry, Inc., Washington D. C., Vol. 34, No. 4, p. 841-849, Sept. 1989.

- (6) Krazinski, J. L., Vanka, S. P., Pearce, J. A., and Roquemore W. M., A Computational Fluid Dynamics and Chemistry Model for Jet Fuel Thermal Stability, ASME Paper No. 90-GT-33, Proceedings of the 35th ASME International Gas Turbine and Aeroengine Congress and Exposition (Combustion and Fuels Committee), Brussels, Belgium, 11-14 June 1990.
- (7) Marteney, P. J., Thermal Decomposition of JP-5 in Long Duration Tests, United Technologies Research Center, R88-957403-23, 1988.
- (8) Taylor, W. F., Deposit Formation from Deoxygenated Hydrocarbons, Part I - General Features, Ind. and Eng. Chem., Prod. Res. and Devel., Vol. 13, No. 2, pp. 133-138, 1974.
- (9) Hazlett, R. N., Hall, J. M., and Matson, M., Reactions of Rerated n-Dodecane Liquid Flowing Over Heated Metal Tubes, Ind. and Eng. Chem., Prod. Res. and Devel., Vol. 16, No. 2, p.171-177, 1977.

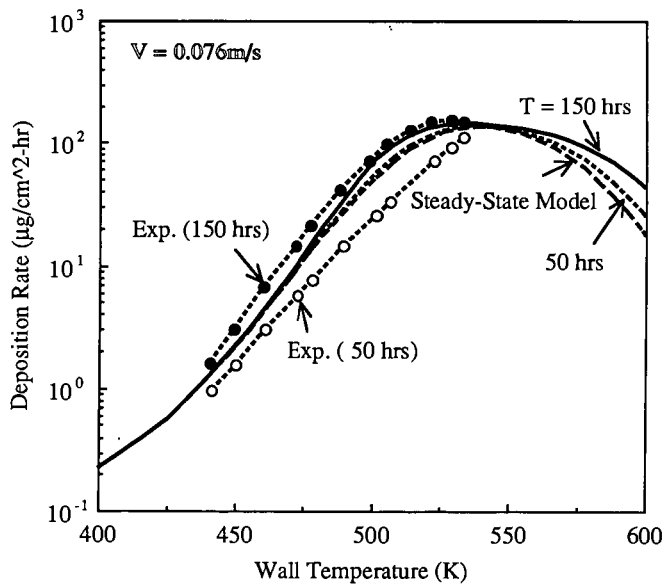
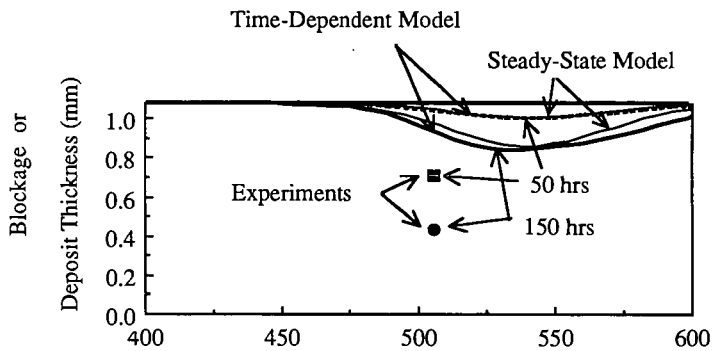


Figure 1. Predicted (without Changing Wall Reaction) and Measured Deposition Rates and Blockages for Long Duration Heated Tube Experiments of Marteny (1989).

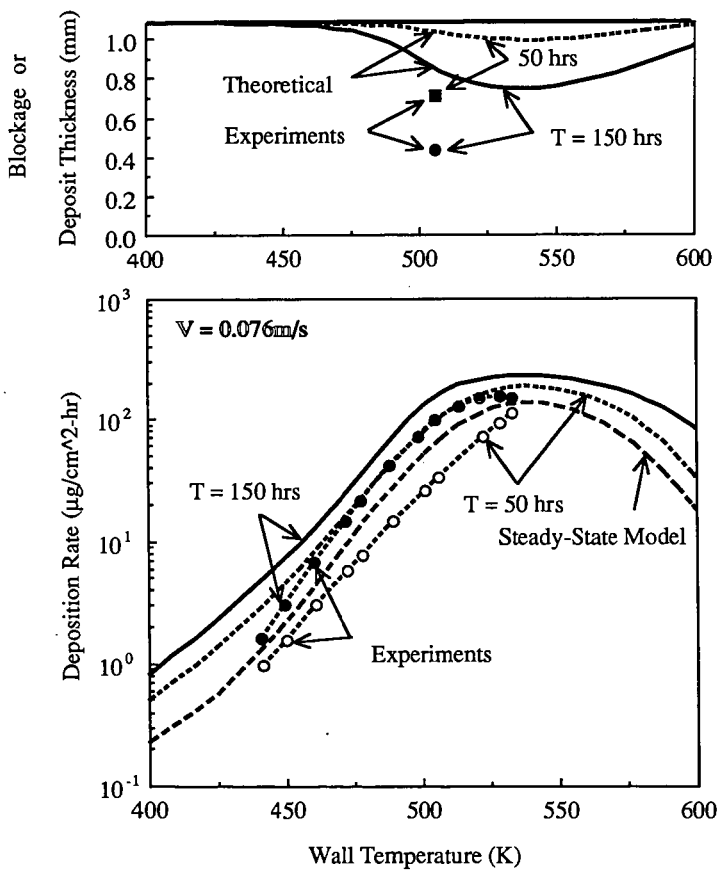


Figure 2. Predicted and Measured Deposition Rates and Blockages for Long Duration Heated Tube Experiments of Marteny (1989).

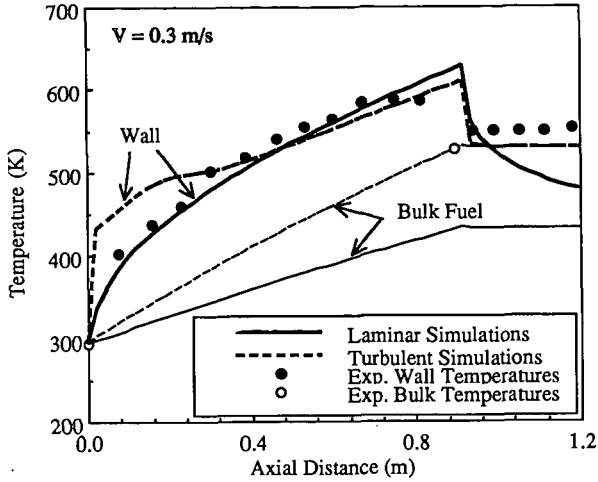


Figure 3. Comparison Between Predicted (Laminar and Turbulent Simulations) and Experimental Data for the Wall and Bulk Fuel Temperatures in the Heated Tube Experiment of Marteny (1989).

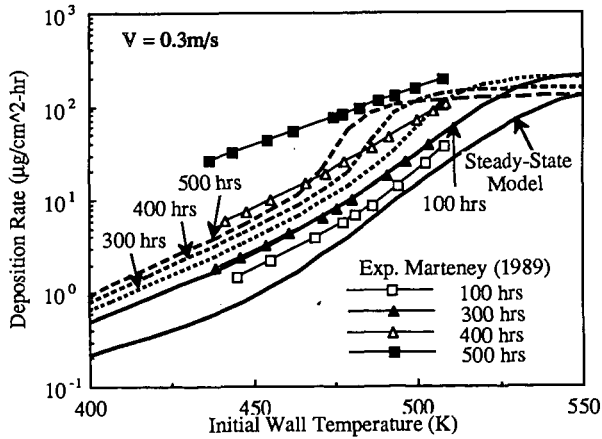


Figure 4. Predicted and Measured Deposition Rates for Long Duration Heated Tube Experiments of Marteny (1989).